Universitat Autònoma de Barcelona

Exploring the pharmacological properties of human antimicrobial ribonucleases

Guillem Prats Ejarque

Universitat Autònoma de Barcelona

DEPARTAMENT DE BIOQUÍMICA I BIOLOGIA MOLECULAR
UNITAT DE BIOQUÍMICA DE BIOCIÈNCIES

Exploring the pharmacological properties of human antimicrobial ribonucleases

Thesis presented by **Guillem Prats Ejarque** to obtain the degree of Doctor in Biochemistry, Molecular Biology and Biomedicine under the supervision of Dr. **Ester Boix Borràs**

Unitat de Biociències del Departament de Bioquímica i Biologia Molecular.
Universitat Autònoma de Barcelona

Dr. Ester Boix Borràs

Guillem Prats Ejarque

Cerdanyola del Vallès, novembre de 2020

"When I take you to the Valley, you'll see the blue hills on the left and the blue hills on the right, the rainbow and the vineyards under the rainbow late in the rainy season, and maybe you'll say, "There it is, that's it!"

But I'll say. "A little farther."

We'll go on, I hope, and you'll see the roofs of the little towns and the hillsides yellow with wild oats, a buzzard soaring and a woman singing by the shadows of a creek in the dry season, and maybe you'll say, "Let's stop here, this is it!"

But I'll say, "A little farther yet."

We'll go on, and you'll hear the quail calling on the mountain by the springs of the river, and looking back you'll see the river running downward through the wild hills behind, below, and you'll say, "Isn't that the Valley?"

And all I will be able to say is "Drink this water of the spring, rest here awhile, we have a long way yet to go and I can't go without you."

--- Ursula K. Le Guin

O dit d'una altra manera...

"La utopía está en el horizonte.

Me acerco dos pasos, ella se aleja dos pasos.

Camino diez pasos y el horizonte se corre diez pasos más allá.

Por mucho que yo camine, nunca, nunca la alcanzaré.

¿Entonces, para qué sirve la utopía?

Para eso sirve: para caminar."

--- Eduardo Galeano

LIST OF PAPERS INCLUDED IN THE THESIS:

I. **Prats-Ejarque, G.**, Blanco, J. A., Salazar, V. A., Nogués, M. V., Moussaoui, M. and Boix, E. Characterization of an RNase with two catalytic centers. Human RNase6 catalytic and phosphate-binding site arrangement favors the endonuclease cleavage of polymeric substrates. *Biochim. Biophys. Acta - Gen. Subj.* **1863,** 105–117 (2019).

II. Pulido, D., **Prats-Ejarque, G.**, Villalba, C., Albacar, M., Moussaoui, M., Andreu, D., Volkmer, R., Torrent, M. and Boix, E. Positional scanning library applied to the human eosinophil cationic protein/RNase 3 N-terminus reveals novel and potent antibiofilm peptides. *Eur. J. Med. Chem.* **152,** 590–599 (2018).

III. **Prats-Ejarque, G.**, Lorente, H., Anguita, R., Lu, Lu., Vázquez, S., Fernández-Millán, P. and Boix, E. Design of an RNase chimera for antimicrobial therapy. *(to be submitted to Int. J. Mol. Sci.)*.

Papers I and II are included as main papers of the thesis and paper III as additional paper related to the thesis.

LIST OF OTHER PUBLISHED PAPERS:

1. **Prats-Ejarque, G.**, Arranz-Trullén, J., Blanco, J. A., Pulido, D., Nogués, M. V., Moussaoui, M. and Boix, E. The first crystal structure of human RNase 6 reveals a novel substrate-binding and cleavage site arrangement. *Biochem. J.* **473,** 1523–36 (2016).
2. Pulido, D., Arranz-Trullén, J., **Prats-Ejarque, G.**, Velázquez, D., Torrent, M., Moussaoui, M. & Boix, E. Insights into the antimicrobial mechanism of action of human RNase6: Structural determinants for bacterial cell agglutination and membrane permeation. *Int. J. Mol. Sci.* **17,** 5–6 (2016).
3. Pulido, D., **Prats-Ejarque, G.**, Villalba, C., Albacar, M., González-López, J. J., Torrent, M., Moussaoui, M. & Boix, E. A novel RNase 3/ECP peptide for *Pseudomonas aeruginosa* biofilm eradication. Combining antimicrobial, lipopolysaccharide binding and cell agglutinating activities. *Antimicrob. Agents Chemother.* **60,** 6313–6325 (2016).
4. **Prats-Ejarque, G.**, Li, J., Ait-Ichou, F., Lorente, H. and Boix, E. Testing a Human Antimicrobial RNase Chimera Against Bacterial Resistance. *Front. Microbiol.* **10,** 1–14 (2019).
5. Lu, L., Arranz-Trullén, J., **Prats-Ejarque, G.**, Pulido, D., Bhakta, S. & Boix, E. Human Antimicrobial RNases Inhibit Intracellular Bacterial Growth and Induce Autophagy in Mycobacteria-Infected Macrophages. *Front. Immunol.* **10,** 1500 (2019).
6. Salazar, V. A., Arranz-Trullén, J., **Prats-Ejarque, G**., Torrent, M., Andreu, D., Pulido, D. & Boix, E. Insight into the antifungal mechanism of action of human RNase N-terminus derived peptides. *Int. J. Mol. Sci.* **20,** 4558 (2019).
7. **Prats-Ejarque, G.**, Lu, L., Salazar, V. A., Moussaoui, M. and Boix, E. Evolutionary Trends in RNA Base Selectivity Within the RNase A Superfamily. *Front. Pharmacol.* **10,** 1–17 (2019).
8. Rangel-Muñoz, N., Suarez-Arnedo, A., Anguita, R., **Prats-Ejarque, G.**, Osma, J. F., Muñoz-Camargo, C., Boix, E., Cruz, J. C. & Salazar, V. A. Magnetite nanoparticles functionalized with RNases against intracellular infection of *Pseudomonas aeruginosa*. *Pharmaceutics* **12**, 1–25 (2020).
9. Lu, L., **Prats-Ejarque, G.***, Wei, R.*, Goetz, M., Wang, G., Torrent, M. & Boix, E. Human RNase3 immune-modulation by catalytic-dependent and independent modes in a macrophage-cell line infection model. *Cell Mol. Life Sci*., in press (2020).

Most of the experimental work of this thesis was performed at the *Human ribonucleases involve in host defence* laboratory (UAB). During the PhD a 3-month stay in 2020, supported by a short-term EMBO fellowship, was spent at the BioNMR laboratory of the Patras University (Greece), under the supervision of Professor Georgios A. Spyroulias.

CONTENTS

ABBREVIATION LIST

Ahx	6-Aminohexanoic acid
AIM	Atg8 interacting motif
AMP	Antimicrobial peptide
CFU	Colony-forming units
CpA	Cytidylyl-3',5'-adenosine
ECP	Eosinophil cationic protein
EDN	Eosinophil-derived neurotoxin
EDTA	Ethylenediaminetetraacetic acid
FBS	Fetal bovine serum
FFT	Fast Fourier transform
FPLC	Fast protein liquid chromatography
HPLC	High-pressure liquid chromatography
HRP	Horseradish peroxidase
IPTG	Isopropyl β-D-1-thiogalactopyranoside
LB	Luria broth
LIR	LC3 interacting region
LPS	Lipopolysaccharide
MEM	Minimum essential media
MOI	Multiplicity of infection
MTT	3-(4,5-dimethylthiazol-2-yl)-2,5-diphenyltetrazolium bromide
ND	Non detected
NPT	Constant pressure equilibration
NVT	Constant volume equilibration
OD	Optical density
PBC	Periodic boundary conditions
PBS	Phosphate-buffered saline
PGN	Peptidoglycan
PMA	Phorbol 12-myristate 13-acetate
PME	Smooth particle mesh of Ewald
Poly(A)	Polyadenylic acid
Poly(C)	Polycytidylic acid
Poly(U)	Polyuridylic acid
P-LINCS	Parallel linear constraint solver
PVDF	Polyvinylidene difluoride
RMSD	Root mean square deviation
RNase	Ribonuclease
RPMI-1640	Roswell Park Memorial Institute 1640
SDS	Sodium dodecyl sulphate
TB	Terrific broth
TBS	Tris-buffered saline
TBST	Tris-buffered saline Tween
TIP3P	Transferible intermolecular potential 3P
TLR	Toll-like receptor
UpA	Uridylyl-3',5'-adenosine
UpG	Uridylyl-3′5′-guanosine
wt	Wild type

SUMMARY

[CATALÀ]

Aquesta tesi s'enfoca en la caracterització estructural i funcional de les propietats biològiques de les RNases antimicrobianes de la superfamília de la RNasa A. Concretament, s'han assolit els següents objectius a curt termini:

La caracterització estructural i funcional de la RNasa 6 per cristal·lografia de raigs X, dinàmica molecular, mutagènesi dirigida i anàlisis enzimàtics destaca el paper clau de les regions remotes d'unió al substrat. A part, hem identificat un possible segon centre actiu en la RNasa 6. Finalment, un estudi evolutiu dels diversos membres de la superfamília de la RNasa A ha revelat una tendència clara, al llarg de l'evolució en vertebrats, des de la preferència de guanina cap a la d'adenina en l'arquitectura de la regió secundària d'unió a bases B_2.

Al llarg del treball experimental realitzat en aquesta tesi, hem buscat la caracterització del mecanisme d'acció bactericida de les RNases, una de les principals línies de recerca del nostre grup de recerca. En aquest treball, ens hem enfocat específicament en l'optimització del pèptid antimicrobià derivat de l'N-terminal de la RNasa 3, ECP(5-17P24-36), i en el disseny d'una RNasa quimèrica antimicrobiana (RNasa 3/1).

Respecte el pèptid ECP(5-17P24-36), s'ha optimitzat mitjançant diverses metodologies, arribant a la conclusió que el millor candidat antimicrobià és el seu enantiòmer total D-ECP(5–17P24–36). Pel que fa a la RNasa 3/1, aquesta incorpora les característiques estructurals de les RNases 1 i 3, combinant així la seva elevada activitat catalítica i bactericida, respectivament. Es va dissenyar un primer constructe amb èxit, malgrat que no presentava els mateixos nivells d'activitat bactericida que la RNasa 3. Aleshores, vam dissenyar dues versions noves de la RNasa 3/1 que incorporaven el loop C-terminal de la RNasa 3, en el qual es va identificar un motiu estructural específic associat al reclutament de l'autofagosoma. És interessant destacar la capacitat de la primera versió de la quimera RNasa 3/1 d'endarrerir l'adquisició de resistència a la colistina en un assaig evolutiu *in vitro* d'exposició a la colistina en cultius d'*Acinetobacter baumannii*.

En global, aquests resultats ajudaran a elucidar el mode d'unió a l'RNA de les ribonucleases i el seu mecanisme antimicrobià, així com la seva contribució en el sistema immunitari innat, amb prometedores aplicacions farmacològiques.

[CASTELLANO]

Esta tesis se enfoca en la caracterización estructural y funcional de las propiedades biológicas de las RNasas antimicrobianas de la superfamilia de la RNasa A. Concretamente, se han alcanzado los siguientes objetivos en el corto plazo:

La caracterización estructural y funcional de la RNasa 6 por cristalografía de rayos X, dinámica molecular, mutagénesis dirigida y análisis enzimáticos destaca el papel clave de las regiones remotas de unión al sustrato. A parte, hemos identificado un posible segundo centro activo en la RNasa 6. Finalmente, un estudio evolutivo de los distintos miembros de la superfamilia de la RNasa A ha revelado una tendencia clara, a lo largo de la evolución en vertebrados, desde la preferencia de la guanina hacia adenina en la arquitectura de la región secundaria de unión a bases B_2.

A lo largo del trabajo experimental realizado en esta tesis, hemos buscado la caracterización del mecanismo de acción bactericida de las RNasas, una de las principales líneas de investigación de nuestro grupo de investigación. En este trabajo, nos hemos enfocado específicamente en la optimización del péptido derivado del N-terminal de la RNasa 3, ECP(5-17P24-36), y en el diseño de una RNasa quimérica antimicrobiana (RNasa 3/1).

Respecto al péptido ECP(5-17P24-36), se ha optimizado mediante varias metodologías, llegando a la conclusión que el mejor candidato antimicrobiano es su enantiómero total D-ECP(5–17P24–36). Por lo que respecta a la RNasa 3/1, esta incorpora las características estructurales de las RNasas 1 y 3, combinando así su elevada actividad catalítica y bactericida, respectivamente. Se diseñó un primer constructo con éxito, pese a que no presentaba los mismos niveles de actividad bactericida que la RNasa 3. Entonces, diseñamos dos nuevas versiones de la RNasa 3/1 que incorporaban el loop C-terminal de la RNasa 3, en el que se identificó un motivo estructural específico asociado al reclutamiento del autofagosoma. Es interesante destacar la capacidad de la primera versión de la quimera RNasa 3/1 de retrasar la adquisición de resistencia a la colistina en un ensayo evolutivo *in vitro* de exposición a la colistina en cultivos de *Acinetobacter baumannii*.

En global, estos resultados ayudarán a elucidar el modo de unión al RNA de las ribonucleasas y su mecanismo antimicrobiano, así como su contribución en el sistema inmunitario innato, con prometedoras aplicaciones farmacológicas.

[ENGLISH]

This thesis project focuses on the structural–functional characterization of the biological properties of antimicrobial RNases from the RNase A superfamily. Specifically, the following short-term goals have been achieved:

Structural and functional characterization of RNase 6 by X-ray crystallography, molecular dynamics, site-directed mutagenesis and enzymatic analysis have highlighted the key role of remote binding subsites. Besides, we have identified in RNase 6 a putative novel secondary active site. In addition, an evolutionary study of several members of the RNase A superfamily have revealed a clear drift from guanine to adenine preference at the secondary base binding site (B_2) architecture along vertebrate evolution.

During this thesis' experimental work, we have pursued the characterization of RNases' bactericidal mechanism of action, a long-term object of study in our research group. Here, we have specifically focused on the optimisation of the antimicrobial peptide derived from RNase 3, ECP(5–17P24–36), and the design of a chimeric antimicrobial RNase (RNase 3/1).

Regarding the N-terminus peptide ECP(5–17P24–36), it has been optimised by several methodologies. We have concluded the best antimicrobial candidate to be its total enantiomer, D-ECP(5–17P24–36). As for RNase 3/1, this chimera encompasses structural features from RNases 1 and 3 parental proteins to combine both high catalytic and bactericidal activities. A first construct was successfully achieved, albeit not reaching the bactericidal activity levels of RNase 3. Therefore, we designed two more versions of RNase 3/1 that incorporate the RNase 3 C-terminus loop. A specific tag motif was identified in that region associated to autophagosome recruitment. Interestingly, the hybrid chimera RNase 3/1 was able to delay the acquisition of bacterial resistance to colistin using an *in vitro* evolutionary exposure assay in *Acinetobacter baumannii* cultures.

Overall, the results shed light on the elucidation of substrate binding architecture and antimicrobial mechanism of action of RNases and their contribution to the innate immune system, with promising pharmacological applications.

1. INTRODUCTION

1.1. The ribonuclease A superfamily

The ribonuclease A superfamily is a vertebrate-specific family of proteins homologous to the bovine pancreatic ribonuclease (RNase A). RNase A is a pyrimidine-specific endonuclease that catalyses the breakdown of single-stranded RNA by cleaving 3',5'-phosphodiester bonds. RNase A was a reference protein in the pioneer biochemistry studies in the 70s, being the first enzyme whose catalytic mechanism was determined before the solving of its 3D-structure. The proteins of this family share several key features. At the structural level, all of them have a high isoelectric point (between 9 and 11), a kidney-shaped structure maintained by three to four disulphide bridges and a common "catalytic triad", formed by two histidines and one lysine at the active site, which cleaves RNA by an acid-base catalysis[1].

In addition to its catalytic function, evolutionary studies suggest that the RNase A family started off as host-defence proteins[2–4]. Antimicrobial and immune-regulatory properties were reported for several family members and their presence in a variety of biological fluids is associated to a protective physiological role[5–10].

1.1.1. The catalytic mechanism

RNases catalyse single-stranded RNA substrates by a two-step acid-base mechanism of transphosphorylation and hydrolysis, which involves two histidines and one lysine[1], as depicted in Figure 1.

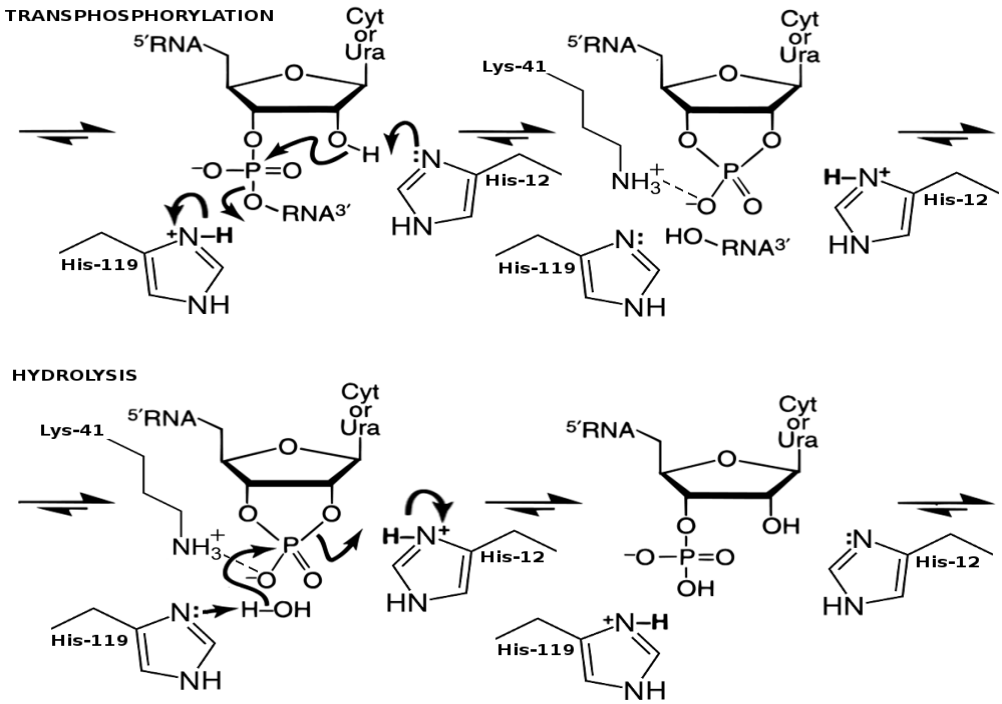

Figure 1. RNA cleavage mechanism of the ribonuclease A superfamily proteins, taking RNase A as a reference. It is an acid-base reaction which involves two histidines and one lysine, consisting of two stages. In the transphosphorylation step, one of the histidines (His12 in RNase A), acting as a base, captures a proton of the ribose hydroxyl, inducing the breakage of the phosphodiester bond and the formation of a 2'3' cyclic phosphodiester bond. This cyclic intermediary is stabilized by the lysine residue. In the hydrolysis step, the other histidine (His119 in RNase A), acting as a base, induces the cleavage of the cyclic phosphodiester bond, returning the enzyme to the initial state. Taken and modified from *Fisher et al. 1998*[11].

The histidines participate in the cleavage of the P-O5' bond of an RNA strand on the 3' side of a pyrimidine residue, while the lysine stabilizes the reaction intermediate[12]. The substrate binds to the enzyme through a multi-subsite structure, where the base at the 3' side of the cleaved bond must be a pyrimidine, while the 5' base can be either a pyrimidine or a purine, even though the latter is preferred[13–16]. These binding sites force the RNA chain to adopt a stretched conformation while the reaction is occurring, facilitating the access of the phosphodiester bond to the active site. The identified subsites are involved in the recognition of base, ribose and phosphate moieties and are globally designated as B_0-B_n, R_o-R_n and p_0-p_n respectively (Figure 2). Non-catalytic phosphate-binding subsites involved in the formation of the enzyme-substrate complex have been characterized by chemical modification, site-directed mutagenesis, molecular modelling, NMR and X-ray crystallography[13,15,17]. Among the main non-catalytic binding sites, we find B_1, which in RNase A is formed by Thr45, Phe120 and Ser123, and B_2, formed by Gln69, Asn71 and Glu111. While B_1, the main base binding site, is pyrimidine-specific, the secondary site B_2 allows the binding of both purines and pyrimidines, although with a clear preference for the former.

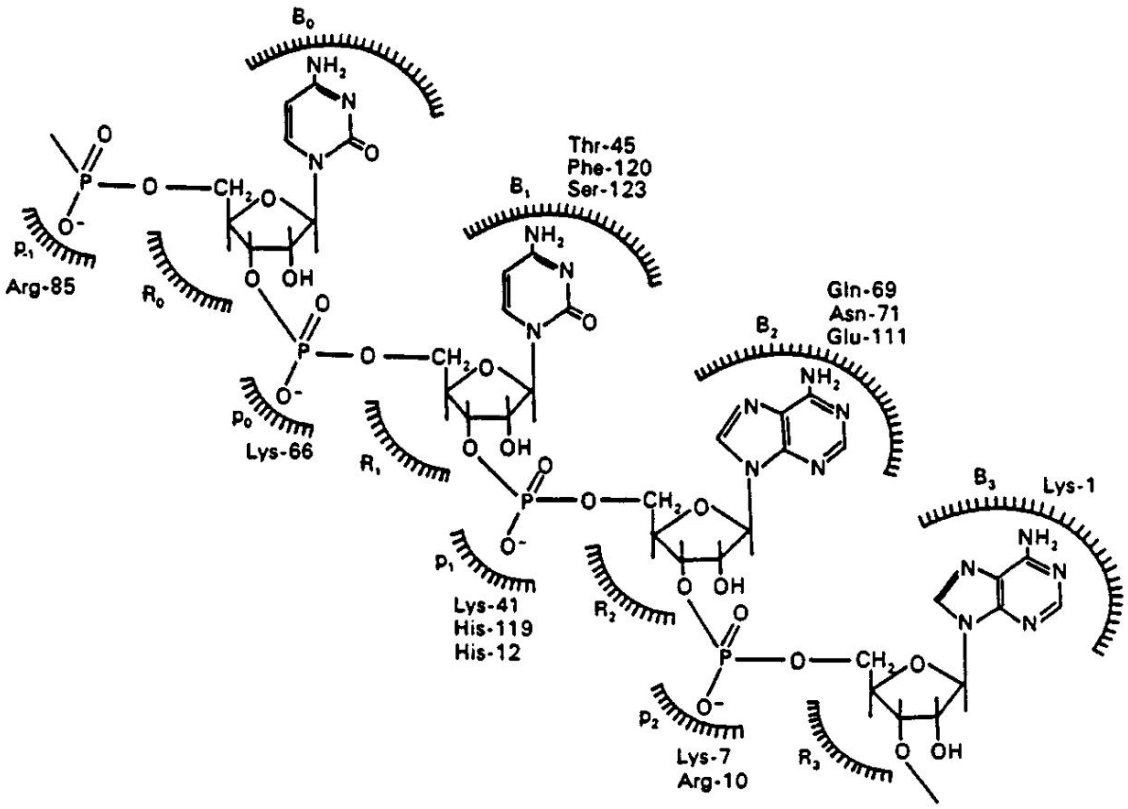

Figure 2. Schematic representation of the active site of RNase A and the adjacent non-catalytic binding sites of phosphate, base and ribose. B_1 is pyrimidine-specific, while B_2 preferentially binds to purines. The phosphate group of the phosphodiester bond which is hydrolysed during the catalysis is the one which is bound to p_1. When known, the residues of each binding site are indicated. Taken and modified from *Parés et al. 1991*[13].

The solved crystal structures of RNase A–nucleotide complexes reported an extended protein binding groove that facilitates RNA interaction[18–20]. In particular, subsite p_2, conformed by residues Lys7 and Arg10[21,22], is described as the main non-catalytic phosphate-binding site[13,14] interacting with the adjacent nucleotide located at the 3' side of subsite p_1. Electrostatic interactions between cationic residues and RNA phosphate groups contribute to enzyme-substrate anchoring and favour an endonuclease activity[15]. On the contrary, a reduction in the number of secondary substrate binding sites is associated to a lower catalytic efficiency in some RNases, such as RNase 3/eosinophil cationic protein (ECP) or RNase 5/angiogenin[23,24]**.** Moreover, a

distinct distribution of phosphate interacting sites in RNase 3, showing a weaker substrate binding at p_2 and an enhanced strength at p_0/p_{-1}, determines a shift towards an exonucleolytic cleavage pattern of RNA[24]. The key contribution of the phosphate secondary sites was also confirmed by site directed mutagenesis in RNase A, where the removal of p_0 and p_2 site determined a shift from endo- to exoribonucleolytic activity[14,25,26].

It is interesting to note that a high evolutionary conservation is observed for the B_1 subsite, whereas a significant variability was visualized for the secondary base selectivity. Interestingly, the observed structural differences at the secondary base site correlate with their substrate specificity and catalytic efficiency[16,27,28]. Likewise, the analysis of the protein conformational changes induced upon nucleotide binding by NMR and molecular dynamics highlighted an evolutionary trend in base interaction selectivity[29–31]. Conserved conformational rearrangements upon ligand binding within closely related members suggested a link between shared protein networks and their characteristic biological properties[31]. A better understanding of the structural determinants that govern the RNases' substrate specificity can help us to explain the divergent functionalities within the family.

1.1.2. The human canonical ribonucleases and their host defence role

The RNase A superfamily includes a series of proteins with antimicrobial and immune-modulatory activities and is considered to have emerged with an ancestral host-defence role[3,10,32]. In humans, there are 13 members of the RNase A superfamily, of which RNases 1–8 are known as the canonical ribonucleases, according to their structural, enzymatic and biological properties[8,33] (Figure 3). Regarding RNases 9–13, although they have a high percentage of identity, they do not present the catalytic triad, common in the rest of the family, and their function is still unknown[34,35].

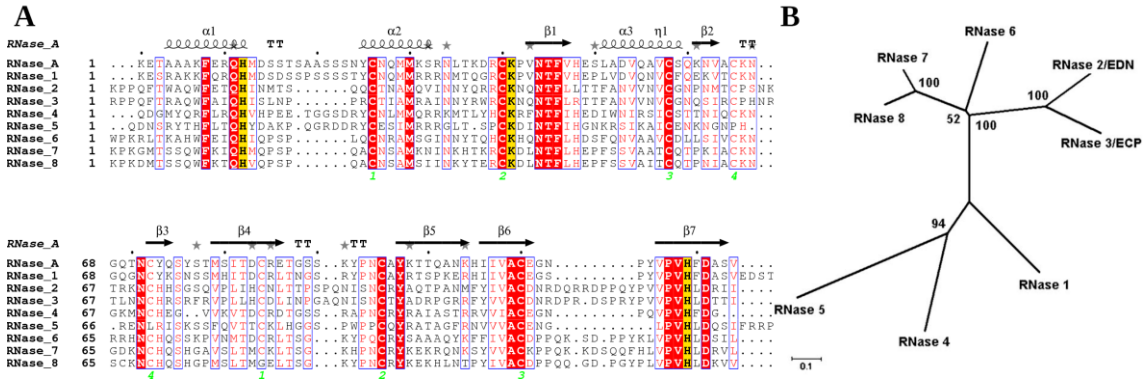

Figure 3. **A)** Sequence alignment of the eight human canonical RNases. The conserved residues are highlighted in red. The non-conserved residues which share similar properties are labelled with red letters. The catalytic triad is highlighted in yellow. The secondary structure is indicated at the top of the alignment. The green numbers represent the disulphide bridges. The alignment has been done with the *Clustal Omega*[36] server, and the figure has been obtained by the *ESPript*[37] server (http://espript.ibcp.fr/ESPript/). **B)** Unrooted phylogenetic tree of the eight human canonical ribonucleases. As shown, RNases 2, 3, 6, 7, and 8 are closely related to one another, forming a separate group from RNase 1, RNase 4 and RNase 5. Taken from *Sorrentino 2010*[8].

Within the canonical RNases, we can differentiate three main phylogenetic lineages (RNase 5, RNases 2/3 and RNases 6–8) related to host defence[2,3,32,38]. In the next sections, the main characteristic features of the canonical RNases will be detailed.

1.1.2.1. RNase 1

Despite its naming, the pancreatic ribonuclease is expressed in a broad range of tissues. In humans there is only one gene copy, in contrast to herbivores, who have several variants. RNase 1 has an optimal pH of 8.0 and is one of the most catalytically active RNases. It is thought to act as an extracellular RNA scavenger, and it could be involved in the nonspecific response to pathogenic RNA molecules[39]. Its interaction with the human ribonuclease inhibitor (Figure 4) is the strongest in the family, the complex having been solved by X-ray crystallography[40–42].

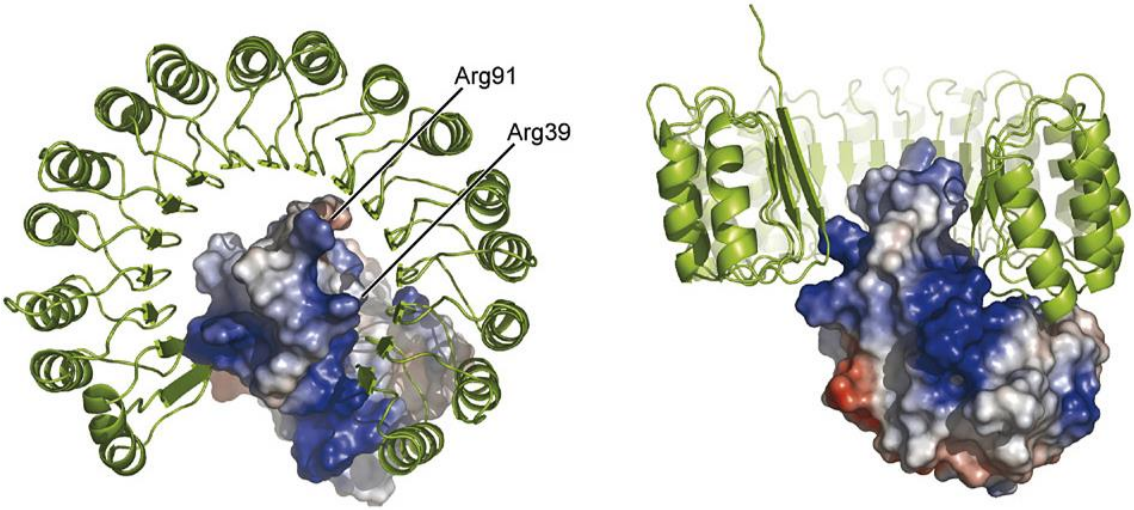

Figure 4. Representation of the interaction between the human ribonuclease inhibitor, hRI (green ribbon) and RNase 1 (electrostatic molecular surface). RNase 1 arginines 39 and 91 are labelled as main responsible for the interaction with the hRI. The intensity of the blue (positive) and red (negative) coloration is indicative of the local electrostatic environment. Images were created by *PyMOL*. Taken and modified from *Johnson et al. 2007*[40].

1.1.2.2. RNases 2 and 3: The eosinophil ribonucleases

The eosinophil ribonucleases, RNase 2 (eosinophil-derived neurotoxin, EDN) and RNase 3 (eosinophil cationic protein, ECP), have been the object of numerous studies[38,43–45] in relation with their antipathogenic activity. They are secretory ribonucleases stored in the secondary granules of eosinophils and released at the focus of infection[46,47]. RNase 2 and 3 genes have diverged after gene duplication, rapidly accumulating non-silent mutations through positive selection pressure[48,49]. RNase 2 acts as a potent modulator of the immune host system, and additionally displays a high antiviral activity against rhinovirus, adenovirus and syncytial respiratory virus in an RNase catalytic activity-dependent manner[50–52]. RNase 3 possesses a highly antimicrobial activity against bacteria[44,46,53–55], and many parasites, such as helminths and protozoa[56]. By contrast, the antimicrobial properties of RNase 3 are not dependent on the ribonuclease activity of the protein[53,57].

Recently, our group has reported that RNase 3, in a macrophage intracellular infection model, is able to modulate the immune response via the epidermal growth factor receptor (EGFR) pathway[58]. Comparative transcriptome profile analysis of macrophages revealed that the protein induces an early pro-inflammatory response in a ribonuclease-independent manner. This pro-inflammatory response would be triggered by a direct activation of the EGF receptor. This was confirmed by observing the inhibition of this response when blocking the EGFR pathway with cetuximab (a monoclonal antibody specific against EGFR) before cell treatment with RNase 3. In addition, the specific blockage of EGFR by Erlotinib indicates that the receptor-associated pathways participate in the protein antibacterial but not antiviral actions. Last, we demonstrated

that endogenous overexpression of RNase 3 in macrophages can inhibit *Mycobacterium aurum* and respiratory syncytial virus (RSV) intracellular proliferation.

1.1.2.3. RNase 4

RNase 4 is the most ancestral among the human RNases. Its sequence is the shortest in length of the human canonical RNases (119 residues) and its sequence identity is about 90% with bovine, porcine and rat RNases. RNase 4 has a strong preference for uridine thanks to its unique active-site pocket, which is conserved in other RNase 4 orthologues, suggesting a strong evolutionary pressure to maintain some specialized biological function[59,60].

1.1.2.4. RNase 5

Commonly known as angiogenin, RNase 5 is a strong inducer of new blood vessel formation[61]. The ribonuclease activity of RNase 5, although weak, is essential for its angiogenic activity[62] and presents a very unusual pattern in comparison to the other canonical RNases, caused by the blockage of the pyrimidine binding site by Gln117. Nevertheless, it has been recently reported that RNase 5 is able to cleave some tRNAs in a specific manner and with high efficiency[63]. Another aspect of interest of RNase 5 is its ability to interact directly with the EGFR and activate its regulatory pathway[64].

1.1.2.5. RNase 6

Since a whole chapter of this thesis is dedicated to the study of RNase 6, we include here more detail on the background of prior research in the field.

The role of the eosinophil ribonucleases in the immune response has been widely studied, as commented above[52,65–67]. However, there are almost no studies of other RNases abundantly expressed in other leukocytes, such as monocytes and neutrophils, like RNase 6. The RNase 6 gene was first identified as a genomic segment and localized in the q11 region of the chromosome 14[68] during the search for a human protein homologous to the RNase k2 (bovine kidney RNase)[69]. Due to its presence in a large variety of tissues and its expression in monocytes and neutrophils, it was proposed that it could play a role in host defence, like other RNases of the family[68].

Recently, more studies have added some light on this hypothesis. Several homologs of this protein are found in mammalian species. As shown in Table 1 and Figure 5, RNase 6 experimented a fast evolutive divergence, probably due to selective evolution pressure (highly remarkable in the early separation between primates and rodents) typical of genes involved in host defence[70].

	Rat	Horse	Cow	Macaque	Human
Mouse	82	66	65	69	68
Rat	—	65	65	65	65
Horse	—	—	75	77	75
Cow	—	—	—	71	73
Macaque	—	—	—	—	94

Table 1. Percentage identity between predicted mature peptide sequences of RNase 6 genes. The sequences used (GenBank codes) for the table are the following: macaque (CB554177), horse (CD536566), cow (AF164025), mouse (NT_039599), rat (NW_047453) and human (U64998). Taken from *Dyer et al. 2004*[70].

Interestingly, even though it has been found that eosinophil RNase 2 and RNase 3 gene lineages have undergone one of the highest rates of divergent evolution to produce paralogous genes[71,72], RNase 6 primate gene lineages appear to have evolved in a more conservative way[69]. On the other hand, the opposite situation has been reported in rodents, in which the evolution of RNase 6 happened at a substantially higher speed[70]. All in all, a similar tendency towards an isoelectric point increase is shared within the eosinophil lineage.

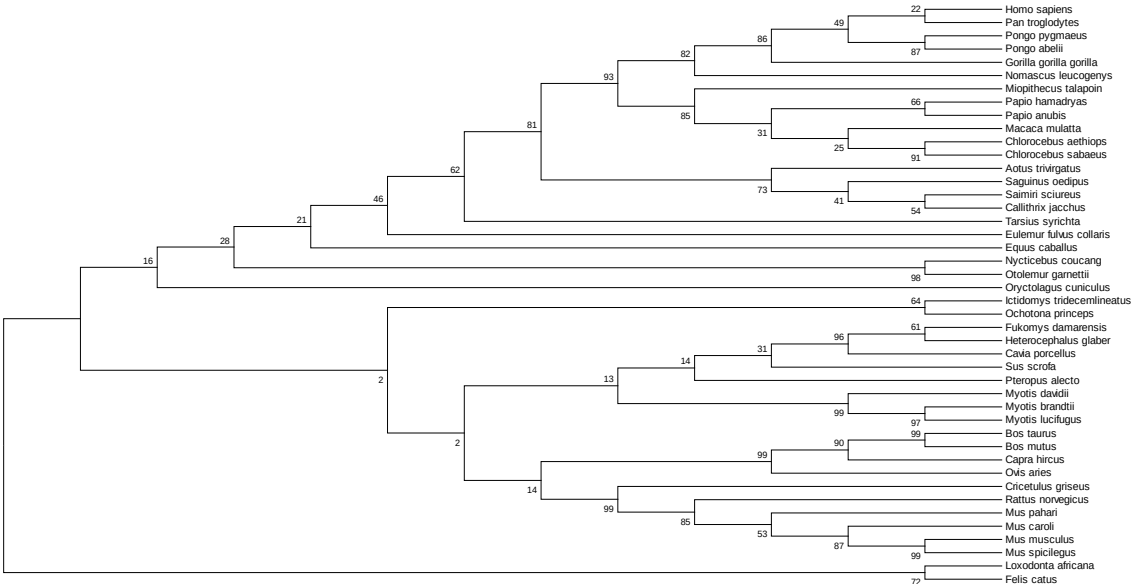

Figure 5. Phylogenetic tree of RNase 6 homologs in several mammal species. The evolutive history has been deduced by the neighbour-joining method[73]. At the end of each branch of the tree is shown the percentage of replicated trees in which the associate taxa have been grouped together by the bootstrap test (5000 replicates)[74]. The evolutive distances have been computed using the Poisson correction method[75] and are represented as the number of amino acid replacements by position. After gap removal, 126 positions have been analysed. The evolutive analysis has been done by MEGA6[76].

Recent studies have added more weight to the hypothesis that RNase 6 may have a host defence function. As it is largely known, human immunodeficiency virus (HIV) suppresses the immune system of the host, reducing dramatically the ability of the patient to respond against pathogens that do not normally surpass the innate defence system. Recently, it has been discovered that the envelope glycoprotein gp120 plays a key role in this inactivation of the immune system. In B cells, gp120 binds with integrin $\alpha_4\beta_7$, inducing a modified pattern of gene expression[77]. One of the downregulated genes by the HIV envelope protein is RNase 6, supporting the hypothesis of its involvement in innate defence.

Another study which supports its putative role *in vivo* is the discovery that macrophages express RNase 6 (as well as RNase 7) in the urinary tract in response to pathogen exposure[66]. This specific response, together with its elevated antibacterial activity against both gram-positive and gram-negative bacteria[78], confirms RNase 6 as another antimicrobial RNase.

By inspection of the alignment of canonical RNases (Figure 3), we can observe that RNase 6 has some particularities that set it apart from other members of this family. All canonical RNases have a cationic or polar residue at the N-terminal position. However, RNase 6 presents a tryptophan residue at this position. This tryptophan is only present in primates; still, all vertebrate homologues have a hydrophobic residue at this position, except for rodents (which have a glutamine). Studies performed in our group[78] have shown that the substitution of Trp1 for alanine completely suppresses the bacterial agglutination activity of RNase 6, considerably reducing the

antimicrobial activity (twofold lower than the wild type protein against both gram-negative and gram-positive strains). The importance of Trp1 in bacterial agglutination is probably due to its large size and hydrophobicity, as well as its exposed position in the structure of RNase 6. Its ability to interact with the membrane of liposomes suggests that this tryptophan could insert partially in the bacterial membrane, similarly to the proposed mechanism for Trp35 of ECP[79].

As it was reported in RNase 3[44], Ile13 also plays a key role in bacterial cell agglutination and antimicrobial activity in RNase 6. The replacement of Ile13 to alanine suppresses completely the agglutination activity and reduces dramatically the antimicrobial activity (~4-fold lower than the wild type protein against gram-negative and gram-positive strains). So, as it was reported in RNase 3, bacterial agglutination appears to be important for the antimicrobial activity of RNase 6.

However, this is probably not the only mechanism of bactericidal activity of RNase 6, because although the antimicrobial activity decreases considerably in both W1A and I13A mutants, the suppression of the agglutination activity cannot completely abolish the antimicrobial activity. One possible explanation of this is the putative role of the α1 helix (where Ile13 and Trp1 are located), which may insert into the bacterial membrane. The suppression of a large hydrophobic patch could hinder the insertion of the helix into the membrane, and would prevent the protein membrane disruption and bactericidal activity.

Another region unique in RNase 6 is the His36/His39 region. This pair of histidines, located in an exposed loop, can only be found in RNase 6 and its primate orthologs. Our recent determination of the 3D structure of RNase 6 by X-ray crystallography in presence of sulphate[80], has revealed that both histidines, along with Lys87, are placed in a way that is analogous to the classic catalytic triad. These residues could act as a secondary active site, with a remarkable preference against polynucleotide substrates, according to the kinetic data[80]. To our knowledge, RNase 6 is the only protein in the family where such a feature has been discovered.

1.1.2.6. RNase 7

RNase 7 is another RNase secreted by a variety of epithelial tissues[81] and displaying a high antimicrobial activity against a wide range of bacteria, regarded as a major contributor to the skin barrier protection[65,82–84]. In contrast to RNases expressed by blood cell types, such as eosinophils, monocytes or neutrophils, i.e. RNases 2,3 and 6, RNase 7 is mainly associated to epithelial cells. Recently, it has been reported that RNase 7 also plays an important role in bacterial clearance in the urinary tract[66].

1.1.2.7. RNase 8

RNase 8 is the most unknown protein of the canonical ribonucleases. Although it has most of the structural features of pancreatic ribonucleases, its uncommon distribution of cysteines makes it particularly interesting. In RNase 8, Cys84 (with RNase 1 numbering), conserved among all other RNases, has changed to glycine, while a new cysteine residue has appeared at position 69 (RNase 1 numbering). Several hypotheses of the different disulphide bond arrangement of RNase 8 have been proposed[85,86] but no 3D structure is available yet. Moreover, contradictory results about its antimicrobial activity have been reported[85,87].

1.1.3. General antimicrobial mechanism of action

Together with their catalytic activity, numerous properties have been described for the RNase A family, mainly related with the innate immune system. These properties are mainly linked with their high antipathogen activity[3,32,88] and the ability of some RNases to activate the immune response through the Toll-like receptors (TLR)[45,89]. For example, human RNase 2 displays both high antiviral activity and a potent immunomodulatory action, however, it does not present any bactericidal activity.

Among the canonical RNases, only the RNases 3, 6 and 7 have been reported to display a significant bactericidal activity. Interestingly, several studies[53,57,79] indicate that the bactericidal activity of RNases is not directly related to their catalytic activity, but is mainly due to their capacity to trigger the breakage of the bacterial cell wall. This bactericidal activity, retained in the N-terminal side of the protein[90–92], is similar to the mechanism that others antimicrobial proteins and peptides (AMPs) present. They share a marked cationicity that facilitates the electrostatic interaction with the negatively charged bacterial surfaces. In addition, they show an abundance of hydrophobic residues, and the presence of dynamic amphipathic modules that can adopt secondary structures upon interaction with the bacterial envelopes[32,93]. A depiction of this general mechanism of action is shown in figure 6.

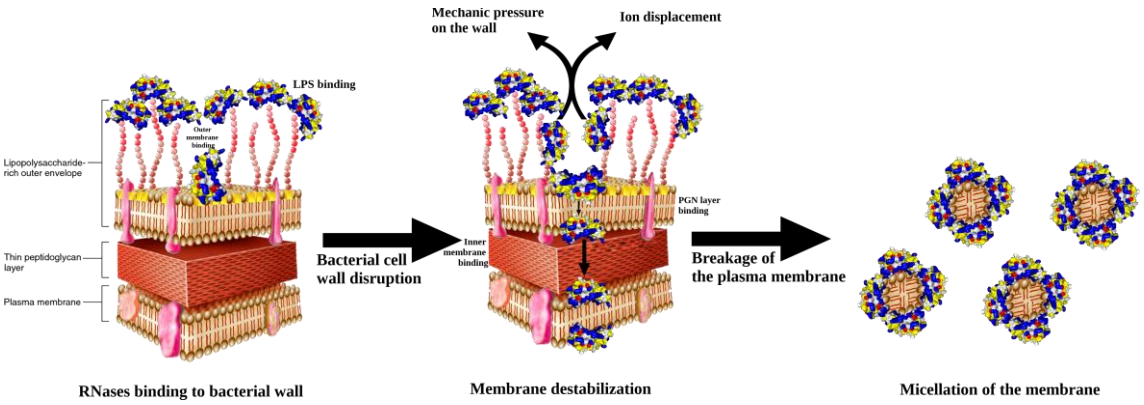

Figure 6. Membrane disruption of gram-negative bacteria by the action of RNases, from binding to the cell wall to breakage of the membrane. The RNases are represented with molecular surface view; in blue, the cationic residues, in red, anionic residues, in yellow, hydrophobic residues. In gram-positive strains the process is similar, with the difference that RNases do not need to break the outside membrane, and, instead of interacting with lipopolysaccharides (LPS), they will bind to teichoic acids (TA) and then, to the peptidoglycan (PGN) layer, until they reach the plasmatic membrane.

Although the exact mechanism of the attack on the bacterial wall remains unclear, it has been proposed[32,79,94] that the RNases bound to lipopolysaccharides (LPS) or teichoic acids (TA) by the cationic regions could form aggregates by interacting with other protein monomers by their hydrophobic regions. These large aggregates, bound to the bacterial wall, would inflict mechanic pressure on the membrane, causing the cell to burst. This bacterial agglutination would help the immune system cells to clear the infection focus. It has been observed that bacterial agglutination is mainly caused by a hydrophobic region of the N-terminus of the protein, in which Ile13 (numbered after RNase 3) would play a key role[44]. Moreover, in gram-negative strains, the competitive displacement of the cations which stabilize the LPS also contributes to this antibacterial activity[32].

1.2. Bacterial resistance mechanisms against antimicrobial agents

Thanks to their genetic plasticity, bacteria have an extraordinary ability to adapt to antimicrobial agents/antibiotic exposure. These resistance mechanisms could be classified into two major strategies: mutational resistance, where the genes related to the antibiotic mechanism of action are mutated, and horizontal gene transfer, where the bacteria acquire foreign DNA coding for the resistance determinant[95].

The mutations in the bacterial genome which result in antimicrobial resistance usually alter the antibiotic action through one of the following mechanisms: modifications of either the antimicrobial agent or the target, a decrease in the drug uptake, the activation of efflux mechanisms and global changes in important metabolic pathways via modulation of regulatory networks.

If we analyse antibiotic resistance from a mechanistic point of view, we can identify four main mechanisms of resistance, which are described below[95].

1.2.1. Modifications of the antimicrobial molecule

The production of enzymes that inactivate the antibiotic, by modifying or even destroying it, is an efficient strategy to acquire bacterial resistance.

1.2.1.1. Chemical alterations of the antibiotic

The expression of enzymes able to introduce changes to the chemical structure of the antibiotic is a resistance mechanism found in both gram-negative and gram-positive bacteria. Most of the antibiotics affected by these modifications act at the ribosome level, inhibiting protein synthesis[96]. The effect of these modifications on the antibiotic is a steric interference in the interaction between the antibiotic and its target. The most frequent biochemical reactions catalysed by these enzymes are acetylation, phosphorylation and adenylation[97].

1.2.1.2. Destruction of the antibiotic molecule

This mechanism is basically found in the case of the β-lactam family. β-lactamase is an enzyme with the ability to cleave the amide bond of the β-lactam ring, triggering the inactivation of the antibiotic molecule. Widely used since the discovery of penicillin, β-lactam antibiotics are nowadays the most popular antibiotic. However, β-lactamases did not appear upon the discovery of penicillin, but instead they are ancient proteins[98,99]. To overcome the penicillin-resistant infections, new β-lactam compounds were designed. From then on, the development of newer generations of β-lactams has systematically been followed by the rapid appearance of enzymes able to destroy the newest compound that reaches the market, being a clear example of antibiotic-driven adaptive bacterial evolution.

1.2.2. Prevention of the compound reaching the antibiotic target

Another common strategy for bacteria to resist antibiotic attack is to protect the bacterial target from the antibiotic compound, by hindering the antibiotic's access to it.

1.2.2.1. Decreasing cell penetration

Since most of the antibiotics used target intracellular components (or the inner membrane in case of gram-negative bacteria), decreasing the penetration capacity of the molecule is an efficient

mechanism to evade an antibiotic attack. The relative hydrophobicity of the molecule is one of the main determinants of its ability to penetrate the bacterial cell wall, mainly through porins, which allow the passage of hydrophilic molecules of varying charge and size[100].

For this reason, alteration of porins is another mechanism of bacterial resistance. Porin-mediated resistance can be achieved by the shift of the type of porins expressed, a change in the level of porin expression and an impairment of the porin function. However, these mechanisms are not able by themselves to confer high-level resistance, and they are usually associated with other mechanisms of resistance, like the increase of the expression of the efflux pumps[101], described below.

1.2.2.2. Efflux pumps

The development of complex bacterial machineries capable of extruding a toxic compound out of the cell can also result in antibiotic resistance. Several classes of efflux pumps have been characterized in both gram-negative and gram-positive strains. Efflux pumps can be substrate-specific or have a broad substrate range, the latter being the usual case in multidrug resistant (MDR) bacteria[102]. The families of efflux pumps differ in terms of structural conformation, energy source, range of substrates they are able to extrude and the type of bacterial organism in which they are distributed[103]. These families are the following; the major facilitator superfamily (MFS), the small multidrug resistance family (SMR), the resistance-nodulation-cell-division family (RND), the ATP-binding cassette family (ABC) and the multidrug and toxic compound extrusion family (MATE)[95,104].

1.2.3. Changes or bypasses of the target sites

Another common strategy to develop antimicrobial resistance is to hinder the antibiotic action through direct interference with its target site. Two main different tactics have been developed by bacteria to achieve this interference: direct protection of the target and modifications of the target site in order to decrease the affinity of the antibiotic molecule.

1.2.3.1. Direct protection of the target

This mechanism of resistance normally involves the expression of a protein that directly competes with the antibiotic for the target site, blocking it[96]. Another way to protect the target is via the indirect interaction of a protein with a remote region of the targeted molecule, which triggers a modification of the binding site, hindering the union of the antibiotic to its target[105].

1.2.3.2. Modification of the target site

The modification of the antibiotic target site is one of the most common mechanisms of antibiotic resistance, which affects almost all the families of antimicrobial compounds. The target changes could consist of point mutations in the genes that encode the target site, enzymatic alterations of the binding site, and/or replacement or bypass of the original target site.

1.2.4. Resistance due to global cell-adaptive processes

Sometimes, the resistance mechanism is not based on specific changes in the metabolism or mutations on the target site, but it is due to a more global phenotypic adaptation. Thanks to millions of years of evolution, bacteria have developed several complex mechanisms to deal with the challenges of a hostile environment. These mechanisms could trigger resistance to an

antibiotic molecule, not as a specific change, but instead as a large-scale adaptation of several metabolic pathways.

1.3. Antimicrobial peptides

1.3.1. General overview

Antimicrobial peptides (AMPs) are small peptides which are effective against a broad spectrum of pathogens: bacteria, viruses, helminths and/or fungi[106,107]. Their wide range of targets and the difficulty to generate resistance[108,109] because of their unspecific action mechanism have made them an object of study as putative new antibiotics. With an average size between 12 to 60 residues, we can divide them in four classes[110]:

- ✓ **Anionic peptides**: Mainly present in the airway epithelia. They require zinc as a cofactor and display activity against both gram-positive and gram-negative bacteria. Dermcidin[111] and maximin H5[112] are examples of these AMPs.
- ✓ **Linear cationic α-helical peptides**, such as magainin and cecropins. These peptides are disordered in solution, but they adopt an α-helical secondary structure once they interact with membranes[113] .
- ✓ **Cationic peptides enriched by specific amino acids** like proline, arginine, and other residues. These peptides are usually linear[114] .
- ✓ **Peptide fragments** originated from larger proteins after their digestion. They are similar in shape and size to other AMPs, and frequently adopt β-turn structures. Lactoferrin and cathelicidins are examples of this class[115].
- ✓ **Charged peptides with a 6-cysteine residue motif**, forming intramolecular disulphide bonds, β-sheets and α-helixes[116]. This is a large and diverse group of small proteins known as defensins, which are present into plants, arthropods and higher animals (birds, reptiles and mammals). It is hypothesised they originated in prokaryotes[117].

1.3.2. Antibacterial action mechanism

The mode of action of antimicrobial peptides is not the same than that of conventional antibiotics. Although some of them penetrate the cell and act against some intracellular targets[114,118], most of the AMPs, with exception of anionic peptides, which are still poorly understood [119]), interact with the negatively-charged bacterial cell wall through electrostatic forces[120], as depicted in Figure 7.

Cationic antimicrobial peptides are amphiphilic molecules, comprising both hydrophobic and hydrophilic residues, aligned on opposite faces, to facilitate their penetration through cell membranes. As a general mechanism, the positive face allows the peptide to bind the bacterial membranes, while the hydrophobic domain penetrates through the phospholipid bilayers[121], triggering bacterial death[122]; however, not all the peptides destabilize and break the membranes in the same manner.

The most studied mechanisms of membrane destabilization are the pore formation and the carpet-like mechanisms. There are three models to explain the pore formation. In the barrel-stave model, the hydrophobic residues of the peptide insert themselves into the membrane, interacting with the acyl chains of the membrane lipids with the charged residues covering the pore. In the toroidal model, the peptides trigger the curvature of the lipid bilayer, with the polar heads of the phospholipids covering the inner part of the pore together with the peptides[124]. In the disordered toroidal model, the bilayer curves in a similar way to form the pore, but the peptides do not cover

the inner part, but one peptide molecule is placed in the inner part, keeping the pore opened, while two other peptide molecules are located near the external face of the membrane.

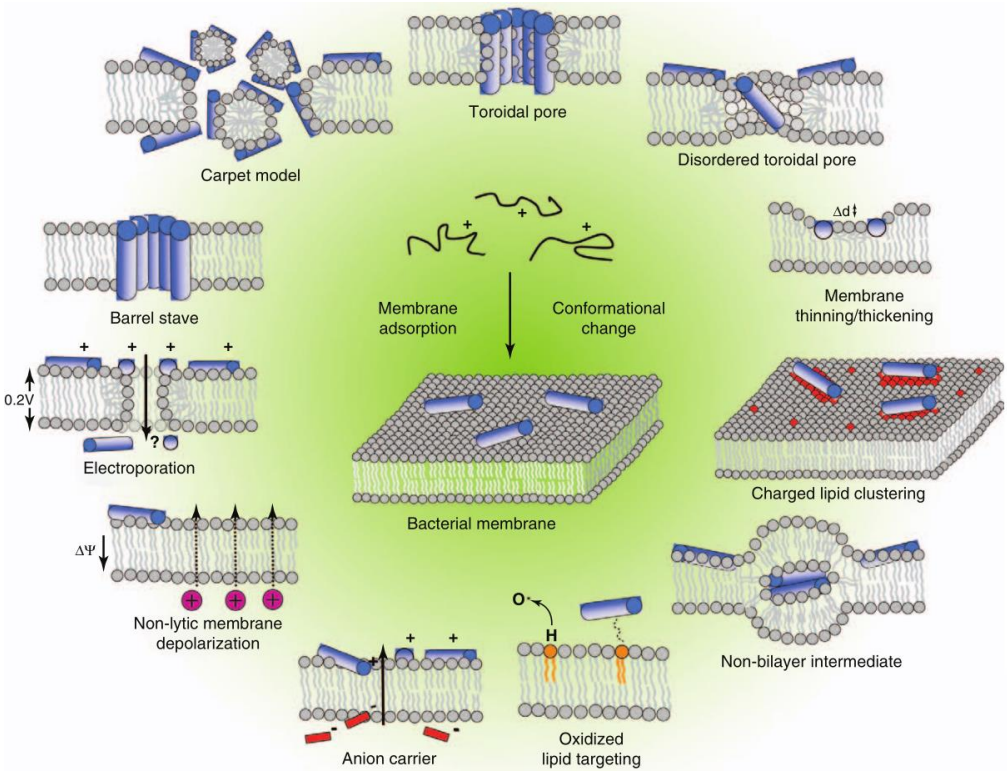

Figure 7. Schematic representation of the action mechanisms of membrane-active AMPs. Taken from *Nguyen et al. 2011*[123].

In the carpet-like mechanism, peptides cover the membrane surface through electrostatic interactions, until they reach a certain point when important changes on the membrane curvature are induced, breaking it and forming micelles[114]. As shown in Figure 7, there are other non-lytic mechanisms involving a membrane alteration (anionic lipid clustering, membrane thinning, intracellular anion expulsion, etc), which finally trigger a depolarization of the membrane or a slower leakage of the cell content[123,125].

1.3.3. Bacterial mechanisms of resistance to antimicrobial peptides

Over time, bacteria have developed several mechanisms to resist the action of the AMPs. These mechanisms can be classified as follows[122]:

- ✓ **Constitutive resistance**
  - **Electrostatic shielding**[126]: Both the anionic charges of the outer part of the cell wall and the cationic charge of the peptide are shielded by ions usually abundant in the extracellular medium, reducing the formation of electrostatic interactions and hindering peptide binding to bacterial structures. Due to this, some AMPs are unable to act at physiological salt conditions. This shielding can also be achieved by overexpression of charged proteins at the cell wall.
  - **Changes in membrane potential during different stages of cell growth**[127–129]: The membrane potential of the bacterial cell is reported to change while the bacterial cell grows, being lower during the lag and the stationary phases (~50 mV) than in the exponential phase (~150 mV)[128]. These differences in the

membrane potential affect the affinity of the peptide for the cell wall components, preventing its activity to a different degree according to each cell growth stage.

- **Biofilm formation**[130–132]: Although AMPs have been characterized as potential tools against biofilms, there are several limitations to their action, besides the common mechanisms of bacterial resistance against AMPs[131]. Biofilms are formed by a bacterial community and an extracellular matrix of exopolysaccharides (negatively charged), among other exopolymers (positively charged)[131,132]. Because of this, the extracellular matrix of the biofilm can work by both sequestration and electrostatic repulsion of the AMPs. By combining the two mechanisms biofilms are protected against both positively and negatively charged peptides[130].

✓ **Inducible resistance**

- **Substitution**[133]: A target site bypass strategy. The cell-wall compound targeted by the AMP is replaced by another compound to avoid the interaction with the peptide. An example is the replacement of the lipid A by analogous compounds[133]. Extreme cases can result not only in the replacement, but the total loss of the targeted molecule, as observed in *Acinetobacter baumannii*, which, as a mechanism of resistance, can lose all the LPS of the cell wall[134].
- **Modification**[135–139]: A target site protection strategy. Some parts of the targeted component are modified (lipid A phosphates to aminoarabinose and ethanolamine groups is one of the best studied example), in order to decrease the antimicrobial peptide affinity to it. Modifications can not only take place at the membrane components. In case the AMP mechanism targets an intracellular component, it can also be modified, like it is reported for the *E. coli* DNA gyrase in response to microcin B17[140].
- **Acylation**[141]: Another target site protection strategy, basically observed in the LPS. The molecule is acylated to avoid, by steric hindering, the interaction with the AMP.
- **Activation of proteolytic enzymes**[142]: A strategy that aims for the destruction of the antibiotic molecule and probably the most typical and specific mechanism against AMPs. Outer membrane, extracellular and even cytoplasmic bacterial proteases degrade the AMP, inactivating it.
- **Efflux pumps**[143]: As with other antibiotics, efflux pump dependant mechanisms have shown to be an efficient mechanism to resist the AMPs that target an intracellular component.

Some of these resistance mechanisms are illustrated in Figure 8. Although bacteria have diverse mechanisms of resistance to AMPs, most AMPs take advantage of the structure and composition of the cell envelope and membrane, common to most bacteria, rather than focusing on specific and replaceable cell components, making it hard to the bacteria to develop a complete resistance against AMPs. Also, the resistance against AMPs reported to date is not as strong as that observed against conventional antibiotics and only has been associated to a limited number of AMPs[116].

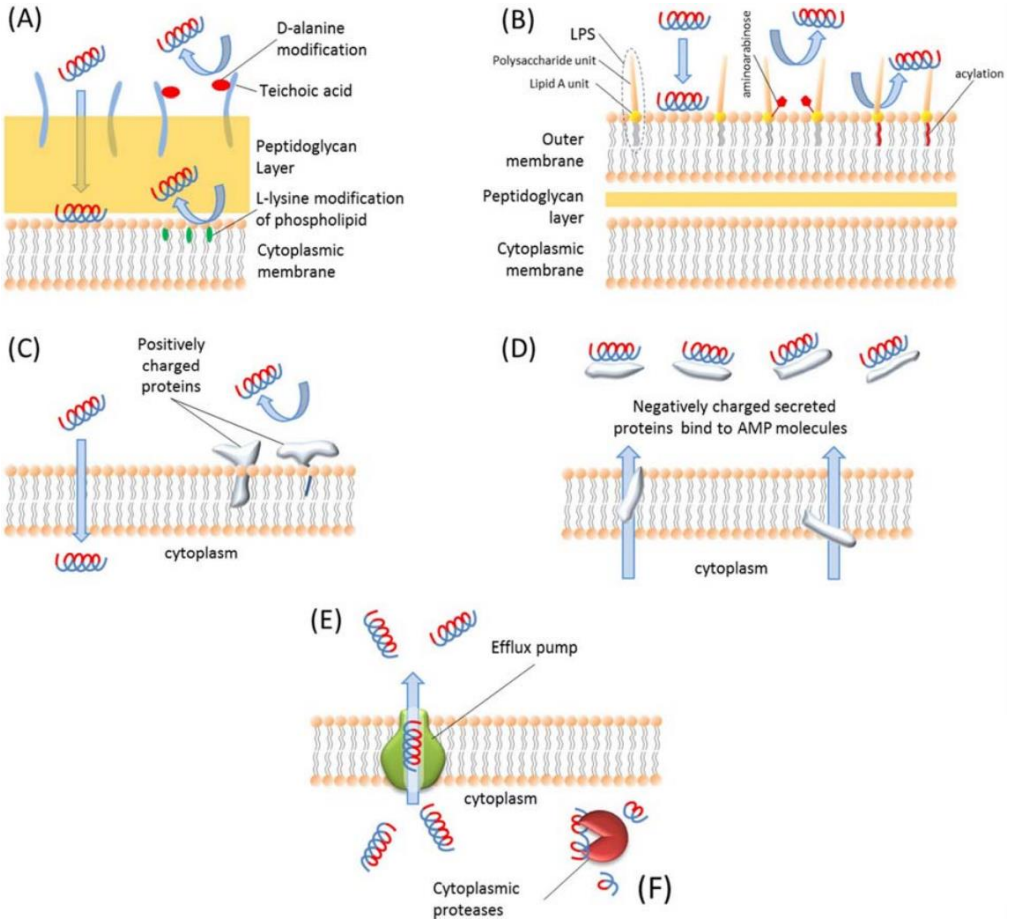

Figure 8. **A**) Gram-positive bacteria resist AMPs via teichoic acid modification of LPS molecules and L-lysine modification of phospholipids. **B**) Gram-negative bacteria resist AMPs by modifying LPS molecules with aminoarabinose or acylation of lipid A unit of LPS molecules. **C**) Bacteria express some positively charged proteins and integrate them in the membrane, so positive charges repulse each other, and AMPs cannot access the cell. **D**) Bacteria produce negatively charged proteins and secrete them to the extracellular environment to bind and block AMPs. **E**) The intracellular AMPs are extruded by efflux pumps. **F**) The AMPs inside the cell are degraded by proteases. Taken from *Bahar and Ren 2013*[120].

1.3.4. The antimicrobial peptides derived from RNase 3

RNase 3, also named the eosinophil cationic protein (ECP), is an RNase with a high antipathogenic activity that is present in the secretion granules of the human eosinophils, together with the eosinophil derived neurotoxin (EDN/RNase 2), the eosinophil peroxidase (EPO) and the major basic protein (MBP). Although the higher relative abundance of MBP points it out as the main responsible of the bactericidal activity of the eosinophils, studies on the parasite *Schistosoma mansoni* showed that ECP is from 8 to 10 times more lethal than MBP[144,145]. The protein displays a high bactericidal[146] and antiparasitic activity (against helminths and protozoa)[46,93,147].

The mechanism of action of bactericidal RNases such as RNase 3 is similar to that of antimicrobial peptides, in that they bind the bacterial cell wall and the membrane through their cationic residues by electrostatic interactions. Then, the hydrophobic residues trigger the destabilisation of the membrane, permeabilizing it and inducing cell death. This mechanism is common for both the gram-negative and gram-positive bacteria, although it may vary by peptide or pathogen type[32,148]. For this reason, in our group we designed several antimicrobial peptides derived from the

sequence of RNase 3, the RNase of the family with highest antimicrobial activity. Specifically, studies from our group indicated that the antibacterial activity of RNase 3 is mostly retained at the N-terminus end[149].

A first study demonstrated that the antimicrobial activity of RNase 3/ECP is retained in the first 45 residues of its N-terminus side[149], which comprises the two first helixes of the protein (see Figure 9). ECP bacterial agglutination ability also corresponds to the first helix, particularly to the 8-16 residues, while the 33-36 residues are involved in destabilisation and breakage of the membranes. On the other hand, the LPS-binding region corresponds to the second helix, although some residues of the first helix like Trp10 and Gln14 are also involved[90]. Combination of LPS binding and agglutination promote the protein antibiofilm activity. Recent studies in our group[150] show that ECP has high activity against bacterial biofilms of *Pseudomonas aeruginosa*, a resistance mechanism in which a bacterial community is formed by the adhesion to a surface through secreted exopolysaccharides. This antibiofilm activity would also be retained at the protein N-terminus side[150].

Based on the structural knowledge, our group aimed to reduce as much as possible the size of the peptide while conserving its antibacterial activity. In a first attempt to minimize the size of the active peptide, eight candidates derived from the ECP(1-45) peptide were synthesised and a shortened peptide version was selected, named ECP(6–17Ahx23–36)[91]. This peptide presented the two first helixes of the protein bound by a molecule of 6-aminohexanoic acid (Ahx).

Starting from this lead peptide, a second generation of peptides was designed by replacing the Ahx for an even shorter variant of the loop that connects the two helixes of the protein, keeping the proline and arginine residues, and removing the non-critical residues before the first helix. Last, the ECP(5–17P24–36) peptide was chosen[91], as depicted in Figure 9, as the best pharmacophore of the parental protein.

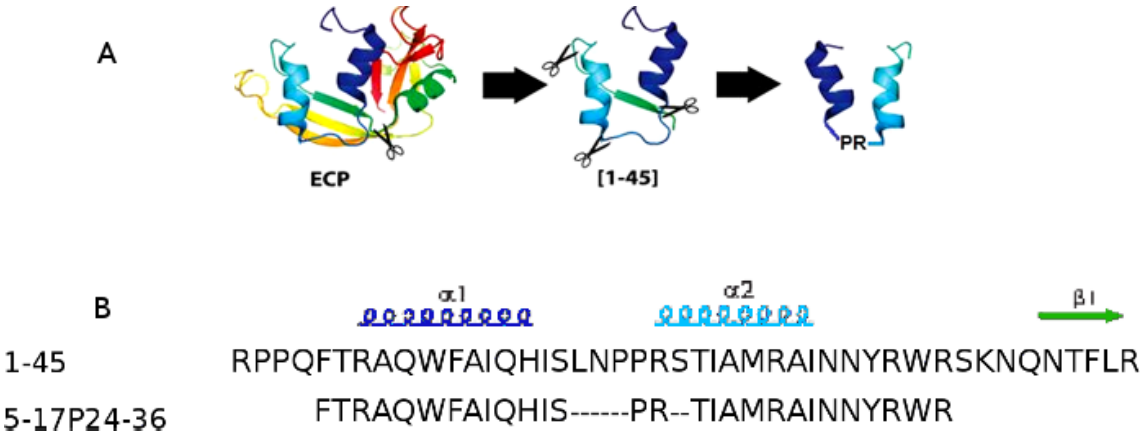

Figure 9. ECP(5–17P24–36) peptide design. (**A**) Structure representation of ECP, its N-terminal peptide and the ECP(5-17P24-36) peptide. (**B**) ECP N-terminal and ECP(5-17P24-36) sequences. The secondary structure elements of the peptide are shown, in basis of the ECP structure. Taken from *Villalba 2015*[151].

2. AIMS OF THE THESIS

The overall objective of the present thesis is to characterize the structure-function relationship of the human antimicrobial RNases both in their antimicrobial and catalytic activities to explore their pharmacological potential. Specifically, the particular aims of this work are:

1. To study the substrate binding mode and catalytic mechanism of RNase 6.

2. To design and select the best antimicrobial peptide derived from RNase 3.

3. To combine RNase 1 catalytic activity and RNase 3 bactericidal activity into a rationally designed chimeric RNase with the final aim to develop novel RNase-based drugs against the emergence of bacterial resistance to antibiotics.

3. RESULTS

CHAPTER I: Exploring RNase 6 RNA binding mode

CHAPTER II: Bactericidal and cytotoxic activity of ECP(5–17P24–36)

CHAPTER III: Design of an RNase chimera for antimicrobial therapy

CHAPTER I: Exploring RNase 6 RNA binding mode

Prats-Ejarque, G., Blanco, J. A., Salazar, V. A., Nogués, V. M., Moussaoui, M., and Boix, E. (2019). Characterization of an RNase with two catalytic centers. Human RNase6 catalytic and phosphate-binding site arrangement favors the endonuclease cleavage of polymeric substrates. *Biochim. Biophys. Acta - Gen. Subj.* **1863**, 105–117. doi:10.1016/j.bbagen.2018.09.021.

CHAPTER II: Bactericidal and cytotoxic activity of ECP(5–17P24–36)

Pulido, D., **Prats-Ejarque, G.**, Villalba, C., Albacar, M., Moussaoui, M., Andreu, D., et al. (2018). Positional scanning library applied to the human eosinophil cationic protein/RNase 3 N-terminus reveals novel and potent antibiofilm peptides. *Eur. J. Med. Chem.* **152**, 590–599. doi:10.1016/j.ejmech.2018.05.012.

CHAPTER III: Design of an RNase chimera for antimicrobial therapy

Design of an RNase chimera for antimicrobial therapy

Authors

Guillem Prats-Ejarque*, Helena Lorente, Lu Lu, Sergi Vázquez, Pablo Fernández-Millán, Ester Boix*

Department of Biochemistry and Molecular Biology, Faculty of Biosciences, UAB, Cerdanyola del Vallès, Spain

*** Correspondence to: Guillem Prats-Ejarque, Ester Boix**

Keywords: RNase, antimicrobial resistance, antibiotic adjuvant, Gram-negative bacteria, antimicrobial peptides.

Abstract

In the last decades, antibiotics resistant bacteria have emerged as a threat for human health. Novel protein-based strategies come out as alternative therapies. Based on the structure- functional of innate immunity proteins, we have designed a chimera construct based on the structure of two human members of the RNase A superfamily: RNase 1, with the highest catalytic activity and the lowest cytotoxicity thanks to its high affinity for the cytosolic ribonuclease inhibitor (RI) and RNase 3, with the highest antipathogen activity, alas with a much-reduced catalytic activity.

We designed a first RNase 3/1-v1 chimera that combined a catalytic activity 40-fold higher than RNase 3 with a high antimicrobial activity, but still not reaching the parental antipathogenic activity of RNase 3. In the second phase, two new chimeric proteins were created that showed an improvement in the antimicrobial activity. Both of these versions (RNase 3/1-v2 and v3) incorporated an antimicrobial RNase 3 loop, while an RNase 1-loop was removed in the RNase 3/1-v3 construct. The stability of the protein 3D structures was validated by molecular dynamics. Experimental results indicated that the RNase 3/1-v3 has acquired both higher antimicrobial and catalytic activities. Unfortunately, the improvement of the RNase 3/1-v3 antimicrobial properties was in detriment of a significant reduction in its affinity for the cytosolic ribonuclease inhibitor (RI). In addition, we tested the ability to induce autophagy in macrophages of the three variants, a property observed in RNase 3, but not shared by RNase 1. Interestingly, RNase 3/1-v1 cannot reproduce RNase3 autophagy induction; in contrast to both RNase 3/1-v2 and v3. We have identified a LIR motif in RNase 3 (^{122}YPVV^{125}), which is uniquely incorporated in both RNase 3/1-v2 and v3 and is associated to autophagosome recruitment, and should facilitate the protein removal of macrophage intracellular infection. The results promise future applied therapeutics.

1 Introduction

Ribonuclease A superfamily is a vertebrate-specific family of proteins homologous to the bovine pancreatic ribonuclease (RNase A). The proteins of this family share, at the structural level, a high isoelectric point (between 9 to 11), a kidney-shaped structure maintained by three to four disulphide bridges and a common “catalytic triad”, conformed

by two histidines and one lysine, which cleaves RNA by an acid-base catalysis (Cuchillo et al., 2011). Interestingly, evolutionary studies suggest that the RNase A family started off as host-defence proteins (Pizzo and D'Alessio, 2007; Rosenberg, 2008; Lomax et al., 2017). Antimicrobial and immune-regulatory properties were reported for several family members and their presence in a variety of biological fluids is associated to a protective physiological role (Hooper et al., 2003; Sorrentino, 2010; Goncalves et al., 2016; Koczera et al., 2016; Xu et al., 2016; Lu et al., 2018).

The antibacterial activity of RNases seems to be unrelated to their ability to degrade RNA (Rosenberg, 1995; Carreras et al., 2003; Torrent et al., 2007, 2011a). However, recent work is showing that catalytic activity has a role in several aspects of the immune system properties of RNase proteins (Kopfnagel et al., 2018; Rademacher et al., 2019; Lu et al., 2020). For example, the antiviral and fungicidal activities of RNases seem to be related to the RNase enzymatic activity (Phipps et al., 2007; Salazar et al., 2016).

Another interesting aspect of RNases, as multifaceted proteins, is their ability to induce autophagy, observed in RNase 3 and 6 (Lu et al., 2019). This autophagy induction ability is a key mechanism to inhibit *Mycobacterium aurum* intracellular growth. In accordance, the expression of both RNases in human macrophage cells is upregulated by the mycobacterial infection, suggesting an *in vivo* physiological role.

Recently, in our group we have designed a chimeric protein that includes some of the antimicrobial regions of RNase 3 (the RNase with highest antibacterial activity) and the skeleton of RNase 1 (the most catalytically active human RNase). This chimeric protein, named RNase 3/1, presents a considerable antibacterial activity, together with a much higher ribonuclease activity and a lower cytotoxicity in comparison to RNase 3. Interestingly, this protein is able to delay the *Acinetobacter baumannii* acquisition of resistance to colistin, when co-administered (Prats-Ejarque et al., 2019). The initial promising results encouraged us to improve the lead chimera construct and ideate two novel variants aimed to target macrophage intracellular infections.

2 Materials

The *Acinetobacter baumannii* strain (CECT 452; ATCC 19606) and *Pseudomonas aeruginosa* strain (CECT 4122; ATCC 15692) are from the Spanish Type Culture Collection (CECT). The *Escherichia coli* BL21(DE3) strain and the pET11c plasmid are from Novagen. MRC-5 and HepG2 cells are from the American Type Cell Culture Collection (ATCC). Mueller-Hinton broth, LPS and RNase A (Type XII) are from Sigma-Aldrich. 3-[4,5-dimethylthiazol-2-yl]-2,5-diphenyl tetrazolium bromide (MTT), isopropyl β-D-1-thiogalactopyranoside (IPTG) and colistin are from Apollo Scientific. 1-aminonaphthalene-3,6,8-trisulfonate (ANTS), α,α′-dipyridinium p-xylene dibromide (DPX) and the fluorescent probe BODIPY TR cadaverine are from Molecular Probes. Toluidine blue is from Merck. RNase3/1 gene was purchased from NZYTech. 1,2-dioleoyl-*sn*-glycero-3-phosphocholine (DOPC) and 1,2-dioleoyl-*sn*-glycero-3-phosphoglycerol (DOPG) were purchased from Avanti Polar Lipids. Human RNase 1

gene was a gift from Prof. Maria Vilanova, Universitat de Girona, Spain. Human RNase 3 sequence was taken from a previously synthesized gene (Boix et al., 1999b).

3 Methods

3.1 Protein expression and purification

The RNase 1, 3 and 3/1 genes were subcloned into the plasmid pET11c for high yield expression in *E. coli* BL21(DE3) strain. The recombinant protein was expressed and purified as previously described (Boix, 2001), with some modifications (Palmer and Wingfield, 2004). Briefly, bacteria were grown in Terrific broth (TB), containing 400 μg/mL ampicillin. Recombinant protein was expressed after cell induction with 1 mM IPTG added when the culture showed an OD600 of 0.6. The cell pellet was collected after 4 h of culture at 37°C. Cells were resuspended in 10 mM Tris/HCl, 2 mM EDTA, pH 8 and 40 μg/mL of lysozyme, and sonicated after 30 minutes. The pellet was suspended in 25 mL of the same buffer with 1% triton X-100 and 1 M urea and was left stirring at room temperature for 30 minutes, before being centrifuged for 30 minutes at 22.000× g. This procedure was repeated until the supernatant was completely transparent. In order to remove the triton X-100, 200 mL of 10 mM Tris-HCl pH 8.5, 2 mM EDTA was added to the pellet and centrifuged again for 30 minutes at 22.000× g. The resulting pellet was resuspended in 25 mL of Tris-acetate 100 mM, pH 8.5, 2 mM EDTA, 6 M guanidine hydrochloride, and 80 mM of DTT. The protein was then refolded for 72 hours at 4ºC by a rapid 100-fold dilution into 100 mM Tris/HCl, pH 8.5, 0.5 M of guanidinium chloride, and 0.5 M L-arginine, and oxidized glutathione (GSSG) was added to obtain a DTT/GSSG ratio of 4. The folded protein was then concentrated, buffer-exchanged against 150 mM sodium acetate, pH 5 and purified by cation-exchange chromatography on a Resource S column (GE Healthcare) equilibrated with the same buffer. The protein was eluted with a linear NaCl gradient from 0 to 2 M in 150 mM sodium acetate, pH 5.

3.2 Mutagenesis

To obtain RNase 3/1-v2 and RNase-v3, two pairs of specific oligonucleotides were designed. Supreme NZYProof polymerase was used for amplification. Next, the parental DNA was digested with *DpnI* and the reaction product was cleaned with the *GenElute PCR Clean-Up kit*. To circulate the plasmid, one end was phosphorylated and the junction of both ends was performed with Anza T4 DNA ligase. Finally, the transformation and sequencing of the obtained plasmid was carried out.

3.3 Molecular dynamic simulations

To analyse the stability of the RNase 3/1 versions, molecular dynamics was performed. All the molecular dynamics were performed with GROMACS 2018.1 (Pronk et al., 2013), using *AMBER99SB-ILDN* (Lindorff-Larsen et al., 2010) as a force field. Proteins were cantered in a dodecahedral box with a distance of 1 nm between the box and the solvent. The unit cell was filled with *TIP3P* water (Jorgensen et al., 1983) at neutral pH and 100 mM of NaCl.

For the neighbour search a Verlet cut-off scheme was used (Páll and Hess, 2013) with a cut-off of 0.9 nm for both Van der Walls and short-range Lennard-Jonnes interactions. For the long-range interactions, smooth particle mesh of Ewald (PME) (Darden et al.,

1993; Essmann et al., 1995) was used with a fourth-order interpolation scheme and 0.1125 nm grid spacing for FFT. The bonds were constrained with P-LINCS algorithm (Hess, 2008) with an integration time step of 2 fs.

The energy of the systems was minimized using the steepest descendant algorithm (Debye, 1909) and equilibrated in two steps. First, an initial constant volume equilibration (NVT) of 1 ns was performed with a temperature of 298 K using a Berendsen modified thermostat (Bussi et al., 2007). Then, 1 ns of constant pressure equilibration (NPT) was run at 1 bar with a Parrinello-Rahman barostat (Parrinello and Rahman, 1981; Nosé and Klein, 1983) at 298 K and the same thermostat. Finally, 50 ns production runs were performed under an NPT ensemble without applying restraints.

3.4 Circular dichroism (CD)

Far-UV CD spectra were obtained from a Jasco-715 (Jasco), as previously described (Torrent et al., 2009). The spectra were registered from 195 to 240 nm at room temperature. Data from four consecutive scans were averaged. Before reading, the sample was centrifuged at 10.000× *g* for 5 minutes. Spectra of RNase 3/1 were obtained at 6 μM in 5 mM sodium phosphate, pH 7.5, with a 0.2 cm path-length quartz cuvette. The percentage of secondary structure was estimated with Spectra Manager II, as described (Yang et al., 1986).

3.5 Activity staining gel

Zymograms were performed following the method previously described (Bravo et al., 1994). 15% polyacrylamide-SDS gels were cast with 0.3 mg/mL of poly(C) (Sigma Aldrich). Then, 20 ng of RNase 1, 3 and 3/1 were loaded, and the gel was run at a constant current of 100 V for 1.5 h. Following, the SDS was removed from the gel with 10 mM Tris/HCl, pH 8, and 10% (v/v) isopropanol. The gel was then incubated during 1 hour in the activity buffer (100 mM Tris/HCl, pH 8) to allow enzymatic digestion of the embedded substrate and then stained with 0.2% (w/v) toluidine blue in 10 mM Tris/HCl, pH 8, for 10 min. Positive bands appeared white against the blue background. The loading buffer had no 2-mercaptoethanol to facilitate recovery of active enzymes.

3.6 Minimum bactericidal concentration (MBC) determination

MBC was defined as the lowest protein/peptide concentration that completely eradicated bacterial cells. RNase3/1was serially diluted from 20 to 0.02 μM in HBS (HEPES 20 mm pH 7.4, NaCl 100 mM). Then, an exponential phase subculture of *E. coli*, *A. baumannii* or *P. aeruginosa* was added, previously adjusted to give a final concentration of approximately $5 \cdot 10^5$ colony-forming units (CFU)/mL in each well and the plate was incubated for 4 hours at 37 ºC and 100 rpm. Finally, samples were plated onto LB Petri dishes (Condalab) and incubated at 37 ºC overnight. All the assays were performed in triplicate.

3.7 Spectrophotometric kinetic analysis

The ribonuclease activity of RNase 1, 3 and the three variants of RNase 3/1 in the presence or absence of ribonuclease inhibitor (rRNasin®, Promega) was assayed against CpA as previously described (Boix et al., 1996). The proteins with or without 40 units of RI were previously incubated for 30 minutes at room temperature. The enzymatic reaction was carried out in a 50 μL quartz cuvette with 1 cm of optical pathlength that contained 50 mM MES-NaOH pH 6, 125 mM NaCl, 1 mM EDTA, 1.2 mM DTT, 0.1% PEG4000, 0.2 mg/mL BSA; the substrate concentration was 100 μM for CpA. The protein concentrations used were 0.1 μM for RNase 3/1-v1 and -v3; 0.25 μM for RNase 3/1-v2. For dinucleotide (CpA, UpA and UpG) kinetics without the presence of the inhibitor, reaction was performed at 50 mM of sodium acetate, pH 5.5 without any previous incubation. The catalytic activity against the dinucleotide CpA was measured as a decrease in absorbance at 286 nm, which corresponds to the first step of the phosphodiester bond cleavage.

3.8 Cytotoxicity assay

Cytotoxicity was measured for the MRC-5 and HepG2 human cell lines using the MTT assay, as described previously (Pulido et al., 2018). Cells were grown in 5% CO_2 at 37 °C with minimal essential medium supplemented with 10% fetal bovine serum (FBS). Cells were plated at 5×10^4 cells/well in a 96-well plate and incubated overnight. Next, the medium was removed and serial dilutions of protein were added at concentrations ranging from 200 to 0.2 μM in 100 μL of medium without serum. After 4 h of incubation, the medium was replaced with fresh medium containing 0.5 mg/mL MTT solution and the mixture was incubated for 2 h in 5% CO_2 at 37 °C. The medium was then removed, and formazan was dissolved by adding acidic isopropanol. The optical density (OD) was recorded by using a Victor^3 plate reader (PerkinElmer, Waltham, MA) set at 550 nm and 630 nm as references. Reference absorbance at 630 nm was used to correct for nonspecific background values. Each experiment was repeated at least three times.

3.9 LPS binding assay

The LPS-binding affinity was assessed using the fluorescent probe BODIPY TR cadaverine (BC) as described (Torrent et al., 2008). RNase 1, 3 and 3/1 were serially diluted in a 96-well fluorescence plate from 20 to 0.02 μM in HEPES 10 mm pH 7.4. Then, LPS (10 μg/mL) and BC (10 μM) were added in the same buffer. Fluorescence measurements were performed on a Victor^3 plate. The BC excitation wavelength was 580 nm, and the emission wavelength was 620 nm. Occupancy factor was calculated as described previously (Torrent et al., 2008).

3.10 Liposome preparation

Large unilamellar vesicles (LUVs) containing DOPC/DOPG (3:2 molar ratio, 1 mM stock concentration) or *E. coli* membrane lipids (5 mg/mL stock concentration) of a defined size were obtained from a vacuum drying lipid chloroform solution. After the chloroform evaporation, liposomes where suspended with 10 mM Tris/HCl, 20 mM NaCl, pH 7.4.

The distribution and the mean hydrodynamic range of the liposomes in suspension was determined by dynamic light scattering (DLS) with a Zetasizer Nano ZS Malvern, and the data was analysed by its built-in software (Zetasizer 7.02).

3.11 Liposome leakage

The ANTS/DPX liposome leakage fluorescence assay was performed as previously described (Pulido et al., 2016). Briefly, a unique population of LUVs DOPC/DOPG (3:2) or *E. coli* liposomes was prepared to encapsulate a solution containing 12.5 mM ANTS, 45 mM DPX, 20 mM NaCl, and 10 mM Tris/HCl, pH 7.5 with 3 freeze-thaw cycles. The ANTS/DPX liposome stock suspension was diluted to 30 µM and incubated at 37 ºC for 1 h with RNase 1, 3 and 3/1, serially diluted from 20 to 0.015 µM in a microtiter fluorescence plate. Fluorescence measurements were performed on a Victor^3 plate reader with an excitation wavelength of 386 nm and an emission wavelength of 535 nm. ED_{50} values were calculated by fitting the data to a dose–response curve with Origin 8.0.

3.12 Macrophage cell culture

Mouse RAW 264.7 cells (NCTC, #91062702) were maintained or passaged in 25 cm^2 tissue culture flasks (BD Biosciences, 353108) using DMEM (Lonza, BE04-687F/U1) and RPMI-1640 (Lonza, BE12-702F) medium with 10% heat-inactivated fetal bovine serum (FBS, Gibco, 26140079) respectively at 37ºC and humidified 5% CO_2 conditions. RAW 264.7 cells were seeded at 5×10^5 cells/well and allowed to attach for 2 h before infection and treatment. The number of viable cells was counted using a Trypan blue (Invitrogen, 15250-061) exclusion assay.

3.13 Growth of mycobacteria culture and macrophage infection

Mycobacterium aurum was purchased from the UK National Collection of Type Cultures (NCTC). Cells cultures of *M. aurum* (NCTC, 10437), *Mycobacterium smegmatis* mc2155 (ATCC, 700084) and *M. bovis* BCG Pasteur (ATCC, 35734) were grown in Middlebrook (MB) 7H9 broth (BD Biosciences, 271310) enriched with 10% (v/v) albumin/dextrose/catalase (ADC; BD Biosciences, 212352) containing 0.05% Tween 80 and 0.05% Glycerol for liquid growth at 37^{0}C for BCG, and in MB7H10 (BD Biosciences, 262710) with 10% (v/v) oleic acid/albumin/dextrose/catalase (OADC; BD Biosciences, 212240) for semi-solid agar growth at 37ºC. Stock cultures of log-phase cells were maintained in glycerol (25% final concentration of glycerol) at -80ºC. The bacteria were vortexed and sonicated using ultrasound sonication bath to obtain a single cell suspension, and then the bacterial concentration was determined by measuring the optical density (OD) of the culture at 600 nm (1 OD=109 CFU/mL). Mid-log phase *M. aurum* cells, harvested in RPMI-1640 complete medium, were co-cultured with RAW264.7 at a multiplicity of infection (MOI) of 10:1 and were incubated at 37 C for 3h, then were washed 3 times with PBS and replaced with fresh media supplied with 50 µg/mL gentamycin (Apollo Scientific, BIG0124) to remove extracellular mycobacteria during further treatment.

3.14 Real-time qPCR assays

Total RNA of the mouse macrophages was extracted using *mirVana™ miRNA Isolation Kit* as described by the manufacturer (Ambion, Life Technologies, AM1560) at each time point (4, 24, 48, 72 h). Total RNA was quantified by NanoDropTM spectrophotometer (Thermo Fisher Scientific, Wilmington, DE USA), and cDNA was synthesized using *iScriptTM cDNA Synthesis Kit* (Bio-Rad, 170-8891). RT-qPCR was performed as previously using the corresponding primers for Mouse *BECN1* and *ATG5* (Lu et al. front immunol 2019). Mouse *BECN1* and *ATG5* genes relative to mouse actin (as a housekeeping gene) were measured in triplicate from cDNA samples by real-time quantitative PCR using CFX96 Real-Time PCR detection system (Bio-Rad, Hercules, CA, USA). The results were analysed by using the relative standard method (Livak and Schmittgen, 2001).

3.15 Acridine orange staining

To quantify autolysosome formation, mouse macrophage cells treated with various compounds were stained with acridine orange as previously reported (Fiorini et al., 2015). Briefly, cells were seeded in 96-well plates (10^4 cells/well) and treated with RNases protein or rapamycin or bafilomycin. At the end of the treatments, cells were washed with prewarmed PBS and stained with 5 µg/ml acridine orange (AO) for 10 min in PBS. After washing with PBS three times, autolysosome formation was performed measuring the red/green fluorescence intensity ratio of AO staining (AO green fluorescence λ_{exc} 485 nm and λ_{em} 535 nm; AO red fluorescence λ_{exc} 430 nm and λ_{em} 590 nm). Values were normalized on cell proliferation by MTT assay.

3.16 Thioflavin-S staining tracking intracellular aggregates

Mouse macrophage cells treated with protein or peptide were stained with Thioflavin-S (Espargaró et al., 2012). Briefly, cells were seeded in 96-well plates (10^5 cells/well) and treated with RNases protein or peptide. At the end of the treatments, cells were washed with prewarmed PBS and stained with 25 µM of Thioflavin-S for 15 min in PBS. After washing with PBS three times, fluorescence intensity was recorded under condition of λ_{exc} 375 nm and λ_{em} 455 nm.

4 Results

4.1 RNase 3/1-v2 and v3 rational design

RNase 3/1 was designed in an effort to combine both the high bactericidal activity of human RNase3 and the high catalytic activity of human RNase1, according to previous structural functional studies (Prats-Ejarque et al., 2019). Using the RNase 1 structure as a scaffold, the following regions of RNase 3, associated to the protein antimicrobial activity, were added: the cationic regions from Arg77 to Arg81 and Arg103 to Arg107 (Carreras et al., 2003, 2005) and the N-terminal region of RNase 3 (Torrent et al., 2009, 2010, 2013; Sánchez et al., 2011). On the other hand, the Asp17-Ser26 flexible loop of

RNase1, considered essential for RNase1 high catalytic activity, was conserved (Doucet et al., 2009; Gagné et al., 2015).

Although the RNase 3/1 initial version (thereafter named RNase 3/1-v1) significantly improved the catalytic activity of RNase 3, conserving a significant antimicrobial activity, its bactericidal activity was considerably lower than RNase 3. For this reason, we decided to modify the initial version and introduce cationicand hydrophobic surface residues, proved to be key for the protein antimicrobial properties (Carreras et al., 2003; Boix et al., 2012). Therefore, we added the RNase 3 antimicrobial loop (113N – 122Y; thereafter R3-L7) in RNase 3/1-v2 and replaced the flexible loop of RNase 1 (14D – 25Y; thereafter R1-L1) by the original shorter loop of the RNase 3 N-terminal (17S – 22R; thereafter R3-L1) in RNase 3/1-v3, as shown in figure 1.

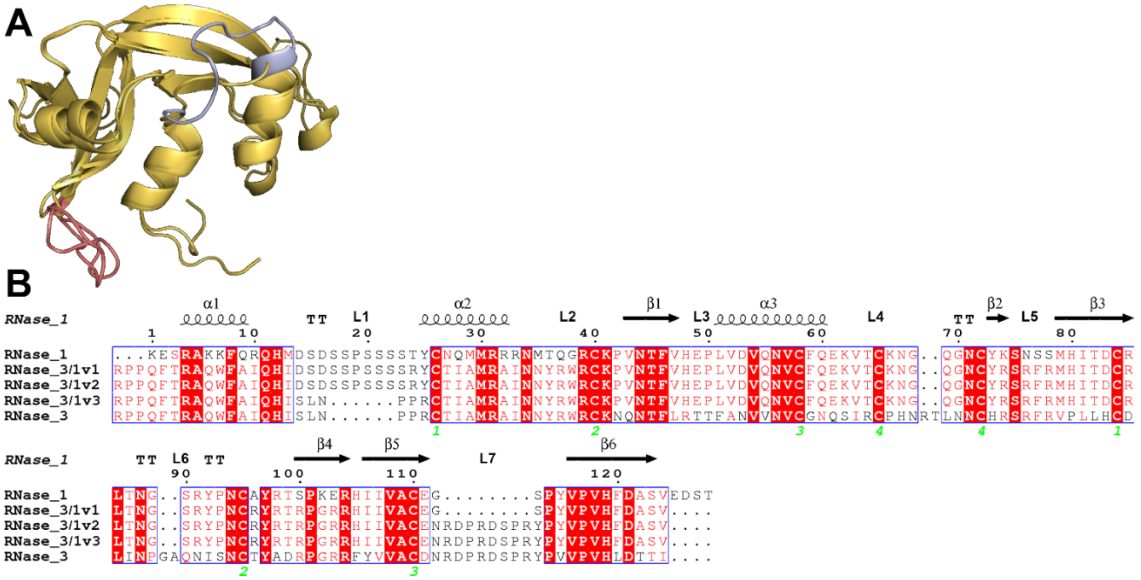

Figure 1. (**a**) Overlapping of the models of RNase 3/1-v1-3 obtained by *Modeller 9.12* (Webb and Sali, 2016). In red, the antimicrobial loop of RNase 3, added in RNase 3/1-v2. In blue, the flexible loop of RNase 1, removed in RNase 3/1-v3. In beige, the RNase 1 skeleton. (**b**) Alignment between RNase 1, 3 and 3/1-v1-3. The fully conserved amino acids are highlighted in red. The residues that are not conserved but have similar properties are marked with red letters. The secondary structure is indicated above the alignment. The green numbers indicate the disulphide bridges. The alignment was done using *Clustal Omega* (Sievers and Higgins, 2018), and the image was obtained with ESPript7 (http://espript.ibcp.fr/ESPript/) (Robert and Gouet, 2014).

To assess the stability of the designed proteins before their recombinant expression, proteins were modelled, and molecular dynamics was performed with those models. The analysis of the molecular dynamics results shows that the three proteins should be stable, considering both the gyration radius and the backbone RMSD of the proteins. Results are shown in figure 2.

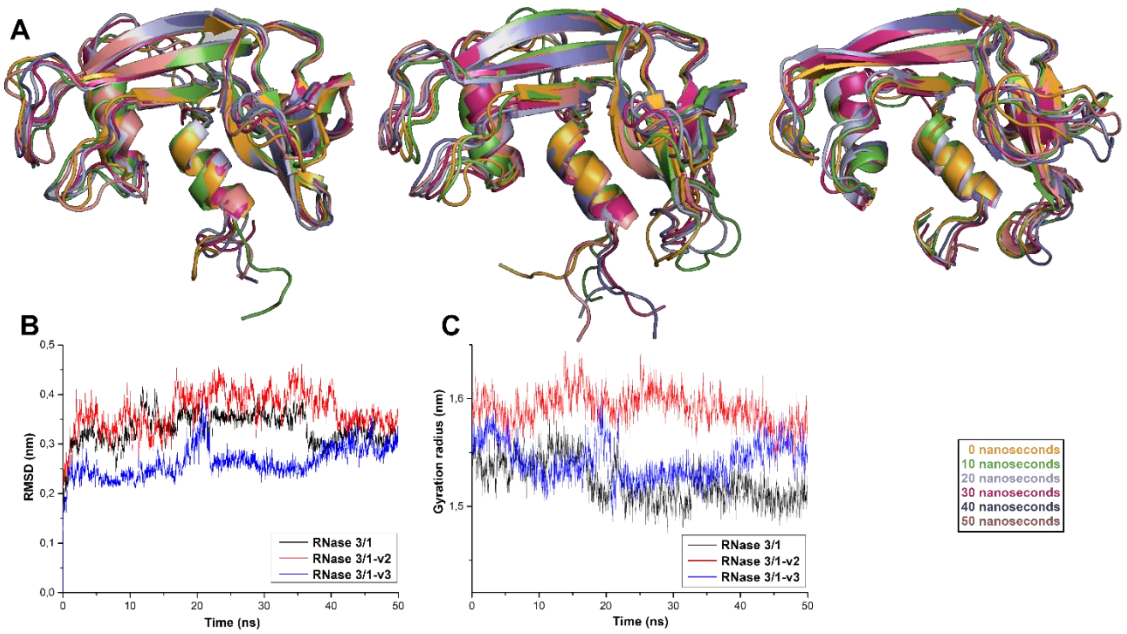

Figure 2. **A**) Overlapping of the three versions of RNase 3/1 after 50 nanoseconds of molecular dynamics. **B**) RMSD variation for the three hybrid RNases. **C**) Gyration radius of the structure of hybrid RNases against time.

The two new versions were successfully expressed in *E. coli* BL21(DE3) cells and purified from inclusion bodies at high yield (between 10 to 40 mg/L, depending on the version). The proper 3D protein folding was checked by circular dichroism (figure S1), giving the characteristic secondary structure percentage distribution of the RNase A family (Fowler et al., 2011).

4.2 Catalytic activity

Following, we assessed the protein catalytic activity using an activity staining gel. Results are shown in figure 3. The data indicates that the RNase3/1-v2 and v3 lowered by half the catalytic activity of the original version towards a polynucleotide substrate, although still retaining a significantly high catalytic activity, only about 3 times lower than RNase 1. Thus, our results indicate that the removal of the R1-L1 loop does not have such a drastic effect in the catalytic activity.

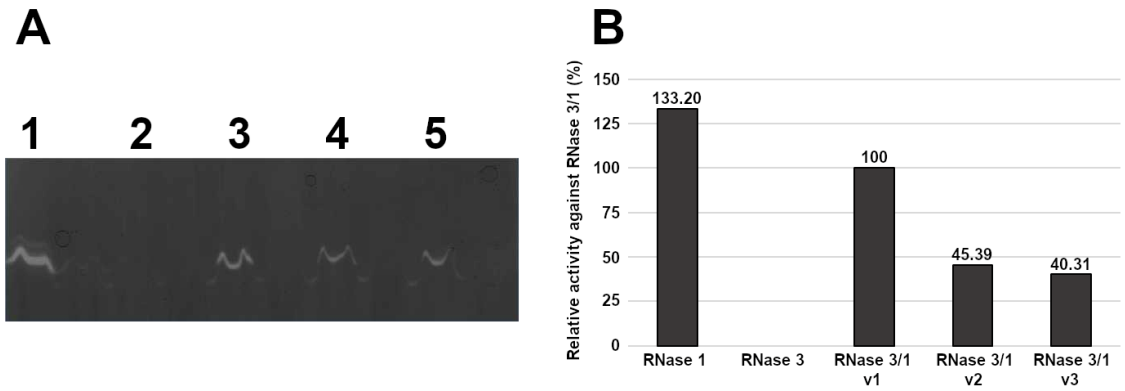

Figure 3. (**a**) Activity staining gel showing the degradation of poly(U) with 15 ng of each protein. RNase 1 (lane 1), RNase 3 (lane 2), RNase 3/1-v1 (lane 3), RNase 3/1-v2 (lane 4) and RNase 3/1-v3 (lane 5). (**b**) Densitometric analysis of the bands of the activity staining gel. Activity is represented by relative activity against RNase 3/1-v1. Quantification was done from a scan image using Quantity One software (Bio-Rad®).

In addition, we also tested the catalytic activity of the different RNase 3/1 versions against dinucleotides (CpA, UpA and UpG) by kinetic spectrophotometry. Results are shown in table 1. As observed in the zymogram, there is a slight decrease of the catalytic activity in comparison with the original RNase 3/1 version. Interestingly, the new RNase 3/1 versions appear to have a more pronounced preference for uridine. Not only that, RNase 3/1-v2 is far more active against adenine than guanidine at the B2 position compared to the other two versions. Again, the suppression of the RNase 1 flexible loop does not seem to have a remarkable effect in the catalytic activity.

Relative catalytic activity against dinucleotides (% respect RNase 3/1-v1)					
	RNase 1	**RNase 3**	**RNase 3/1-v1**	**RNase 3/1-v2**	**RNase 3/1-v3**
CpA	640.84	1.73	100	37.24	35.17
UpA	940.26	0.79	100	73.44	130.08
UpG	124.19	N.D.	100	22.78	84.51
U/C	10.02	3.13	6.83	13.47	25.27
A/G	1322.34	∞[1]	207.37	757.68	353.18

[1] As no activity was detected for UpG, the A/G ratio is expressed as infinite

Table 1. Comparison of the relative catalytic activity against dinucleotides assayed by spectrophotometry. B1 and B2 relative ratio is indicated. The relative activity was determined by an spectrophotometric method at 286 nm, measuring the cleavage of the phosphodiester bond for 2 minutes, with enzyme concentrations between 0.1 to 1 µM. Each assay was performed in triplicate in 50 mM sodium acetate, pH 5.5, using a 0.3 cm pathlength quartz cuvette.

4.3 Bactericidal activity

In view of these results, we wanted to check whether the incorporation of the bactericidal loop really improved the antimicrobial activity of the RNase 3/1-v2 and 3, as predicted. Therefore, we determined the minimum bactericidal concentration (MBC) for the hybrid

and parental RNases. Interestingly, the addition of the R3-L7 loop, when the R1-L1 loop is not present (being the case of RNase 3/1-v2), resulted in a decrease of the antimicrobial activity for *A. baumannii* and *P. aeruginosa*, while no improvement of the activity is detected in *E. coli*. In contrast, in RNase 3/1-v3, where the R1-L1 loop of the N-terminal is replaced by R3-L1, a significant improvement of the antimicrobial activity is detected. Results are shown in table 2.

	MBC_{100} (μM)				
	RNase 1	**RNase 3**	**RNase 3/1-v1**	**RNase 3/1-v2**	**RNase 3/1-v3**
E. coli	> 20	1.88 ± 0.88	6.25 ± 2.17	6.25 ± 2.17	0.78 ± 0.27
A. baumannii	> 20	0.6 ± 0.07	6.25 ± 2.17	16.67 ± 2.89	1.56 ± 1.89
P. aeruginosa	18.33 ± 2.89	0.6 ± 0.07	3.13 ± 1.08	18.33 ± 2.89	1.25 ± 0.54

Table 2. Bactericidal activity of RNases 1, 3 and the three versions of RNase 3/1 against three bacterial Gram-negative species in comparison to RNases 1 and 3. MBC_{100} was determined as the lowest concentration of peptide where no cells were detected by CFU counting in HBS.

Following, we evaluated whether the RNase 3/1 versions retained the high LPS-binding affinity observed in RNase 3. LPS-binding affinity was estimated by a displacement assay using the fluorescent BODYPY-cadaverine (BC) probe as previously described (Torrent et al., 2008). Results indicated that all the versions of RNase3/1 retained a similar LPS-binding affinity, nearly equivalent to RNase 3, being v3 the one with highest affinity (Table 3).

In addition, the liposome leakage ability of the RNases was evaluated. As shown in Table 3, RNase 3/1 retained a similar liposome leakage activity to RNase 3, while RNase 1 does not present any membrane disruption ability.

	LPS binding (LBC_{50}) (μM)	**Liposome leakage (LC_{20}) (μM)**	
		DOPC:DOPG	***E. coli***
RNase 1	1.50 ± 0.28	N. D.	N. D.
RNase 3	0.38 ± 0.03	1.19 ± 0.19	1.87 ± 0.42
RNase 3/1-v1	0.59 ± 0.02	1.18 ± 0.36	0.86 ± 0.18
RNase 3/1-v2	0.66 ± 0.08	3.31 ± 0.67	0.56 ± 0.26
RNase 3/1-v3	0.42 ± 0.07	3.34 ± 0.39	0.36 ± 0.77

Table 3. LPS-binding affinity and liposome leakage activity of RNases 1, 3 and 3/1. The LPS binding concentration at the 50% displacement concentration (LBC_{50}) values have been determined from a dose-response curve adjusted by *OriginPro 8* statistical software. Liposome leakage was measured as the protein concentration that induces 20% of liposome leakage (LC_{20}). Experimental data plots are shown in figures S2 and S3, respectively.

4.4 Interaction with the RNase Inhibitor (RI) and cytotoxicity

The presence of the ubiquitous ribonuclease inhibitor (RI) within the cytosol of human somatic cells protects the cells from cellular RNA degradation (Rutkoski et al., 2005; Rutkoski and Raines, 2008). The RI binds with a very high affinity to all tested human members of the RNase A superfamily and prevents their cytotoxicity (Dickson et al., 2005; Rutkoski and Raines, 2008; Lomax et al., 2014). Its affinity varies depending on the RNase, being RNase 1 the human RNase with highest affinity with the inhibitor, while RNase 3 presents one of the lowest affinities (Rutkoski and Raines, 2008). Preserving high levels of inhibition by the ribonuclease inhibitor (RI) was one of the main goals of the initial design of RNase 3/1, to ensure host cell protection from the protein catalytic activity and potential associated cytotoxicity. Therefore, we evaluated the percentage of RI inhibition of the three RNase 3/1 versions by comparing their catalytic efficiency using CpA as a substrate. Similar inhibition percentage are registered for both v1 and v2. However, the last version shows a significant reduction in the inhibition percentage values (Table 4).

Next, the potential cytotoxicity of the three protein versions against host tissues was evaluated *in vitro* using two human cell lines: immortalized lung fibroblasts (MRC-5) and tumour hepatic cells (HepG2).

The results indicated that RNase 3/1-v2, as observed for v1, shows no toxicity at the maximum concentration tested (200 µM), while RNase 3/1-v3 appears to be slightly toxic in contrast with the preceding versions, although still conserving low toxicity levels (Table 4). The results correlate with the calculated inhibition ability of the RI against the tested RNases.

	RNase 1	**RNase 3**	**RNase 3/1-v1**	**RNase 3/1-v2**	**RNase 3/1-v3**
RI Inhibition (%)	100[a]	11[b]	68	44.1	13.92
	Cell toxicity (IC_{50})				
Lung fibroblasts (µM)	N.D.	> 100	N.D.	N.D.	31.875 ± 10.625
Hepatocarcinoma epithelial cells (µM)	N.D.	134.66 ± 0.95	N.D.	N.D.	> 170

Table 4. Ribonuclease inhibitor (RI) percentage of inhibition was determined by comparing the catalytic activity against CpA with or without presence of the inhibitor. Values represents the percentage of inhibition. Cell toxicity (IC_{50}) was determined as the concentration of protein where 50% of cells were still alive, in the corresponding medium. Cytotoxicity was determined by the MTT assay. Each assay was performed in triplicate. N.D. means that, at the highest tested concentration (200 µM), no reduction of cell viability was detected. Cell toxicity values of RNase 3/1-v1 are taken from (Prats-Ejarque et al., 2019). [a] Data estimated from RNasin® (Promega) datasheet. [b]Data estimated from (Domachowske et al., 1998).

4.5 RNase 3/1 autophagy induction

On the other hand, RNases activity on host cells is not only detrimental. Indeed, diverse immunomodulation activities, such as anti-inflammatory action, have been attributed to secretory RNases (Venge et al., 1999; Lu et al., 2018). Interestingly, a screening of seven human canonical RNases 1-7 in our laboratory highlighted the ability of RNase 3 to induce autophagy in macrophages, which was proven to be essential against intracellular mycobacterial infection (Lu et al., 2019). Contrarily, the same experimental results showed that RNase 1 does not activate autophagy.

Therefore, we envisaged here to test whether the hybrid RNase 3/1 chimera conserved the autophagy induction capacity. Towards this aim we assayed the activity of the three RNase 3/1 versions in comparison to RNase1 and RNase3 parental proteins. Autophagy induction was evaluated selecting the early and late autophagy markers *BECN1* and *ATG5*, which are essential in the autophagosome formation and maturation, respectively. Results are shown in figure 4. Results highlighted that the only v2 and v3 chimera retained RNase3 ability to induce autophagy. Sequence comparison between the first RNase3/1 chimera and the latter two versions pointed to R3-L7 loop in RNase3, which was the unique sequence region absent in RNase3/1-v1 and present in RNase3 and RNase 3/1 v2 and v3.

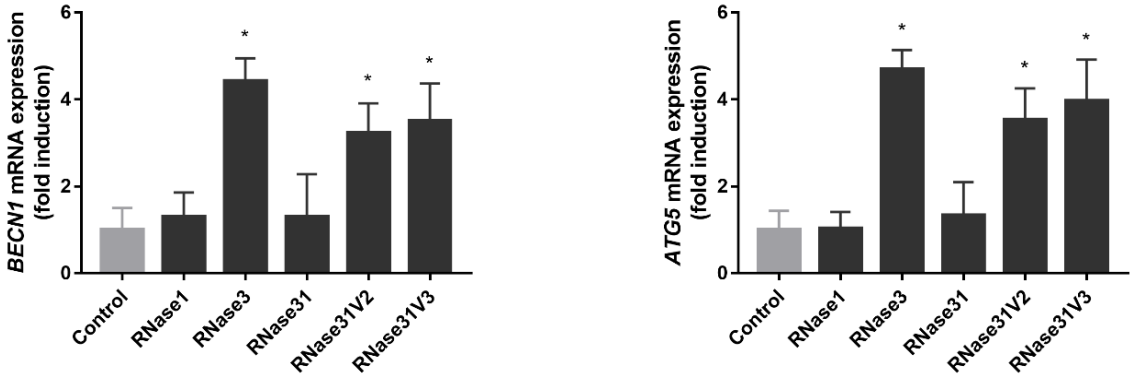

Figure 4. RAW 264.7 macrophages were infected with *M. aurum* and treated by 10 µM of proteins (RNase 1, 3 and 3/1 v1-3) for 24 hours. Real-time qPCR measured the relative expression of *BECN1* and *ATG5* genes, normalized by housekeeping gene *β-actin*. Results are shown from 3 independent experiments (mean ± SD). * indicates significant difference compared with control group ($p < 0.05$).

Moreover, our previous work discarded that the catalytic activity was involved in the protein autophagy induction activity (Lu et al. 2019). Complementarily, we analysed here the main region of RNase 3 associated to its antimicrobial activity: the protein N-terminus (Torrent et al., 2009). The peptide RN3(1-45) was tested to confirm whether or not this region was involved in the autophagy induction mechanism. In addition, we tested two RNase3 single mutants at the N-terminus residues previously identified to be key for the protein membrane interaction and cell agglutination activities (residues Ile13 and Trp35) (Carreras et al., 2003; Torrent et al., 2007, 2012). The involvement of the N-terminus

region was discarded, as the RN3(1-45) peptide could not reproduce the RNase3 protein induction of autophagy (Figures S2-A and S2-B). Besides, single mutations at residues 13 and 35 did not abolish the protein induction of *BECN1* and *ATG5* expression, as also observed for the catalytically defective mutant. From these results, we can conclude that the N-terminal region is not contributing to the autophagy induction activity.

In addition, in our previous work we observed that macrophage incubation with RNase3 was associated to an increase in the content of acidic vesicle formation (Lu et al., 2019), which could be attributed to the autolysosomal compartment during the autophagosome maturation. Here, we inspected whether the RNase3 protein ability to aggregate membrane vesicles, a capacity not found in RNase1, could be responsible for the formation of autolysosomes. A positive correlation was observed for RNase3 (Figure S2-C). Interestingly, the results indicate that the formation of acidic vesicles is not associated to the protein aggregation ability, as the I13A mutant, which is devoid of the aggregation activity (Torrent et al., 2012) is still triggering the increase in acidic vesicles (Figure S2-C). On the contrary, the protein N-terminus peptide RN3(1-45), which has a positive aggregation activity but cannot induce the autophagy process, is also not able to trigger the formation of acidic vesicles. Likewise, no correlation between autophagy induction and liposome or protein aggregation could be inferred from our results (Figure S3 and S4). Put together, the analysis of the RT-qPCR and autolysosome formation results indicate that neither the agglutination, nor the ribonuclease activity would be responsible for autophagy induction. Instead, the comparison of the three chimera variants indicate that the inclusion of the R3-L7 loop in the RNase 3/1 sequence is required for the autophagy induction.

Therefore, we could ascribe unambiguously the observed autophagy activity to the L7 specific loop of RNase 3. Next, we screened the human RNases sequences, to find out whether the R3-L7 loop include any target region essential for the autophagosome-lysosomal protein routing. By applying a software for the identification of subcellular localization targeting regions we identified a lysosome tag near the R3-L7 loop (^{122}YPVV^{125}) in RNase3 (figure S5 and table S1). This region is also present in RNase 1, but it is located in the β6, instead of being exposed in the loop. If we compare the three RNase3/1 variants we can see how the R3-L7 loop of RNase 3 includes the identified autophagosome targeting tag (Figure 5). Specifically, the sequence encompass not only a lysosome tag, but also an LC3-interacting region (LIR) motif (Birgisdottir et al., 2013; Popelka and Klionsky, 2015), with a consensus sequence, [W/F/Y]xx[L/I/V], present at the antimicrobial loop (^{122}YPVV^{125}).

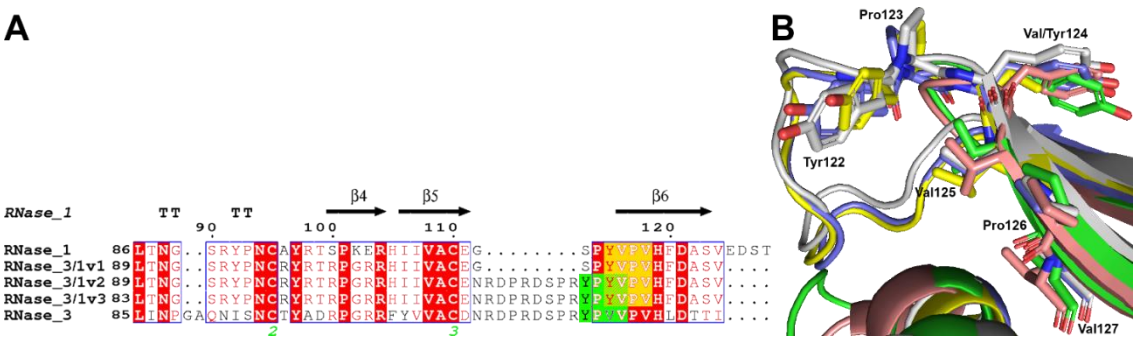

Figure 5. A) Sequence alignment of the C-terminal of RNases 1, 3 and the three versions of RNase 3/1. In yellow the sequence tag which, being in the β6 sheet, does not act as LIR tag. In green, the LIR tag. **B**) Zoom of the putative LIR-AIM tag found. In salmon, RNase 1 (2k11.pdb); in yellow, RNase 3 (1qmt.pdb); in green, RNase 3/1-v1; in grey, RNase 3/-1-v2; in blue, RNase 3/1-v3 predicted structures. The residues of the putative tag are shown. Sequence numbering is according to the RNase 3. Picture was done by PyMOL 2.3.4, (Schrödinger LLC).

5 Discussion

RNase 3/1 was designed to achieve a chimeric RNase which was able to combine, on one hand, the high catalytic activity of RNase 1 and its affinity to ribonuclease inhibitor, and, on the other hand, the high antimicrobial activity of RNase 3. After a first characterization of the first version of RNase 3/1, which showed its potential as an antimicrobial protein (Prats-Ejarque et al., 2019), we decided to try to improve its activity into two new versions of the chimeric protein, RNase 3/1-v2 and RNase 3/1-v3. These two new versions of the protein present a catalytic activity lower than RNase 3/1-v1 against poly(U) and CpA (about 40 %). Interestingly, an enhancement of uridine versus cytidine preference at the main base binding site (B1) was observed for the constructs, and in particular for v3 (see table 1).

On the other hand, comparison of the secondary base (B2) preference of the three chimera versions highlighted the contribution of both parental proteins in the catalytic efficiency (Table 1). However, the data is also emphasizing the main contribution of the B1 specificity over the secondary base selectivity. Surprisingly, the addition of the L7 loop of RNase 3 (113N – 122Y) induced a more pronounced reduction of the catalytic activity than the deletion of the flexible loop of RNase 1 (14D – 25Y), reported as key for the high catalytic efficiency of the latter (Gagné and Doucet, 2013). However, we should take into consideration the possibility that the absence of the 113-122 loop may indirectly alter the N-terminus position, based on the observed interaction between the C and N-terminus revealed by NMR and X-ray structural data of RNase 3 (Mallorquí-Fernández et al., 2000)(García-Mayoral et al., 2010).

Indeed, further insight into the predicted structures of the three RNase 3/1 versions by molecular dynamics allowed us to interpret the obtained results (see figure 6). In basis of the structural changes predicted by molecular dynamics, the R3-L7 loop would interact

with the N-terminal triggering a displacement of the first helix (see boxes 1 and 5 of figure 6). In the case of RNase 3/1-v2, this change in the interactions would affect the Lys44 of the active site, which weakly binds to the Gln14 (see boxes 2 and 3 of figure 6). The high cationic charge and side chain length of the R3-L7 loop, which places it nearby B2, would interfere in the interaction of the substrate with the binding sites, triggering a decrease of the catalytic activity. In the case of RNase 3/1-v3, the replacement of the flexible loop of RNase 1 by the more rigid loop of RNase 3, reduces the capacity of the two first helixes to readapt at the active site, provoking a major displacement of both helixes (see box 4 of figure 6) and forming a hydrophobic core similar to the one described for RNase 3 (Mallorquí-Fernández et al., 2000).

Surprisingly, due to the higher similitude to RNase 3, together with the decrease of the catalytic activity, we expected an increase of the cytidine preference, instead of the remarkable increase of the preference for uridine in the B_1 subsite observed in RNase 3/1-v2 and RNase 3/1-v3.

A closer look shows that the inclusion of Arg103 in the three versions of RNase 3/1 (Arg101 in RNase 3) could be involved in the higher preference for uridine. Arg103 can interact with Asp86, which binds to Thr48. This threonine residue (Thr45 in RNase A) has been reported to provide alternative binding modes to selectively accommodate either uridine or cytidine (Raines, 1998).

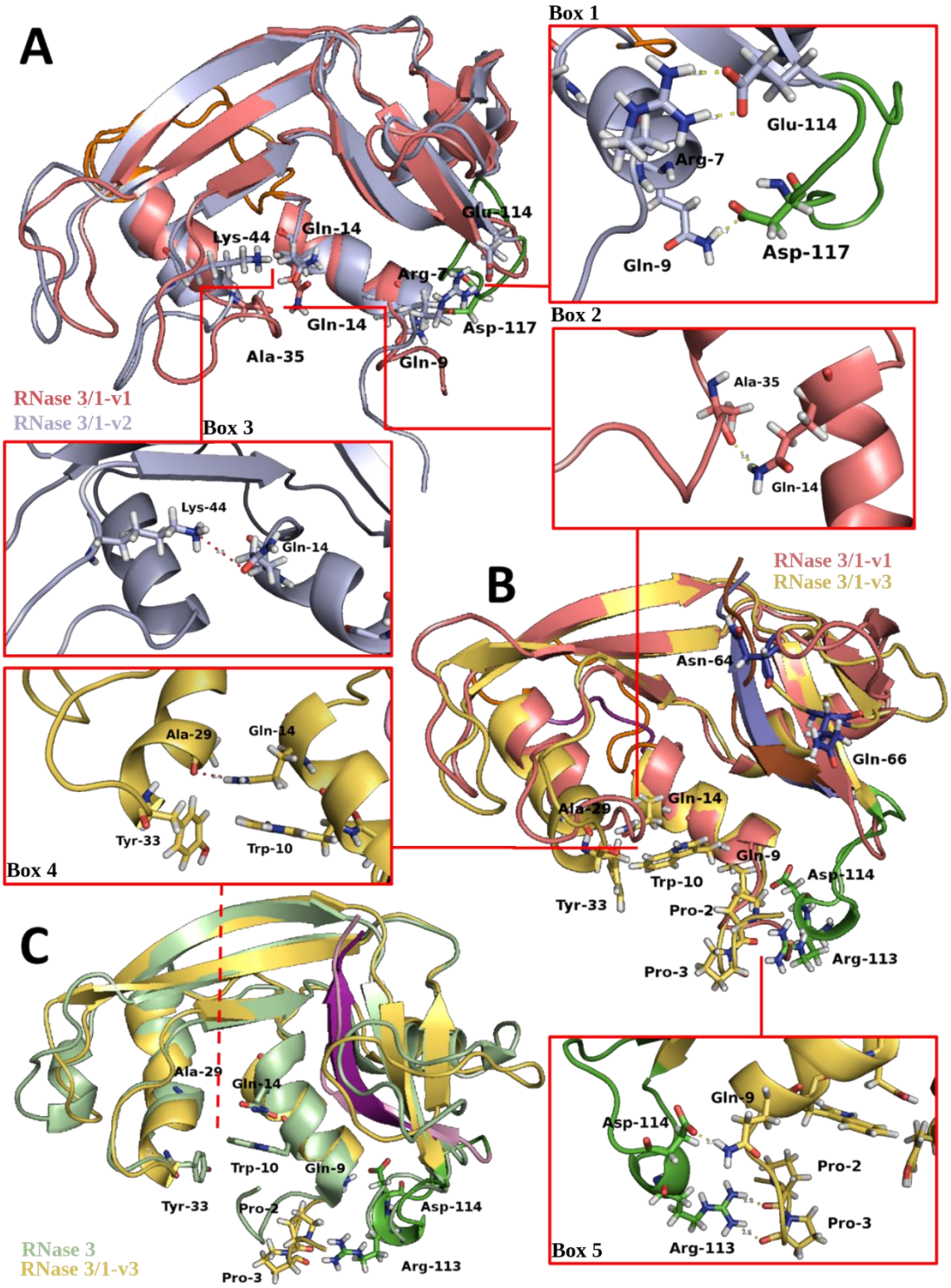

Figure 6. Overlapping of the different RNase 3/1 versions after 50 ns of molecular dynamics. Green numbers indicate the position of the α-helix in the RNase. Hydrogen bonds are shown. **A**) Overlapping of RNase 3/1-v1 with RNase 3/1-v2. In **box 1**, zoom of the interaction region of the N-terminal with the R3-L7 loop (dark green), which pulls down the α1 helix in RNase 3/1-v2, contrarily of the case of RNase 31-v1. In **box 2 and 3**, zoom of the hydrophobic cluster of RNase 3/1 and RNase 3/1-v2, which stabilizes the α1 helix. **B**) Overlapping of RNase 3/1-v1 and RNase 3/1-v3. As can be observed, when

the loop 14D – 25Y (magenta) is replaced by the loop 17S – 22R of RNase 3 (orange) there is an approaching between the α1 and α2 helixes. In blue, the β-sheet of the C-terminal of RNase 3/1 is highlighted; the region is partially destructured in RNase 3/1-v3 (pink). In **box 4**, zoom of the hydrophobic cluster that stabilizes the active site of RNase 3/1-v3, thanks to a weak hydrogen bond and a π-π interaction between Tyr33 and Trp10. In **box 5**, zoom of the interaction region of the N-terminal with the R3-L7 loop. **C**) Overlapping of RNase 3 (1qmt.pdb) (Boix et al., 1999a) and RNase 3/1-v3. The discontinuous line indicates the similarity between the clusters of both RNases. C-terminal β-sheet is highlighted in magenta.

Notwithstanding, the main goal of our work was to achieve a final chimera endowed with a high antimicrobial activity. The results indicate that addition of the R3-L7 loop reduces the antimicrobial activity of RNase 3/1, which is partly recovered by the incorporation of the R1-L1 loop. Whereas R1-L1 is long and flexible, R3-L1 is short and rigid. A wider spacing between both N-terminal helixes (essential for RNase 3 antibacterial activity (Torrent et al., 2011b)) could affect its bacterial membrane disruption ability. In accordance, when removing the R1-L1 loop (RNase 3/1-v3), we observe an increase of the LPS-binding and the antimicrobial activity, probably due to its more similar structure to RNase 3.

On the other hand, the increase of the antimicrobial activity of RNase 3/1-v3 is achieved at the cost of a slight increase of the protein toxicity in the tested human cell lines. On the contrary, no increase of the cytotoxicity is observed for RNase 3/1-v2. Considering the obtained results for RI inhibition (see table 4), we can conclude that the R1-L1 loop of RNase 1 is important for the interaction with the RI. Therefore, we suspect that the reduction of the protein interaction with the RI would be the main cause for the increase of the cytotoxicity of RNase 3/1-v3. Redesigning this loop to keep the antimicrobial and catalytic activities while enhancing the RI interaction should be the next step in this chimeric protein rational design.

Recent studies in our group showed that RNase 3 has the ability to induce autophagy in human macrophages, a property not shared by RNase 1 (Lu et al., 2019). Taking into account these results, we tested here the autophagy-inducing ability of our chimeric proteins. Interestingly, although RNase 3/1-v1 has no ability to induce autophagy, the other two versions (where we added the R3-L7 loop) do present the ability to induce autophagy.

Recently, it has been reported that RNase 2 (which share about 70% amino acid identity with RNase 3 and also includes an equivalent L7 loop, see figure S5), colocalizes with endosomal and lysosomal markers (Ostendorf et al., 2020). The protein endolysosomal localization will allow the compartment RNA degradation and subsequent activation of TLR8, inducing an immune response. Interestingly, the authors suggest that the cooperative activity of RNase 2 together with RNase T2, which also allows the activation of the TLR8 pathway, will be mainly due to uridine release from foreign RNA cleavage. To note, while RNase 2 cleaves at dinucleotides with a preference for uridine at B1,

RNase T2 preferentially cuts the substrate when an uridine is found at the B2 site. The TLR 8 activation by uridine could explain the observed preference for uridine at the B1 site in human eosinophil RNases (Sorrentino, 2010; Boix et al., 2013).

It has been reported that Toll-like receptors are able to induce selective autophagy as an immune response (Delgado et al., 2008; Delgado and Deretic, 2009; Campbell and Spector, 2012; Oh and Lee, 2014; Franco et al., 2017). Considering the recently reported mechanism of stimulation of TLR8 by RNase 2 (Ostendorf et al., 2020) and the importance of autophagy in the intracellular antimicrobial action of RNases (Lu et al., 2019), TLR activation could be the factor that triggers autophagy during RNases immune response to cell infection.

Nevertheless, as mentioned before, we did not observe any difference in the autophagy induction levels when a catalytically inactive RNase (H15A) was assayed (Lu et al., 2019) (Figure S2). Likewise, correlation between autophagy induction and agglutinating activity was also discarded (Figure S3). Moreover, when comparing the three versions of RNase 3/1, we identify the R3-L7 as the unique region absent in v1, the only construct devoid of autophagy activity. Moreover, screening on all canonical RNases for putative tag sequences associated to protein subcellular localization (figure S5 and table S1) revealed the presence of specific motives associated to lysosomal compartment and autophagosome formation. Of particular interest is the motif YXXΨ (where Ψ is a hydrophobic residue), found in RNases 1-3 and 6-8, and reported to bind to a subunit of the clathrin associate protein complexes AP1 and AP2 (Ohno et al., 1995, 1998; Boll et al., 1996; Owen and Evans, 1998; Kurten, 2003). To note, this observed tag (^{122}YPVV^{125}), is not only a stimulator of the clathrin complex, but also an LC3-interacting region (LIR) motif (Birgisdottir et al., 2013; Popelka and Klionsky, 2015), whose consensus sequence [W/F/Y]xx[L/I/V] also coincides with the sequence found in the antimicrobial loop (^{122}YPVV^{125}).

Although the tag sequence is present in the parental RNases 1, 3 and the three versions of RNase 3/1, its structural arrangement is distinct in each protein. While in the case of RNase 1 and RNase 3/1-v1 the tag falls into the β6 sheet (figure 6), in RNase 3 and the other two versions of RNases 3/1, this tag falls in an intrinsically disordered protein region (IDPR), the R3-L7 loop. As it has been reported recently (Popelka and Klionsky, 2015), the functional LIR are short linear motifs which arise from an IDPR.

LIR motifs are present in both autophagy receptors and adaptors, which are recognized by Atg8 (LC3) proteins (Noda et al., 2010; Birgisdottir et al., 2013; Wild et al., 2014). Atg8 proteins are essential for the autophagosome formation, as well as its membrane elongation and the final closure and the fusion with lysosome (Yang and Klionsky, 2009; Klionsky and Deretic, 2011; Johansen and Lamark, 2020). In selective autophagy, the Atg8 proteins located on the inner membrane are involved on the recruitment of the autophagosome cargo by binding to autophagy receptors (Birgisdottir et al., 2013; Johansen and Lamark, 2020).

The sequence found in RNase 3 is an Y-type motif (the motifs which present tyrosine in the beginning of the consensus sequence. The Y-type motifs are reported to be the less common of the LIR motifs (Birgisdottir et al., 2013), and the ones with lowest affinity with LC3 proteins (Rozenknop et al., 2011). Taking this into account, the RNase recruitment by Atg8 proteins would take place at a lower ratio than autophagy receptors. Which could be the role then of the RNase recruitment into the autophagosome cargo? We suggest that the presence of RNases in the autophagosome could be involved in the killing of the pathogen inside the autophagosome, as well as the removal of the pathogenic RNA.

In the light of these data, taking into account that the activation of the autophagy does not seem to be associated with the catalytic activity (figure S2) (Lu et al., 2019), it would be tempting to conclude that it is the LIR motif the one responsible of the autophagosome recruitment. However, an overall outlook of the general pathway leads us to think that, as suggested before (Chakrabarti et al., 2012; Siddiqui and Malathi, 2012; Fiorini et al., 2014, 2015; Ostendorf et al., 2020), the catalytic activity might also contribute to the autophagic response. We can speculate that the RNase recruited by LC3 into the autophagosome, could help to remove the bacteria inside the vesicle.

Altogether, we can hypothesize that the inclusion of the R3-L7 loop improves the antibacterial activity, not only because of its higher cationicity, but also due to its ability to induce autophagy.

Overall, a global side-by-side comparison of the parental and chimeric proteins properties, as illustrated in Figure 7, corroborates a successful strategy: the structure-based approach has assisted us in the design of a novel antimicrobial protein. Notwithstanding, further work is required to optimize our construct to ensure the non-toxicity and maximum biological activity of our lead protein for potential antimicrobial therapy.

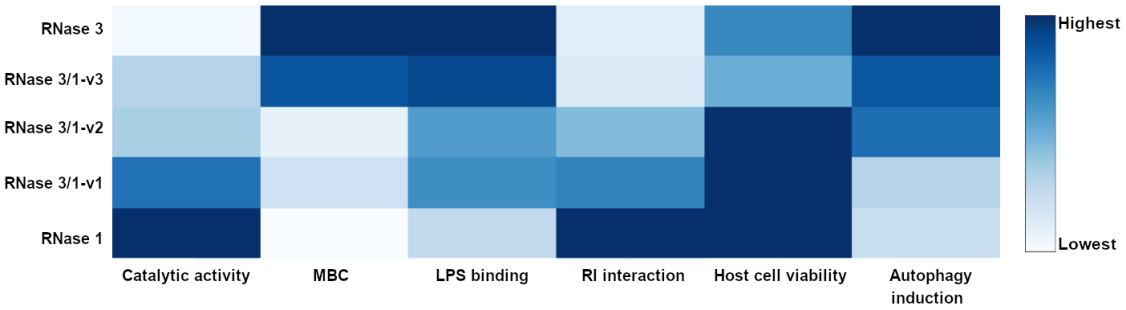

Figure 7. Heatmap depiction for activity comparison of RNase 1, 3 and the three versions of RNase 3/1. All the results were normalized as relative to the highest detected activity and the heatmap was depicted by Plotly and GIMP.

6 Conclusions

In this work we designed and characterized three chimeric proteins that combines RNase 1 high catalytic activity together with RNase 3 antimicrobial properties. A first RNase 3/1 chimera achieved a significant increase in the protein catalytic activity respect to RNase 3 but could not fully reproduce its antimicrobial efficiency. Two new versions (RNase 3/1-v2 and v3) incorporate a C-terminal loop key for the protein antimicrobial and autophagy activity. In addition, the RNase3/1-v3 lacks an N-terminal loop, which provides flexibility to RNase1 but may induce some reshaping of the overall 3D conformation due to potential steric clashes between the N and C- terminus regions. The RNase3/1-v3 shows an enhanced antimicrobial activity and catalytic activity in relation to v2. However, the removal of the flexible N-terminal loop in our third construct is in detriment of its RI interaction and slightly increases the protein toxicity. Interestingly, we have found an LIR motif in RNase 3, which is present in the RNase 3/1-v2 and v3 versions and is associated to the autophagosome formation. The presence of the LIR tag correlates with the observed autophagy induction activity. Further work is needed to increase the affinity to the ribonuclease inhibitor, reducing its cytotoxicity.

7 Conflict of Interest

The authors declare that the research was conducted in the absence of any commercial or financial relationships that could be construed as a potential conflict of interest.

8 Author Contributions

EB and GP conceived and designed the experiments. HL, GP, LL, RA and SV performed the experimental work. EB, GP and HL analysed the data. EB and GP drafted the manuscript. EB, GP and HL revised the final manuscript. All authors approved the final manuscript version.

9 Funding

Research work was supported by the Ministerio de Economía y Competitividad (SAF2015-66007P; PID2019-106123GB-I00) and by AGAUR, Generalitat de Catalunya (2016PROD00060; 2019LLAV00002), co-financed by FEDER funds. GP is a recipient of a PIF (UAB) predoctoral fellowship. LL was a recipient of a CSC predoctoral fellowship.

10 Acknowledgments

The authors wish to thank Clara Villalba for thoroughly revising the manuscript, and the *Laboratori d'Anàlisi i Fotodocumentació* (UAB), where RT-qPCR were performed.

11 References

Birgisdottir, Å. B., Lamark, T., and Johansen, T. (2013). The LIR motif - crucial for selective autophagy. *J. Cell Sci.* 126, 3237–3247. doi:10.1242/jcs.126128.

Boix, E. (2001). “Eosinophil Cationic Protein,” in *Methods in Enzymology* (Elsevier

Masson SAS), 287–305. doi:10.1016/S0076-6879(01)41159-1.

Boix, E., Blanco, J. a., Nogués, M. V., and Moussaoui, M. (2013). Nucleotide binding architecture for secreted cytotoxic endoribonucleases. *Biochimie* 95, 1087–1097. doi:10.1016/j.biochi.2012.12.015.

Boix, E., Leonidas, D. D., Nikolovski, Z., Nogués, M. V., Cuchillo, C. M., and Acharya, K. R. (1999a). Crystal structure of eosinophil cationic protein at 2.4 A resolution. *Biochemistry* 38, 16794–16801. doi:10.1021/bi9919145.

Boix, E., Nikolovski, Z., Moiseyev, G. P., Rosenberg, H. F., Cuchillo, C. M., and Nogués, M. V. (1999b). Kinetic and Product Distribution Analysis of Human Eosinophil Cationic Protein Indicates a Subsite Arrangement That Favors Exonuclease-type Activity. *J. Biol. Chem.* 274, 15605–15614. doi:10.1074/jbc.274.22.15605.

Boix, E., Salazar, V. a., Torrent, M., Pulido, D., Nogués, M. V., and Moussaoui, M. (2012). Structural determinants of the eosinophil cationic protein antimicrobial activity. *Biol. Chem.* 393, 801–815. doi:10.1515/hsz-2012-0160.

Boix, E., Wu, Y., Vasandani, V. M., Saxena, S. K., Ardelt, W., Ladner, J., et al. (1996). Role of the N terminus in RNase A homologues: differences in catalytic activity, ribonuclease inhibitor interaction and cytotoxicity. *J. Mol. Biol.* 257, 992–1007. doi:10.1006/jmbi.1996.0218.

Boll, W., Ohno, H., Songyang, Z., Rapoport, I., Cantley, L. C., Bonifacino, J. S., et al. (1996). Sequence requirements for the recognition of tyrosine-based endocytic signals by clathrin AP-2 complexes. *EMBO J.* 15, 5789–5795. doi:10.1002/j.1460-2075.1996.tb00965.x.

Bravo, J., Fernandez, E., Ribo, M., Dellorens, R., and Cuchillo, C. M. (1994). A Versatile Negative-Staining Ribonuclease Zymogram. *Anal. Biochem.* 219, 82–86. doi:10.1006/abio.1994.1234.

Bussi, G., Donadio, D., and Parrinello, M. (2007). Canonical sampling through velocity rescaling. *J. Chem. Phys.* 126. doi:10.1063/1.2408420.

Campbell, G. R., and Spector, S. A. (2012). Toll-Like Receptor 8 Ligands Activate a Vitamin D Mediated Autophagic Response that Inhibits Human Immunodeficiency Virus Type 1. *PLoS Pathog.* 8. doi:10.1371/journal.ppat.1003017.

Carreras, E., Boix, E., Navarro, S., Rosenberg, H. F., Cuchillo, C. M., and Nogués, M. V. (2005). Surface-exposed amino acids of eosinophil cationic protein play a critical role in the inhibition of mammalian cell proliferation. *Mol. Cell. Biochem.* 272, 1–7. doi:10.1007/s11010-005-4777-2.

Carreras, E., Boix, E., Rosenberg, H. F., Cuchillo, C. M., and Nogués, M. V. (2003). Both aromatic and cationic residues contribute to the membrane-lytic and bactericidal activity of eosinophil cationic protein. *Biochemistry* 42, 6636–6644. doi:10.1021/bi0273011.

Chakrabarti, a., Ghosh, P. K., Banerjee, S., Gaughan, C., and Silverman, R. H. (2012). RNase L Triggers Autophagy in Response to Viral Infections. *J. Virol.* 86, 11311–

11321. doi:10.1128/JVI.00270-12.

Cuchillo, C. M., Nogués, M. V., and Raines, R. T. (2011). Bovine Pancreatic Ribonuclease: Fifty Years of the First Enzymatic Reaction Mechanism. *Biochemistry* 50, 7835–7841. doi:10.1021/bi201075b.

Darden, T., York, D., and Pedersen, L. (1993). Particle mesh Ewald: An N·log(N) method for Ewald sums in large systems. *J. Chem. Phys.* 98, 10089. doi:10.1063/1.464397.

Debye, P. (1909). Näherungsformeln für die Zylinderfunktionen für große Werte des Arguments und unbeschränkt veränderliche Werte des Index. *Math. Ann.* 67, 535–558. doi:10.1007/BF01450097.

Delgado, M. A., and Deretic, V. (2009). Toll-like receptors in control of immunological autophagy. *Cell Death Differ.* 16, 976–983. doi:10.1038/cdd.2009.40.

Delgado, M. A., Elmaoued, R. A., Davis, A. S., Kyei, G., and Deretic, V. (2008). Toll-like receptors control autophagy. *EMBO J.* 27, 1110–1121. doi:10.1038/emboj.2008.31.

Dickson, K. A., Haigis, M. C., and Raines, R. T. (2005). Ribonuclease Inhibitor: Structure and Function. *Prog. Nucleic Acid Res. Mol. Biol.* 80, 349–374. doi:10.1016/S0079-6603(05)80009-1.

Domachowske, J. B., Dyer, K. D., Adams, A. G., Leto, T. L., and Rosenberg, H. F. (1998). Eosinophil cationic protein/RNase 3 is another RNase A-family ribonuclease with direct antiviral activity. *Nucleic Acids Res.* 26, 3358–3363. doi:10.1093/nar/26.14.3358.

Doucet, N., Watt, E. D., and Loria, J. P. (2009). The flexibility of a distant loop modulates active site motion and product release in ribonuclease A. *Biochemistry* 48, 7160–7168. doi:10.1021/bi900830g.

Espargaró, A., Sabate, R., and Ventura, S. (2012). Thioflavin-S staining coupled to flow cytometry. A screening tool to detect in vivo protein aggregation. *Mol. Biosyst.* 8, 2839–2844. doi:10.1039/c2mb25214g.

Essmann, U., Perera, L., Berkowitz, M. L., Darden, T., Lee, H., and Pedersen, L. G. (1995). A smooth particle mesh Ewald method. *J. Chem. Phys.* 103, 8577. doi:10.1063/1.470117.

Fiorini, C., Cordani, M., Gotte, G., Picone, D., and Donadelli, M. (2015). Onconase induces autophagy sensitizing pancreatic cancer cells to gemcitabine and activates Akt/mTOR pathway in a ROS-dependent manner. *Biochim. Biophys. Acta - Mol. Cell Res.* 1853, 549–560. doi:10.1016/j.bbamcr.2014.12.016.

Fiorini, C., Gotte, G., Donnarumma, F., Picone, D., and Donadelli, M. (2014). Bovine seminal ribonuclease triggers Beclin1-mediated autophagic cell death in pancreatic cancer cells. *Biochim. Biophys. Acta - Mol. Cell Res.* 1843, 976–984. doi:10.1016/j.bbamcr.2014.01.025.

Fowler, C. B., Evers, D. L., O'Leary, T. J., and Mason, J. T. (2011). Antigen retrieval

causes protein unfolding: Evidence for a linear epitope model of recovered immunoreactivity. *J. Histochem. Cytochem.* 59, 366–381. doi:10.1369/0022155411400866.

Franco, L. H., Fleuri, A. K. A., Pellison, N. C., Quirino, G. F. S., Horta, C. V., De Carvalho, R. V. H., et al. (2017). Autophagy downstream of endosomal Toll-like receptor signaling in macrophages is a key mechanism for resistance to Leishmania major infection. *J. Biol. Chem.* 292, 13087–13096. doi:10.1074/jbc.M117.780981.

Gagné, D., and Doucet, N. (2013). Structural and functional importance of local and global conformational fluctuations in the RNase A superfamily. *FEBS J.* 280, 5596–5607. doi:10.1111/febs.12371.

Gagné, D., French, R. L., Narayanan, C., Simonović, M., Agarwal, P. K., and Doucet, N. (2015). Perturbation of the Conformational Dynamics of an Active-Site Loop Alters Enzyme Activity. *Structure* 23, 2256–2266. doi:10.1016/j.str.2015.10.011.

García-Mayoral, M. F., Moussaoui, M., De La Torre, B. G., Andreu, D., Boix, E., Nogués, M. V., et al. (2010). NMR structural determinants of eosinophil cationic protein binding to membrane and heparin mimetics. *Biophys. J.* 98, 2702–2711. doi:10.1016/j.bpj.2010.02.039.

Goncalves, K. A., Silberstein, L., Li, S., Severe, N., Hu, M. G., Yang, H., et al. (2016). Angiogenin Promotes Hematopoietic Regeneration by Dichotomously Regulating Quiescence of Stem and Progenitor Cells. *Cell* 166, 894–906. doi:10.1016/j.cell.2016.06.042.

Hess, B. (2008). P-LINCS: A parallel linear constraint solver for molecular simulation. *J. Chem. Theory Comput.* 4, 116–122. doi:10.1021/ct700200b.

Hooper, L. V, Stappenbeck, T. S., Hong, C. V, and Gordon, J. I. (2003). Angiogenins: a new class of microbicidal proteins involved in innate immunity. *Nat. Immunol.* 4, 269–273. doi:10.1038/ni888.

Johansen, T., and Lamark, T. (2020). Selective Autophagy: ATG8 Family Proteins, LIR Motifs and Cargo Receptors. *J. Mol. Biol.* 432, 80–103. doi:10.1016/j.jmb.2019.07.016.

Jorgensen, W. L., Chandrasekhar, J., Madura, J. D., Impey, R. W., and Klein, M. L. (1983). Comparison of simple potential functions for simulating liquid water. *J. Chem. Phys.* 79, 926. doi:10.1063/1.445869.

Klionsky, D., and Deretic, V. (2011). Autophagy: molecular mechanisms and disease outcomes. *Nat. Rev. Mol. Cell Biol.*, 2011. Available at: http://www.bostonbiochem.com/sites/bostonbiochem.com/files/new-scientific-poster-autophagy-molecular-mechanisms-and-disease-outcomes.pdf.

Koczera, P., Martin, L., Marx, G., and Schuerholz, T. (2016). The ribonuclease a superfamily in humans: Canonical RNases as the buttress of innate immunity. *Int. J. Mol. Sci.* 17.

Kopfnagel, V., Wagenknecht, S., Harder, J., Hofmann, K., Kleine, M., Buch, A., et al.

(2018). RNase 7 Strongly Promotes TLR9-Mediated DNA Sensing by Human Plasmacytoid Dendritic Cells. *J. Invest. Dermatol.* 138, 872–881. doi:10.1016/j.jid.2017.09.052.

Kurten, R. C. (2003). Sorting motifs in receptor trafficking. *Adv. Drug Deliv. Rev.* 55, 1405–1419. doi:10.1016/j.addr.2003.07.003.

Lindorff-Larsen, K., Piana, S., Palmo, K., Maragakis, P., Klepeis, J. L., Dror, R. O., et al. (2010). Improved side-chain torsion potentials for the Amber ff99SB protein force field. *Proteins Struct. Funct. Bioinforma.* 78, 1950–1958. doi:10.1002/prot.22711.

Livak, K. J., and Schmittgen, T. D. (2001). Analysis of relative gene expression data using real-time quantitative PCR and the 2-ΔΔCT method. *Methods* 25, 402–408. doi:10.1006/meth.2001.1262.

Lomax, J. E., Bianchetti, C. M., Chang, A., Phillips, G. N., Fox, B. G., and Raines, R. T. (2014). Functional evolution of ribonuclease inhibitor: Insights from birds and reptiles. *J. Mol. Biol.* 426, 3041–3056. doi:10.1016/j.jmb.2014.06.007.

Lomax, J. E., Eller, C. H., and Raines, R. T. (2017). Comparative functional analysis of ribonuclease 1 homologs: Molecular insights into evolving vertebrate physiology. *Biochem. J.* 474, 2219–2233. doi:10.1042/BCJ20170173.

Lu, L., Arranz-Trullén, J., Prats-Ejarque, G., Pulido, D., Bhakta, S., and Boix, E. (2019). Human Antimicrobial RNases Inhibit Intracellular Bacterial Growth and Induce Autophagy in Mycobacteria-Infected Macrophages. *Front. Immunol.* 10. doi:10.3389/fimmu.2019.01500.

Lu, L., Li, J., Moussaoui, M., and Boix, E. (2018). Immune modulation by human secreted RNases at the extracellular space. *Front. Immunol.* 9, 1–20. doi:10.3389/fimmu.2018.01012.

Lu, L., Wei, R., Prats-Ejarque, G., Goetz, M., Wang, G., Torrent, M., et al. (2020). Human RNase3 immune-modulation by catalytic-dependent and independent modes in a macrophage-cell line infection model. *Cell Mol. Life Sci.*, Accepted Manuscript.

Mallorquí-Fernández, G., Pous, J., Peracaula, R., Aymamí, J., Maeda, T., Tada, H., et al. (2000). Three-dimensional crystal structure of human eosinophil cationic protein (RNase 3) at 1.75 Å resolution. *J. Mol. Biol.* 300, 1297–1307. doi:10.1006/JMBI.2000.3939.

Noda, N. N., Ohsumi, Y., and Inagaki, F. (2010). Atg8-family interacting motif crucial for selective autophagy. *FEBS Lett.* 584, 1379–1385. doi:10.1016/j.febslet.2010.01.018.

Nosé, S., and Klein, M. L. (1983). Constant pressure molecular dynamics for molecular systems. *Mol. Phys.* 50, 1055–1076. doi:10.1080/00268978300102851.

Oh, J. E., and Lee, H. K. (2014). Pattern recognition receptors and autophagy. *Front. Immunol.* 5, 1–7. doi:10.3389/fimmu.2014.00300.

Ohno, H., Aguilar, R. C., Yeh, D., Taura, D., Saito, T., and Bonifacino, J. S. (1998). The

medium subunits of adaptor complexes recognize distinct but overlapping sets of tyrosine-based sorting signals. *J. Biol. Chem.* 273, 25915–25921. doi:10.1074/jbc.273.40.25915.

Ohno, H., Stewart, J., Fournier, M. C., Bosshart, H., Rhee, I., Miyatake, S., et al. (1995). Interaction of tyrosine-based sorting signals with clathrin-associated proteins. *Science (80-.).* 269, 1872–1875. doi:10.1126/science.7569928.

Ostendorf, T., Zillinger, T., Andryka, K., Schlee-Guimaraes, T. M., Schmitz, S., Marx, S., et al. (2020). Immune Sensing of Synthetic, Bacterial, and Protozoan RNA by Toll-like Receptor 8 Requires Coordinated Processing by RNase T2 and RNase 2. *Immunity* 52, 591-605.e6. doi:10.1016/j.immuni.2020.03.009.

Owen, D. J., and Evans, P. R. (1998). A structural explanation for the recognition of tyrosine-based endocytotic signals. *Science (80-.).* 282, 1327–1332. doi:10.1126/science.282.5392.1327.

Páll, S., and Hess, B. (2013). A flexible algorithm for calculating pair interactions on SIMD architectures. *Comput. Phys. Commun.* 184, 2641–2650. doi:10.1016/j.cpc.2013.06.003.

Palmer, I., and Wingfield, P. T. (2004). "Preparation and Extraction of Insoluble (Inclusion-Body) Proteins from Escherichia coli," in *Current Protocols in Protein Science* (Hoboken, NJ, USA: John Wiley & Sons, Inc.), 6.3.1-6.3.18. doi:10.1002/0471140864.ps0603s38.

Parrinello, M., and Rahman, A. (1981). Polymorphic transitions in single crystals: A new molecular dynamics method. *J. Appl. Phys.* 52, 7182–7190. doi:10.1063/1.328693.

Phipps, S., En Lam, C., Mahalingam, S., Newhouse, M., Ramirez, R., Rosenberg, H. F., et al. (2007). Eosinophils contribute to innate antiviral immunity and promote clearance of respiratory syncytial virus. *Blood* 110, 1578–1586. doi:10.1182/blood-2007-01-071340.

Pizzo, E., and D'Alessio, G. (2007). The success of the RNase scaffold in the advance of biosciences and in evolution. *Gene* 406, 8–12. doi:10.1016/j.gene.2007.05.006.

Popelka, H., and Klionsky, D. J. (2015). Analysis of the native conformation of the LIR/AIM motif in the Atg8/LC3/GABARAP-binding proteins. *Autophagy* 11, 2153–2159. doi:10.1080/15548627.2015.1111503.

Prats-Ejarque, G., Li, J., Ait-Ichou, F., Lorente, H., and Boix, E. (2019). Testing a Human Antimicrobial RNase Chimera Against Bacterial Resistance. *Front. Microbiol.* 10, 1–14. doi:10.3389/fmicb.2019.01357.

Pronk, S., Páll, S., Schulz, R., Larsson, P., Bjelkmar, P., Apostolov, R., et al. (2013). GROMACS 4.5: A high-throughput and highly parallel open source molecular simulation toolkit. *Bioinformatics* 29, 845–854. doi:10.1093/bioinformatics/btt055.

Pulido, D., Arranz-Trullén, J., Prats-Ejarque, G., Velázquez, D., Torrent, M., Moussaoui, M., et al. (2016). Insights into the Antimicrobial Mechanism of Action of Human RNase6: Structural Determinants for Bacterial Cell Agglutination and Membrane

Permeation. *Int. J. Mol. Sci.* 17, 552. doi:10.3390/ijms17040552.

Pulido, D., Villalba, C., Prats-Ejarque, G., Albacar, M., Moussaoui, M., Andreu, D., et al. (2018). Positional scanning library applied to the human eosinophil cationic protein/RNase 3 N-terminus reveals novel and potent antibiofilm peptides. *Eur. J. Med. Chem.* 152, 590–599. doi:10.1016/j.ejmech.2018.05.012.

Rademacher, F., Dreyer, S., Kopfnagel, V., Gläser, R., Werfel, T., and Harder, J. (2019). The Antimicrobial and Immunomodulatory Function of RNase 7 in Skin. *Front. Immunol.* 10, 1–11. doi:10.3389/fimmu.2019.02553.

Raines, R. T. (1998). Ribonuclease A. *Chem. Rev.* 98, 1045–1066. doi:10.1021/cr960427h.

Robert, X., and Gouet, P. (2014). Deciphering key features in protein structures with the new ENDscript server. *Nucleic Acids Res.* 42, 320–324. doi:10.1093/nar/gku316.

Rosenberg, H. F. (1995). Recombinant human eosinophil cationic protein. Ribonuclease activity is not essential for cytotoxicity. *J. Biol. Chem.* 270, 7876–7881.

Rosenberg, H. F. (2008). RNase A ribonucleases and host defense: an evolving story. *J. Leukoc. Biol.* 83, 1079–1087. doi:10.1189/jlb.1107725.

Rozenknop, A., Rogov, V. V., Rogova, N. Y., Löhr, F., Güntert, P., Dikic, I., et al. (2011). Characterization of the interaction of GABARAPL-1 with the LIR motif of NBR1. *J. Mol. Biol.* 410, 477–487. doi:10.1016/j.jmb.2011.05.003.

Rutkoski, T. J., Kurten, E. L., Mitchell, J. C., and Raines, R. T. (2005). Disruption of shape-complementarity markers to create cytotoxic variants of ribonuclease A. *J. Mol. Biol.* 354, 41–54. doi:10.1016/j.jmb.2005.08.007.

Rutkoski, T. J., and Raines, R. T. (2008). Evasion of ribonuclease inhibitor as a determinant of ribonuclease cytotoxicity. *Curr. Pharm. Biotechnol.* 9, 185–189. doi:10.2174/138920108784567344.

Salazar, V. A., Arranz-Trullén, J., Navarro, S., Blanco, J. A., Sánchez, D., Moussaoui, M., et al. (2016). Exploring the mechanisms of action of human secretory RNase 3 and RNase 7 against Candida albicans. *Microbiologyopen*, 1–16. doi:10.1002/mbo3.373.

Sánchez, D., Moussaoui, M., Carreras, E., Torrent, M., Nogués, V., and Boix, E. (2011). Mapping the eosinophil cationic protein antimicrobial activity by chemical and enzymatic cleavage. *Biochimie* 93, 331–338. doi:10.1016/j.biochi.2010.10.005.

Siddiqui, M. A., and Malathi, K. (2012). RNase L induces autophagy via c-Jun N-terminal kinase and double-stranded RNA-dependent protein kinase signaling pathways. *J. Biol. Chem.* 287, 43651–43664. doi:10.1074/jbc.M112.399964.

Sievers, F., and Higgins, D. G. (2018). Clustal Omega for making accurate alignments of many protein sequences. *Protein Sci.* 27, 135–145. doi:10.1002/pro.3290.

Sorrentino, S. (2010). The eight human “canonical” ribonucleases: Molecular diversity,

catalytic properties, and special biological actions of the enzyme proteins. *FEBS Lett.* 584, 2194–2200. doi:10.1016/j.febslet.2010.04.018.

Torrent, M., Andreu, D., Nogués, V. M., and Boix, E. (2011a). Connecting peptide physicochemical and antimicrobial properties by a rational prediction model. *PLoS One* 6, e16968. doi:10.1371/journal.pone.0016968.

Torrent, M., Cuyás, E., Carreras, E., Navarro, S., López, O., De La Maza, A., et al. (2007). Topography studies on the membrane interaction mechanism of the eosinophil cationic protein. *Biochemistry* 46, 720–733. doi:10.1021/bi061190e.

Torrent, M., de la Torre, B. G., Nogués, V. M., Andreu, D., and Boix, E. (2009). Bactericidal and membrane disruption activities of the eosinophil cationic protein are largely retained in an N-terminal fragment. *Biochem. J.* 421, 425–434. doi:10.1042/BJ20082330.

Torrent, M., Navarro, S., Moussaoui, M., Nogu?s, M. V., and Boix, E. (2008). Eosinophil Cationic Protein High-Affinity Binding to Bacteria-Wall Lipopolysaccharides and Peptidoglycans. *Biochemistry* 47, 3544–3555. doi:10.1021/bi702065b.

Torrent, M., Odorizzi, F., Nogués, M. V., Boix, E., Nogues, M. V, and Boix, E. (2010). Eosinophil cationic protein aggregation: identification of an N-terminus amyloid prone region. *Biomacromolecules* 11, 1983–1990. doi:10.1021/bm100334u.

Torrent, M., Pulido, D., de la Torre, B. G., García-Mayoral, M. F., Nogués, M. V., Bruix, M., et al. (2011b). Refining the Eosinophil Cationic Protein Antibacterial Pharmacophore by Rational Structure Minimization. *J. Med. Chem.* 54, 5237–5244. doi:10.1021/jm200701g.

Torrent, M., Pulido, D., Nogués, M. V., and Boix, E. (2012). Exploring New Biological Functions of Amyloids: Bacteria Cell Agglutination Mediated by Host Protein Aggregation. *PLoS Pathog.* 8. doi:10.1371/journal.ppat.1003005.

Torrent, M., Pulido, D., Valle, J., Nogués, M. V., Andreu, D., and Boix, E. (2013). Ribonucleases as a host-defence family: evidence of evolutionarily conserved antimicrobial activity at the N-terminus. *Biochem. J.* 456, 99–108. doi:10.1042/BJ20130123.

Venge, P., Byström, J., Carlson, M., Håkansson, L., Karawacjzyk, M., Peterson, C., et al. (1999). Eosinophil cationic protein (ECP): Molecular and biological properties and the use of ECP as a marker of eosinophil activation in disease. *Clin. Exp. Allergy* 29, 1172–1186. doi:10.1046/j.1365-2222.1999.00542.x.

Webb, B., and Sali, A. (2016). Comparative Protein Structure Modeling Using MODELLER. *Curr. Protoc. Protein Sci.*, 2.9.1-2.9.37. doi:10.1002/cpps.20.

Wild, P., McEwan, D. G., and Dikic, I. (2014). The LC3 interactome at a glance. *J. Cell Sci.* 127, 3–9. doi:10.1242/jcs.140426.

Xu, L., Liao, W. L., Lu, Q. J., Li, C. G., Yuan, Y., Xu, Z. Y., et al. (2016). ANG Promotes Proliferation and Invasion of the Cell of Lung Squamous Carcinoma by Directly Up-Regulating HMGA2. *J. Cancer* 7, 862–871. doi:10.7150/jca.14440.

Yang, J. T., Wu, C. S. C., and Martinez, H. M. (1986). Calculation of Protein Conformation from Circular Dichroism. *Methods Enzymol.* 130, 208–269. doi:10.1016/0076-6879(86)30013-2.

Yang, Z., and Klionsky, D. J. (2009). An overview of the molecular mechanism of autophagy. *Curr. Top. Microbiol. Immunol.* 335, 1–32. doi:10.1007/978-3-642-00302-8-1.

Design of an RNase chimera for antimicrobial therapy
Supplementary material

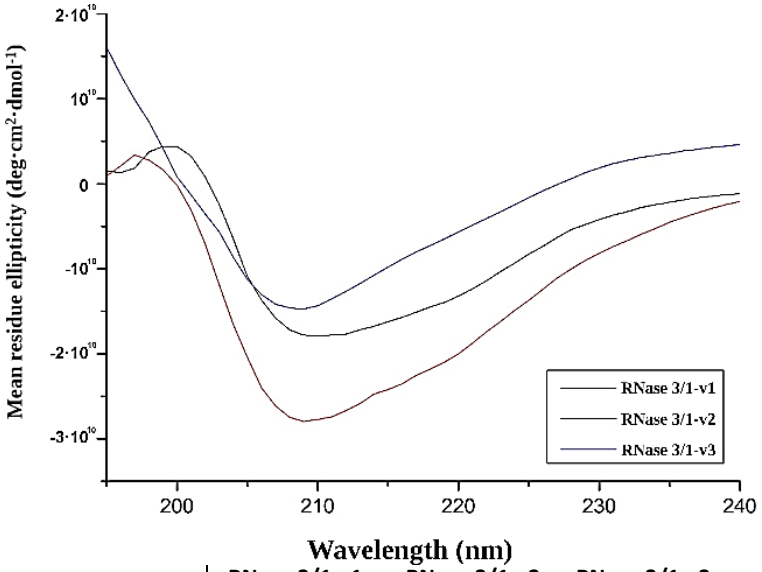

	RNase 3/1-v1	RNase 3/1-v2	RNase 3/1-v3
α-helix	18.3	14.1	18.6
β-sheet	59.4	41.6	62.8
Random coil	16.6	28.7	18.6

Figure S1. Circular dichroism spectra of the three versions of RNase 3/1. The embedded table indicates the estimated % of secondary structures for each construct.

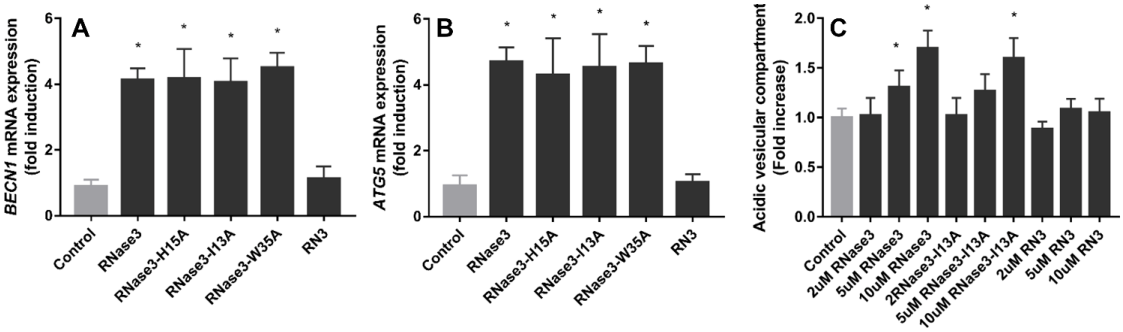

Figure S2. RAW 264.7 macrophages were treated by 10 µM of proteins or peptide (RNase 3, I13A, H15A and W35A and the RN(1-45)) for 24 hours. **Real-time qPCR measured the relative expression** of *BECN1* (**A**) and *ATG5* (**B**) genes, normalized by housekeeping gene *β-actin*. **Autolysosome formation measured by AO staining** (**C**). Results are shown from 3 (**A** and **B**) or 8 (**C**) independent experiments (mean ± SD). * indicates significant difference compared with control group ($p < 0.05$). RNase 3-H15A data are taken from (Lu et al., 2019).

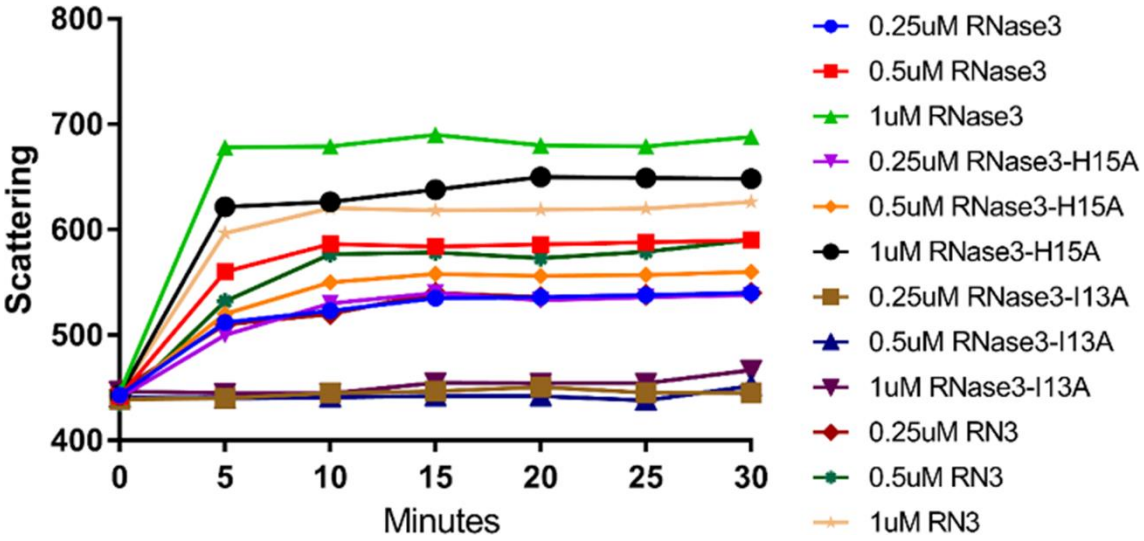

Figure S3. Liposome aggregation by different timing points and/or concentration of protein or peptide. Kinetic of RNase 3 derivates in aggregating liposomes. Protein or peptide was incubated with 200 µM of liposomes at room temperature, the scattering intensity was recorded every 5 minutes, while no protein added is indicated as 0 minute point.

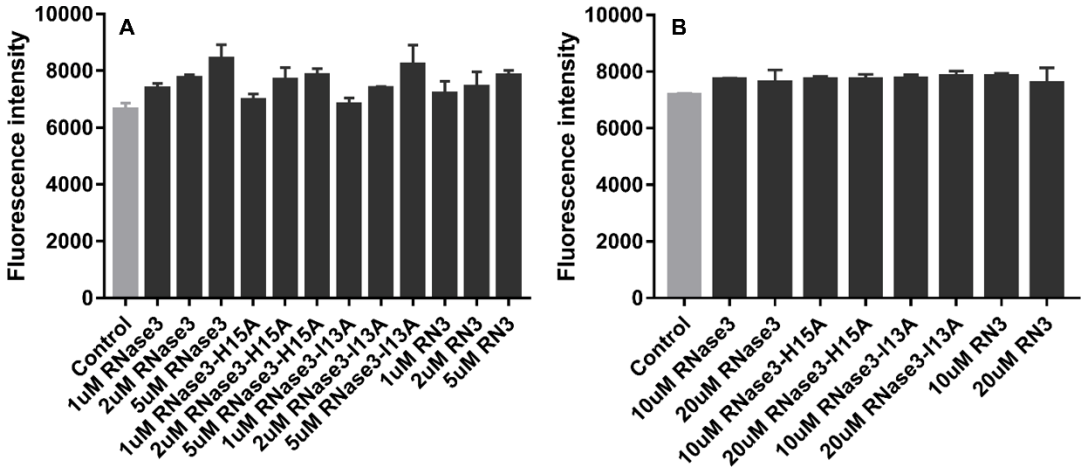

Figure S4. RAW 264.7 macrophages were infected with *M. aurum* and treated by 10 µM of proteins or peptide (RNase 3, I13A, H15A and W35A and the RN(1-45)) for 1 hour and then stained for 15 minutes by Thioflavin-S.

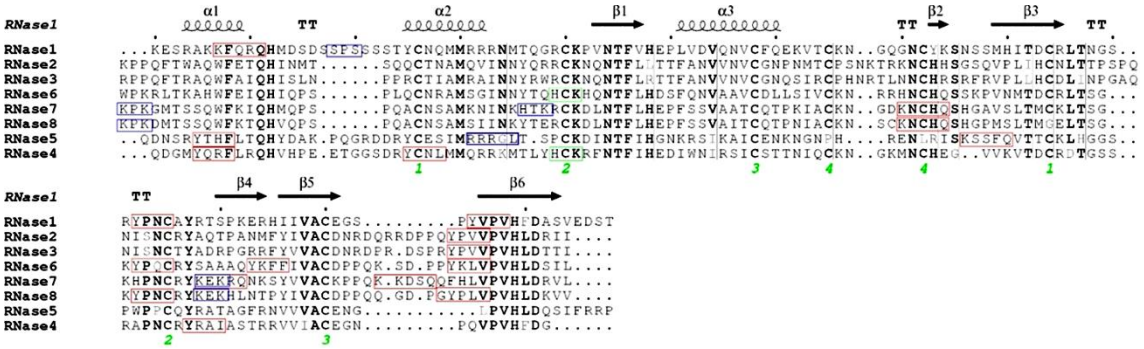

Figure S5. Putative signal tag of the subcellular localization of human RNases. Red box indicates the tag for lysosome; blue for endoplasmic reticulum and green for nucleus. Green numbers indicate disulphide bonds. The tags were identified by *LocSigDB* (Negi et al., 2015). Sequences are detailed in table S1.

Table S1. Prediction of the subcellular localization of human RNases by signal tag

	Signal	Aminoacid number/tag	Localization
RNase 1	Yx{2}[VILFWCM]	91-95/YPNC; 114-118/YVPV	Lysosome
	Kx{3}Q	6-11/KFQRQ	Lysosome
	SPS	17-20/SPS	Nucleus
RNase 2	Yx{2}[VILFWCM]	122-126/YPVV	Lysosome
RNase 3	Yx{2}[VILFWCM]	121-125YPVV	Lysosome
RNase 4	Yx{2}[VILFWCM]	4-8/YQRF; 23-27/YCNL; 93-97/YRAT	Lysosome
	[HK]x{1}K	37-40/HCK	Endoplasmic reticulum
RNase 5	Yx{2}[VILFWCM]	5-9/YTFH	Lysosome
	Kx{3}Q	72-77/KSSFQ	Lysosome
	RRRGL	30-35/RRRGL	Nucleus
RNase 6	Yx{2}[VILFWCM]	87-91/YPQC; 98-102/YKFF; 115-119/YKLV	Lysosome
	[HK]x{1}K	35-38/HCK	Endoplasmic reticulum
RNase 7	Kx{3}Q	66-71/KNCHQ; 93-98/KEKRQ; 110-115/KKDSQ	Lysosome
	[HK]x{1}K	0-3/KPK; 32-35/HTK; 93-96/KEK	Endoplasmic reticulum
RNase 8	Yx{2}[VILFWCM]	87-91/YPNC; 115-119/YPLV	Lysosome
	Kx{3}Q	66-71/KNCHQ	Lysosome
	GYx{2}[VILFWCM]	114-119/GYPLV	Lysosome
	[HK]x{1}K	0-3/KPK; 93-96/KEK	Endoplasmic reticulum

4. GENERAL DISCUSSION AND FUTURE PERSPECTIVES

4.1. Exploring RNase 6 RNA binding mode

The RNase 6 three dimensional structure was first solved at 1.72 Å in presence of sulphates[80]. This structure allowed us to identify an analogue region to the canonical RNase catalytic triad (His36, His39 and Lys87). Kinetic data suggested that these residues could act as a secondary active site, with a remarkable preference for polynucleotide substrates. In this thesis two alternative crystal forms of human RNase 6 at atomic resolution (1.04 Å and 1.10 Å) have been characterized (Figure 10). Several aspects of the kinetical behaviour of RNase 6 can be explained thanks to these structures.

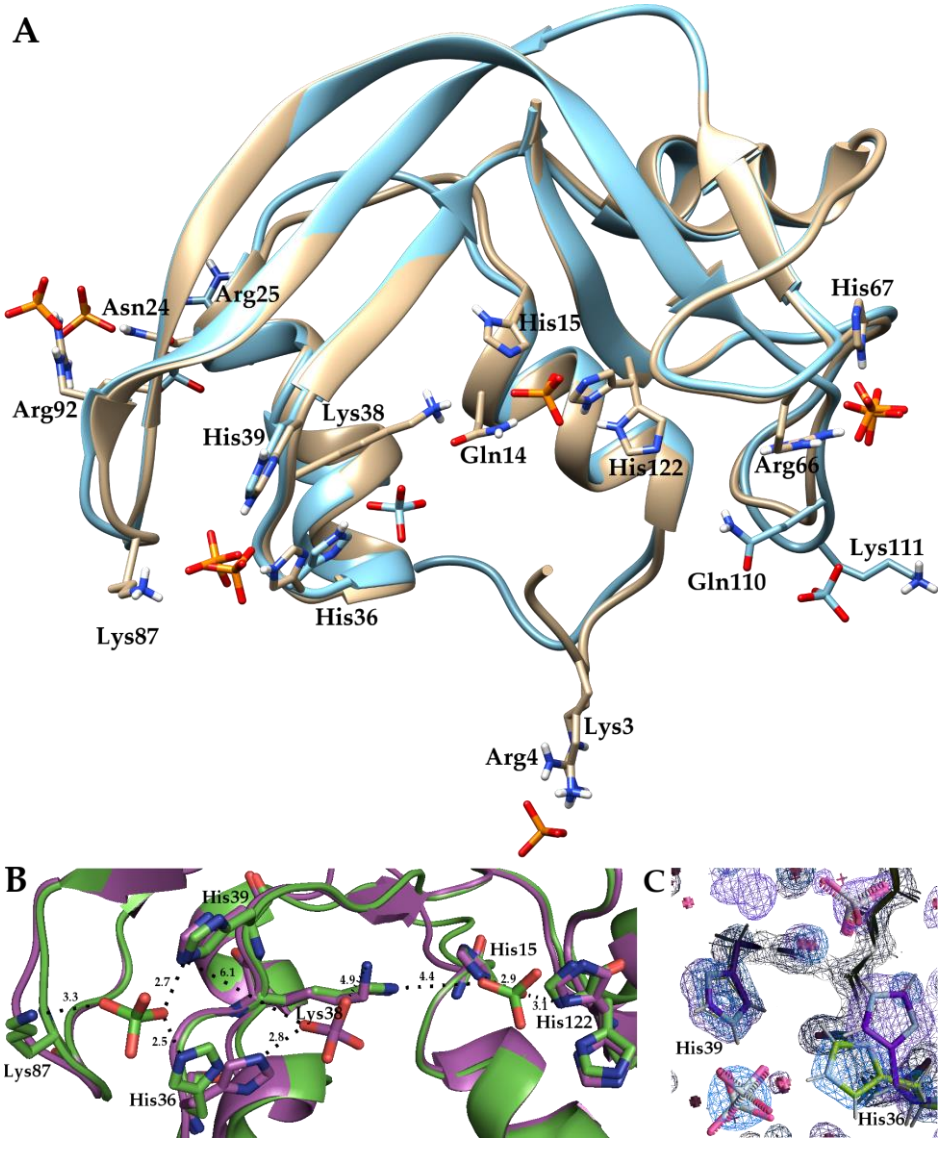

Figure 10. **A**) Overlapping of the two new crystallographic structures of RNase 6. The cubic form (PDB ID:5OAB) is drawn in ocher and the orthorhombic form (PDB ID:6ENP) in blue. The corresponding phosphate anions are shown in orange and blue respectively). The protein phosphate interacting residues are shown. **B**) Detail binding interactions at both active sites. In green, 5OAB.pdb, in magenta 6ENP.pdb. The distances between residues and phosphates are indicated. The hydrogen bond interactions are shown in yellow. The picture was drawn with *PyMOL 1.7.2* (Schrödinger, LLC). **C**) Detail of the His36/39 region. $2F_o$ -F_c maps at 1.5 σ RMSD of 5OAB (blue) and 6ENP (magenta). Maps were superposed with PHENIX[152] and the image has been obtained with Coot 0.8[153].

First of all, the phosphate anions bound to the RNase 6 structure allowed us to identify the unique substrate binding mode of RNase 6. The present data confirm our previous molecular dynamic studies using an RNase 6-heptanucleotide complex that outlined an extended cationic cavity groove all along the enzyme cleft[80]. Combining all the current available information, we can identify nine phosphate-binding sites in the RNase 6 structure that could outline a subsite binding architecture adapted for the interaction with extended oligonucleotides.

Secondly, analysis of structural data suggested the presence of a secondary active site. Site-directed mutagenesis and kinetic studies confirmed the presence of an additional catalytic triad conformed by His36/His39 and Lys87. It is important to highlight the role of His36. Thanks to the flexibility of this residue, significant differences among the three solved structures are observed, in the site conformed by His36 and His39, one of phosphates being located at a putative p_{-2} position, and another phosphate in the p_{-3} ascribed position, interacting with His36 and Lys87 (see Figure 10). The observed flexibility of His36 depending on the crystallization conditions suggests a similar role to that of the main active site His122, which can acquire an "active" or "inactive" position, as observed for His119 in RNase A[154–157].

In the case of His36 in RNase 6 the "inactive" position would be facing the main active site, while the "active" form would be facing His39/Lys87. It is interesting to note that the active position of the histidine might be promoted by the presence of an adjacent base at the 3′ end, as observed for RNase A. In both RNase A and RNase 6 main active sites, the His 119/122 imidazole ring helps to fix the base ring at the B_2 site by stacking interactions, as suggested by molecular dynamics for His36 in RNase 6 (see Chapter I).

These observations on the present structures also support the previously suggested putative role of Lys87 as stabilizer of the transition state intermediate during catalysis at the RNase 6 secondary active site[80]. By comparison of the new solved structures with the previously one, some variability at Lys87 side chain conformation can be observed, which might illustrate its phosphate-binding mode flexibility. Besides, the enzymatic analysis of the K87A mutant confirms the main contribution of Lys87 in the RNase cleavage of polymeric substrate. Therefore, we can conclude that Lys87 together with the His36/His39 pair conform a secondary catalytic triad. Thereby the catalytic triad His36/His39/Lys87 would mimic the enzyme main active site (His15/His122/Lys38). The kinetic comparison between RNase 6 and RNase A engineered double mutant K7H/R10H (with an added second catalytic triad) indicates that the presence of two catalytic sites enhances the endonuclease-type cleavage pattern. In addition, the extended phosphate-binding subsite arrangement of RNase 6, expanding at both 3′ and 5′ ends, would favour the enzyme catalysis of polymeric substrates.

Conversion of a secondary substrate binding site into a catalytic site, as engineered in the RNase A-K7H/R10H double mutant, might have taken place during primate evolution to shape a novel RNase endowed with an enhanced catalytic cleavage of extended RNA substrates. Natural and engineered oligomeric RNases have been studied previously[158,159]. In contrast, the present arrangement of two active sites within a single RNase monomeric entity constitutes an alternative and unique catalytic strategy with potentialities to explore.

Work is currently in progress, in collaboration with the group of Professor Georgios A. Spyroulias (Patras University), to elucidate RNase 6 binding mode to oligonucleotides in solution by NMR.

Interestingly, we observe that the secondary active site is only present in the higher primate versions of RNase 6, which have incorporated His39 residue (see Additional Figure 1 in the annexes section). On the contrary, Lys87 is present in both lower and higher primates.

Comparison of RNase 6 orthologues suggests an evolutionary shift to convert a secondary phosphate binding site into a novel additional catalytic site.

Taking into account the prior observations in RNase 6, together with other studied antimicrobial RNases, we wanted to elucidate the changes in RNases' binding mode and catalytic sites throughout evolution, to explore if any shift has taken place in their selectivity towards specific cellular RNA targets and eventual physiological roles.

To do this, we have compared the catalytic activity of the human canonical RNases, using UpA, UpG and UpI dinucleotides as a substrate. Interestingly, when we compare the A/G ratio at B_2 site for the studied canonical RNases, we observe a pronounced evolutionary tendency from guanine to adenine preference, which follows the same order as the proposed evolutionary order of emergence of the RNases (from ancient to modern: 5, 4, 1 and 6/7/8–2/3 group, see Figure 3B) [34,35,86]. This result is in agreement with previously reported kinetic data, where lower order vertebrates, such as amphibians and reptiles, show a preference for guanine[160,161], while mammalian RNases have a clear preference for adenine[16].

In addition to the kinetics results, our molecular dynamics study using UpA, UpG and UpI enabled us to outline the main residues involved in the RNases' distinct specificities for B_2. First, bidentate interactions can mainly discriminate between binding to either adenine or guanine at N1/N6 or N1/O6 groups respectively. In addition, we observe specific interactions at N7/N6 for adenine versus N7/O6 for guanine; and eventually specific binding at guanine N1/N2 group. We can observe the conserved binding mode for adenine of Asn71 in RNase A, and counterparts, together with L4 loop main chain atoms. On their turn, lower order vertebrates tend to present an arginine that facilitates the interactions at N7/O6 for guanine recognition, as reported for other nucleotide-binding proteins[162].

Overall, our results indicate an evolutionary drift tendency from guanine to adenine preference. Additional Figure 2 depicts a general summary of the results. Interestingly, a close inspection of the residues potentially involved in the enzyme B_2 site reveals that the main contributors (Asn71 and Glu111 in RNase A and equivalent counterparts) are present in all the family members. Notwithstanding, significant differences in L4 loop extension and contribution of complementary residues can facilitate a distinct binding mode that confers discrimination between both purine bases. Overall, Asn, Glu/Asp and Arg bidentate side chains provide selective binding to adenine N1/N6 and N6/N7 versus guanine N1/O6, O6/N7 and N1/N2 groups.

However, we are aware of the intrinsic limitations of drawing conclusions based merely on dinucleotide substrates. A comprehensive analysis of the protein nucleotide recognition pattern should take into account the contribution of an extended substrate binding site architecture as demonstrated by many structural and kinetic studies[12,15,20,21,161,164,165]. Interestingly, recent work on the protein motion and ligand binding energies using a pentanucleotide suggests that induced conformational changes take place upon RNA interaction with secondary binding sites and can eventually provide a synergistic addition effect[30]. The cooperative participation of secondary substrate binding sites could explain the low binding affinity for mono- and dinucleotides and is also significantly limiting the potency of molecular dynamics predictions, when working with such probes. In any case, our present results, together with previously reported data, are definitely indicating an evolutionary trend in subsite selectivity within the vertebrate-specific RNase A superfamily that should respond to changing environmental conditions and adaptation to novel physiological needs.

Further work would be required to draw a more complete scenario of the dynamic interaction between the RNA and the RNases. We are confident that ongoing NMR studies would shed light on the contribution of the distinct protein subsites in the substrate specificity and cleavage mechanism.

4.2. Bactericidal and cytotoxic activity of an RNase 3 derived peptide: ECP(5–17P24–36)

Apart from the catalytic activity of RNases, one of the most interesting aspects of this protein family is the bactericidal capacity of many of its members, which is mainly retained at the N-terminal fragment[90,92]. As explained before, RNase 3 (also named the eosinophil cationic protein, ECP) is the most bactericidal member of the family. Previous work located at the N-terminus the main active region of the protein. A first 45-mer was identified that mostly retained the parental protein bactericidal activity[149]. Although the peptide bactericidal activity was high, we wanted to reduce its size, while improving its efficiency and reducing its cytotoxicity to host cells, in order to widen the therapeutic window. A second generation of peptides was designed, and a lead peptide was selected where the two first protein helices were linked with a proline residue as a connector (see Figure 9).

To further improve the properties of the ECP(5–17P24–36) peptide, a scan library of 546 peptides was prepared and the contribution of sequence positioning and amino acid singularity was evaluated. The main conclusion of this scanning is that the N-terminus of the protein has already been optimized through evolution to ensure antimicrobial activity. In consonance with the bibliography[166], the sequence specific incorporation of hydrophobic as well as positively charged amino acids enhanced the antimicrobial, agglutinating and LPS-binding activities of the peptides. Unfortunately, most substitutions improving antimicrobial activity are in detriment of cytotoxicity. However, three substitutions were identified that enhanced the peptide antibiofilm activity: T6I, W10I and Q14I (see Chapter II).

These three mutations expanded the N-terminus aggregation prone region and produced novel peptides that combined enhanced bactericidal and agglutinating activities, while retaining a similar LPS binding and low mammalian cytotoxicity. The selected candidates exerted a two- to threefold increase of the anti-biofilm effectivity compared to the original peptide. Interestingly, the W10I version reduced the peptide cytotoxicity respect to the parental lead peptide in the tested mammalian cell lines, and was considered for future studies.

Single-point mutations are not the only way to improve the bactericidal activity of peptides. Non-standard amino acids have proved to be an interesting choice to improve this bactericidal activity[167]. Among all the considerations that must be taken when designing antimicrobial peptides, hydrophobicity and relative positive charge are key players. A certain level of hydrophobicity is necessary to interact with the membrane and destabilise it. Excessive hydrophobicity, although significantly improving the antimicrobial activity, comes with the drawback of increasing the peptide cytotoxicity. Due to the general negative charge of the bacterial cell wall in comparison to eukaryotic cells, increasing the global positive charge of the peptide normally results in an improvement of the bactericidal activity while not posing a substantial cytotoxicity risk.

Taking all that into account, and due to the abundance of arginines in ECP(5–17P24–36) peptide, which are the main effectors of its antimicrobial activity, the substitution of these arginines for cationic residues with less hydrophobicity[166] was considered. Non-standard amino acids, such as ornithine, homoarginine or 2,4-diaminobutyric acid (Dab) were selected to reduce the peptide cytotoxicity while conserving its antibacterial activity and ensure resistance to bacterial proteases.

For that reason, we designed three new peptides in which arginines were replaced. Replacement by less cationic residues (Dab and ornithine, which have an amino group at the sidechain, instead of a guanidine group) led to a clear decrease of the bactericidal activity, while also reduced the cytotoxicity of the ornithine variant. Instead, homoarginine, which has the same charge as arginine, but with one carbon more in length, kept a similar bactericidal activity while increasing dramatically the cytotoxicity (Additional Table 1 in annexes section). Considering these data, norarginine, an arginine with one carbon less, appears as a worthy alternative for arginine replacement in future work.

Unfortunately, none of these candidate peptides solved one of the main drawbacks of ECP(5–17P24–36), which is its low bactericidal activity when bacteria are in rich medium growing conditions (evaluated by the calculation of the minimum inhibitory concentration, MIC). We suspected that this low efficiency in rich media conditions was due to the peptide sensitivity to bacterial proteases (a known resistance mechanism against antimicrobial peptides[168]). For this reason, we synthesised the total D enantiomer of our peptide to protect the molecule against both bacterial and host proteases. The D enantiomeric peptide retained an equivalent 2D structural fold, as confirmed by circular dichroism (Additional Figure 3), displaying high antimicrobial activity, even in rich medium growing conditions (Additional Table 1). However, the improvement in the peptide efficiency was in detriment of a slight increase of its cytotoxicity (Additional Table 1). This increase of the cytotoxicity was not enough to exceed the so-called therapeutic window, so we chose this candidate for starting the *in vivo* experimental part of this project (assays are currently in process in an acute infection mouse model using *Acinetobacter baumannii*).

4.3. RNase 3/1 efficiently combines RNase 1 catalytic activity and RNase 3 bactericidal properties

4.3.1. Design of an RNase 3/1 chimera

RNase 3/1 was designed to achieve a chimeric RNase which was able to combine, on one hand, the high catalytic activity of RNase 1 and its affinity to the ribonuclease inhibitor, and, on the other hand, the high antimicrobial activity of RNase 3. The RNase 3/1 form conserves the RNase 1 scaffold that provides the essential requirements for an elevated catalytic activity[1,12,15,169,170] and encompasses the key features of RNase 3 antimicrobial activity[53,55,93,171,172]. The experimental results confirmed that our new construct successfully combines a high catalytic activity together with a high bactericidal activity for all tested gram-negative species. In addition, the RNase 3/1 variant retained the characteristic high affinity for LPS of RNase 3[94] together with its membrane leakage activity[79,149]. On the other hand, RNase 3/1 shares with RNase 1 its non-toxicity to the tested human cell lines. Indeed, human secretory RNases' harmlessness *in vivo* is ensured thanks to the presence in the cytosol of all human tissue cells of the RNase inhibitor (RI), a horseshoe-shaped protein that binds to the human secretory RNase members[42] in a 1:1 stoichiometry with an unusually high affinity (at the fM-nM range). The RI is ubiquitous and protects the host cells from the potential toxicity of secretory RNases[173]. Therefore, our RNase chimera combines a high affinity for the bacterial wall together with an elevated catalytic efficiency and no toxicity to the host.

4.3.2. Rational design of two new versions of RNase 3/1 helps to understand the biological activities of RNases

Although the RNase 3/1 first chimeric version (thereafter named RNase 3/1-v1) significantly improved the catalytic activity of RNase 3, conserving a significant antimicrobial activity, its bactericidal efficiency was considerably lower than that of RNase 3. For this reason, we decided to modify this initial version and introduce cationic and hydrophobic surface residues, proved to

be key for the protein antimicrobial properties[53]. Therefore, we added the RNase 3 antimicrobial loop (N113 – Y122; thereafter R3-L7) in RNase 3/1-v2[55] and replaced the flexible loop of RNase 1 (D14 – Y25; thereafter R1-L1) by the original shorter loop of the RNase 3 N-terminal (S17 – R22; thereafter R3-L1) in RNase 3/1-v3.

Although these two new versions of the protein present a catalytic activity about 40% lower than RNase 3/1-v1, they were still far more active than RNase 3, which has only about 3% of the activity displayed by the chimera (see Chapter III). In addition, a significant shift of the preference from cytidine to uridine is observed in the RNase versions. The sequences of all the protein chimera are shown in Figure 11A.

Surprisingly, the addition of the L7 loop of RNase 3 (N113 – Y122; R3-L7) induced a more pronounced reduction of the catalytic activity than the deletion of the flexible loop of RNase 1 (D14 – Y25; R1-L1), reported as key for the catalytic efficiency of the protein[29]. Probably, the absence of the 113–122 loop may indirectly alter the N-terminus relative position, considering the observed interaction between the C and N-terminus in NMR and X-ray structural data of RNase 3[175,176].

Unfortunately, the antimicrobial activity of RNase 3/1 is significantly reduced when adding the R3-L7 loop in the absence of the R1-L1 loop. L1 is located at the N-terminal and links the first two helixes (needed for the antibacterial activity[91]). While R1-L1 is a long and flexible loop, R3-L1 is short and rigid. The greater separation of both helixes could decrease its bacterial membrane disruption ability. Indeed, when replacing the R1-L1 loop by R3-L1 (RNase 3/1-v3), we can observe a significant increase of the LPS-binding and the antimicrobial activity, probably due to its final 3D structure being more similar to RNase 3.

Recently solved crystal structures of the hybrid constructs (see Additional Figure 4) confirmed the conclusions extracted from the molecular dynamics (see Chapter III), that is, R1-L1 promotes higher flexibility to the first two helices, rearranging the hydrophobic cluster of the protein, while R3-L7, when interacting with the first helix, pulls the helix slightly displacing the p1 catalytic site.

On the other hand, no increase of the cytotoxicity is observed for the RNase 3/1-v2. Considering the obtained results on the protein inhibition by the RI, we can conclude that the R1-L1 loop of RNase 1 is important for the interaction with the RI. Overall, a comparative analysis of all the tested properties of the parental proteins and three chimeras (Figure 11B) indicate that the enhanced antimicrobial and catalytic activities of version 3 are in detriment of a slight increase in its cytotoxicity. We observe a pronounced decrease of the RI inhibition when the R1-L1 loop is removed. Further work is needed to increase the affinity to the ribonuclease inhibitor, reducing its cytotoxicity. Redesigning this loop to keep the antimicrobial and catalytic activities while enhancing the RI interaction should be the next step in the rational design of this chimeric protein.

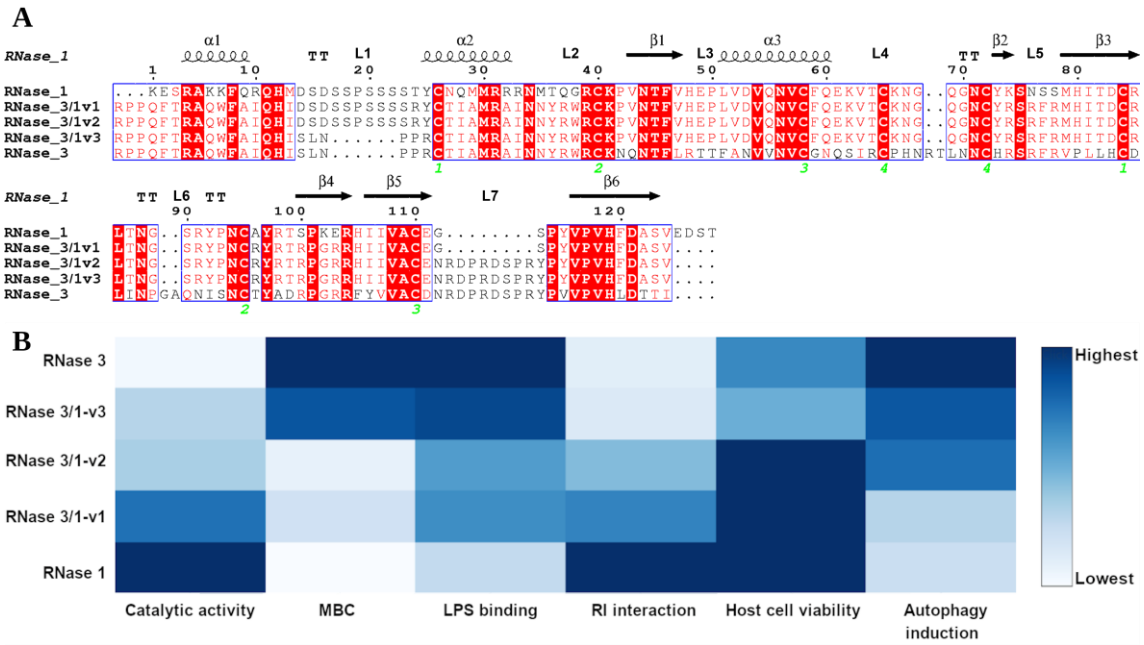

Figure 11. **A**) Alignment between RNase 1, RNase 3 and the three versions of RNase 3/1. The fully conserved amino acids are highlighted in red. The residues that are not conserved but have similar properties are marked with red letters. The secondary structure is indicated above the alignment. The green numbers indicate the disulphide bridges. The alignment was done using *Clustal Omega*[36], and the image was obtained with *ESPript7* (http://espript.ibcp.fr/ESPript/)[37]. **B**) Heatmap depiction for activity comparison of RNase 1, 3 and the three versions of RNase 3/1. All the results were normalized as relative to the highest detected activity and the heatmap was depicted using Plotly and GIMP[174].

Finally, thanks to the comparison between the three versions of RNase 3/1 we have identified a LIR motif (^{122}YPVV^{125}), whose particular structural arrangement in versions 2 and 3 as an intrinsically disordered protein region (IDPR) makes it fully functional. The region will adopt an equivalent conformation as in RNase 3 but not in RNase 1. LC3-interacting region (LIR) motifs are present in both autophagy receptors and adaptors, which are recognized by Atg8 (LC3) proteins[177–179]. Atg8 proteins are essential for the autophagosome formation, as well as its membrane elongation and the final closure and the fusion with lysosome[180–182]. In selective autophagy, the Atg8 proteins located on the inner membrane of the autophagosome are involved in the recruitment of the autophagosome cargo by binding to autophagy receptors[178,182].

The sequence found in RNase 3 is a Y-type motif (LIR motifs with a tyrosine at the beginning of the consensus sequence). Y-type motifs are reported to be the least common of the LIR motifs [178], and the ones with lowest affinity for LC3 proteins[183]. Taking this into account, RNase 3 would be recruited into the autophagosome by Atg8 proteins at a lower ratio than autophagy receptors. Which could then be the role of the RNase recruitment into the autophagosome cargo? The presence of RNases in the autophagosome could be involved in the killing of the pathogen inside the autophagosome, as well as the removal of the pathogenic RNA.

Further work is currently ongoing to confirm this hypothesis. Previous data from intracellular infection models done with human macrophages in our group showed that the higher the autophagy induction of RNases, the lower the intracellular MIC[184]. We expect the same behaviour with the different versions of RNase 3/1, and we have yet to test their intracellular MIC. If that is the result, we are going to include this LIR-AIM motif in the next version of the chimeric protein.

4.3.3. RNase 3/1 is able to reduce *Acinetobacter baumannii* resistance acquisition to antibiotics

It has often been claimed by several authors that resistance against antimicrobial peptides is almost impossible to obtain due to their unspecific mechanism of action, mostly associated to the attack on the bacterial cell wall. Indeed, this was the mechanism identified for the designed RNase 3 derived peptide ECP(5–17P24–36). However, some years ago, Perron and coworkers[108] proved that high resistance against antimicrobial peptides could also be achieved, although requiring longer exposition cycles. More recently, several other examples of resistance acquired against antimicrobial peptides have been reported. Of particular interest is the findings reported by Mossat and colleagues[134] that showed that exposure of *A. baumannii* at high bacterial concentration, to very high doses of colistin (polymyxin E, an AMP used in the clinics as a last-resort antibiotic for multidrug resistant infections), induced the emergence of bacterial resistance. The authors observed that resistant strains have undergone a total loss of the bacterial cell wall, the main target of colistin. The capacity of *A. baumannii* to reach such an extreme response clearly proves that bacterial plasticity is far higher than initially expected.

With the hypothesis that ribonuclease activity could block interbacterial communication by degrading RNA molecules, we decided to combine colistin treatment with the RNase 3/1-v1 chimera. We should mention here that when the project started the other two versions of RNase 3/1 had not been designed yet. Hindering RNA transference, which has been reported to be an essential mechanism for bacterial communication[185], could be an interesting way to delay bacterial resistance.

Towards this end, a systematic resistance assay was optimized that allowed us to observe, with a good statistical significance (n=40), the ability of RNase 3/1 to reduce the emergence of bacterial resistance against colistin[186]. The construct's efficacy to inhibit the emergence of *A. baumannii* resistance to colistin at a concentration below its effective bactericidal activity indicates that the mechanism of action of RNase 3/1 is probably due to a combination of the protein specific properties and not merely to a direct bactericidal action (Additional Figure 5).

Although further studies will be necessary to confirm this hypothesis, we speculate that the RNase 3/1 activities might interfere with the bacterial community quorum sensing and thereby delay the bacterial resistance acquisition process. Currently, we are analysing the potential combinatorial effect of our RNase construct in the presence of other families of conventional antibiotics, to discard any specific synergistic effect unique to the antimicrobial mechanism of colistin. In addition, to fully interpret our results, it is important to analyse whether the antibiotic resistome profile differs between the control bacterial cells, exposed only to colistin, and the bacterial cultures treated with both colistin and RNase 3/1.

Despite our promising results, we are very conscious on the limitations of the data presented in this work. We do not yet have enough data to determine the specific mechanism underlying RNase 3/1 reduction of the emergence of bacterial resistance, although preliminary results from our group indicate that the catalytic activity is involved in the delay of bacterial resistance. In case we confirm that the catalytic activity is responsible for our observations, blocking horizontal transference of RNAs could be a promising new way to prevent the emergence of new resistance mechanisms and extend the usable life of the current antibiotics. However, blocking RNA horizontal transference without blocking gene transference is, most probably, an insufficient strategy to completely abolish bacterial resistance.

4.4. Conclusion remarks

To sum up, this thesis sheds light by diverse methodological approaches on the structural-functional relationship of host defence ribonucleases and their pharmacological potential. Prior work in this laboratory suggested the presence of a secondary active site in RNase 6, unique in the family. In this thesis, the role of this secondary active site, together with its extended substrate binding mode, has been confirmed thanks to the determination of two new high-resolution structures at different crystallization conditions bound to phosphate ions. Secondly, this thesis has explored the potential of RNase-based antimicrobial agents. Specifically, two approaches have been taken. First, of all, optimisation of an RNase 3-derived peptide, ECP(5–17P24–36), identified three potential candidates with enhanced antibiofilm activity and no significant toxicity. Finally, in basis of the prior knowledge, an RNase 1/3 chimeric protein has been designed, which possesses RNase 3 antimicrobial activity and also retains most of the catalytic activity of RNase 1. Preliminary results showed the potential of this chimeric protein to reduce the acquisition of *A. baumannii* resistance to the antimicrobial peptide colistin.

Altogether, our results emphasize once more the applicability of host defence proteins to design novel anti-infective therapies. Although, as mentioned before, it is necessary to fully characterize the mechanism through which RNase 3/1 hinders the bacterial resistance acquisition, RNases and their derivatives appear, again, as promising new lead compounds in the fight against antimicrobial resistance.

5. CONCLUSIONS

I. Exploring RNase 6 RNA binding mode

- **a.** RNase 6 atomic structures (5OAB.pdb, at 1.10 Å in cubic form and 6ENP.pdb, at 1.04 Å in orthorhombic form) outline an extended phosphate-binding region, having up to nine phosphate-binding subsites.
- **b.** RNase 6's dual catalytic site architecture is unique within the RNase A superfamily. Its H36/H39/K87 secondary catalytic triad is only present in RNase 6 higher primates orthologs.
- **c.** RNase 6 substrate-binding arrangement favors the endonucleolytic cleavage of RNA.

II. Bactericidal and cytotoxic activity of the RNase 3-derived peptide ECP(5–17P24–36)

- **a.** The scanning of a library of 546 peptides with single substitutions of the ECP(5–17P24–36) lead peptide showed that the RNase 3 N-terminal is already optimized by evolution to ensure antimicrobial activity.
- **b.** Although most substitutions improving antimicrobial activity are in detriment of cytotoxicity, three substitutions (T6I, W10I and Q14I) were identified that enhanced the peptide antibiofilm activity without a significant increase in its toxicity.
- **c.** Due to the slightly higher cytotoxicity of Q14I and T6I, W10I was selected as the best candidate for future optimization of the peptide.
- **d.** None of the modifications of the reference peptide by replacing arginines with non-standard amino acids resulted in a promising candidate due to either a lower antimicrobial activity or a higher cytotoxicity.
- **e.** Instead, D-ECP(5–17P24–36) proved to be a very efficient peptide with very high antimicrobial activity against all the bacterial species tested, while its moderate increase of toxicity to tested human cell lines was still acceptable within the limits of the therapeutic window.

III. Rational design of an RNase 3/1 chimera for antimicrobial therapy

- **a.** RNase 3/1-v1 combines efficiently the high catalytic activity of RNase 1 with the specific antimicrobial properties of RNase 3.
- **b.** Due to the significantly lower antimicrobial activity of RNase 3/1-v1 in comparison with RNase 3, we successfully designed two new versions of RNase 3/1, named as -v2 and -v3.
- **c.** RNase 3/1-v2 shows a significant lower antimicrobial and catalytic activity than RNase 3/1-v1, and a slight reduction of the affinity with the ribonuclease inhibitor, but with no toxicity to human cells.
- **d.** RNase 3/1-v3 shows an enhanced antimicrobial activity and catalytic activity in relation to v2, albeit in detriment of its interaction with the human ribonuclease inhibitor and consequent slight increase of the protein toxicity to host cells.
- **e.** The two new versions, RNase 3/1-v2 and v3, incorporate a C-terminal loop that is key for antimicrobial activity and autophagy induction.
- **f.** Interestingly, we have found an LIR motif in RNase 3, which is present in the RNase 3/1-v2 and v3 versions and is associated to the autophagosome formation. The presence of the LIR tag correlates with the observed autophagy induction activity.
- **g.** Further work is needed to increase the affinity of RNase 3/1 to the ribonuclease inhibitor, in order to reduce its cytotoxicity.
- **h.** RNase 3/1-v1 reduces the calculated colistin MIC value when coadministered with colistin. The present data anticipate the potential development of RNase-based lead molecules as antibiotic adjuvant candidates.

6. ANNEXES

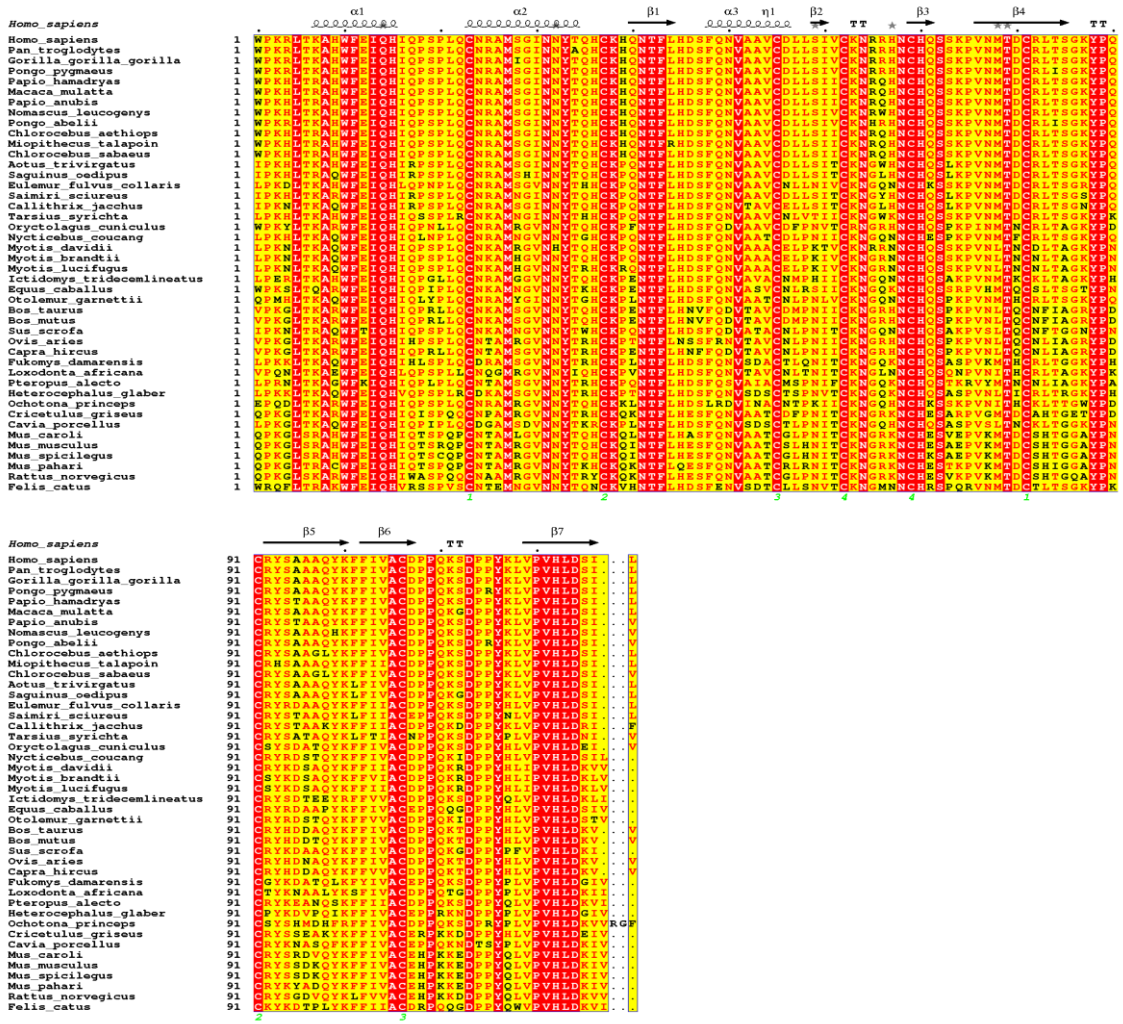

Additional Figure 1. Alignment between several orthologs of RNase 6. The active site is highlighted in yellow. The four disulphide bonds are labelled with green numbers. The alignment was performed using *T-coffee*, and the picture was drawn using *ESPript* (http://espript.ibcp.fr/ESPript/).

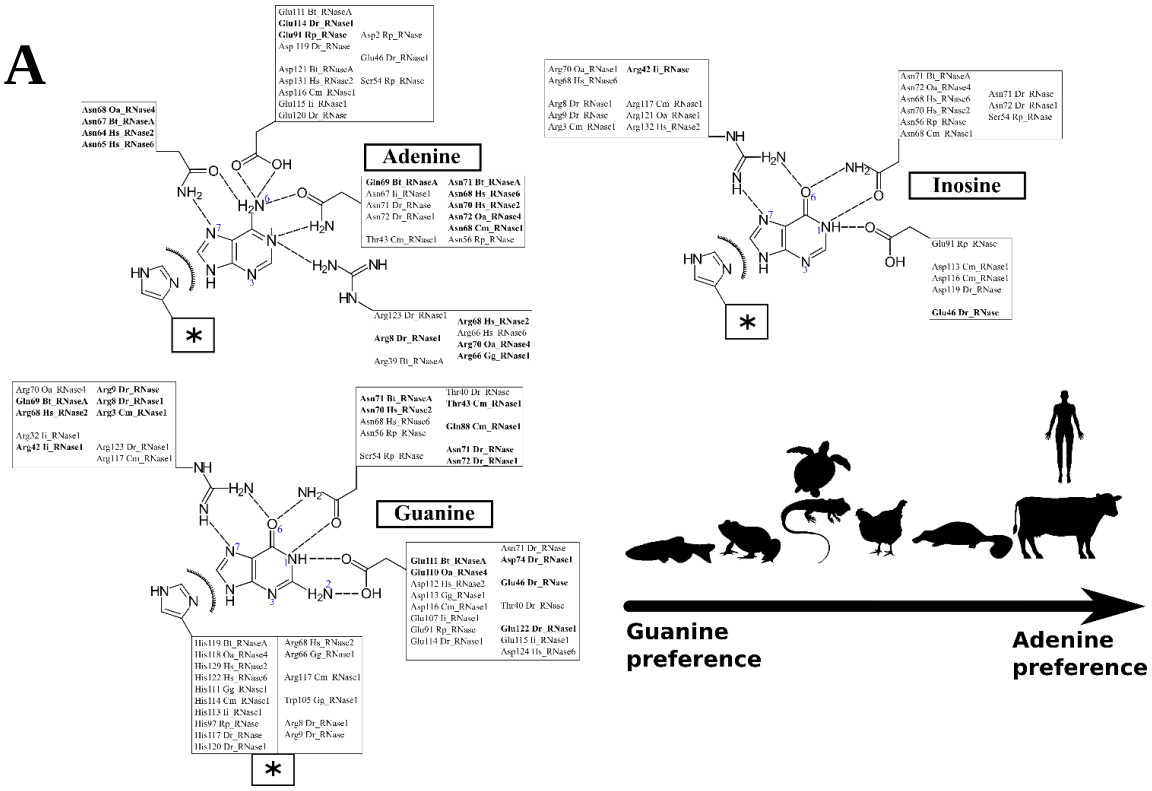

Additional Figure 2. **A)** Schematic representation of the predominant interactions observed during the 100 ns of each simulation run. Only the interactions present during more than 30% of the total dynamic runs were considered. The interactions observed in more than 50% of the total dynamic runs are highlighted in bold. Protein residues are listed according to RNase A numbering reference. Since there are no significant differences between the histidine interactions among the three dinucleotides, all the interactions are grouped in the * box. **B)** Schematic depiction of the main interactions identified by molecular dynamics according to the two main family classes (mammalian versus non-mammalian RNases). In dark and light red, the main and secondary specific interactions characteristic for either mammalian or non-mammalian RNases and in grey, the other interactions observed in all the RNases analysed. Representative icon labels for humans and fishes illustrate the predominant interaction mode for each RNase class. Taken and modified from *Prats-Ejarque et al. 2019*[163].

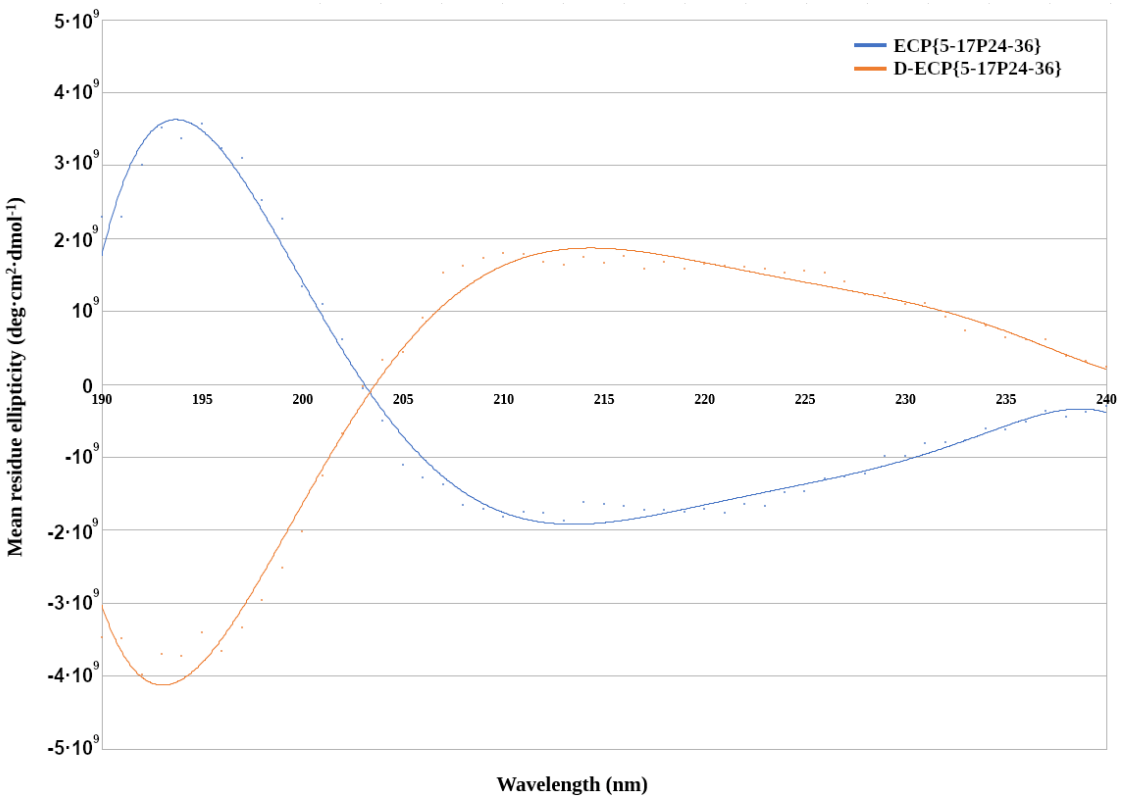

Additional Figure 3. Circular dichroism spectra of ECP(5–17P24–36) and its enantiomer. Measures were performed in Tris 5 mM pH 7.4, 1 mM SDS and a peptide concentration of 16 µM with a Jasco J-715 spectropolarimeter, as previously described[91].

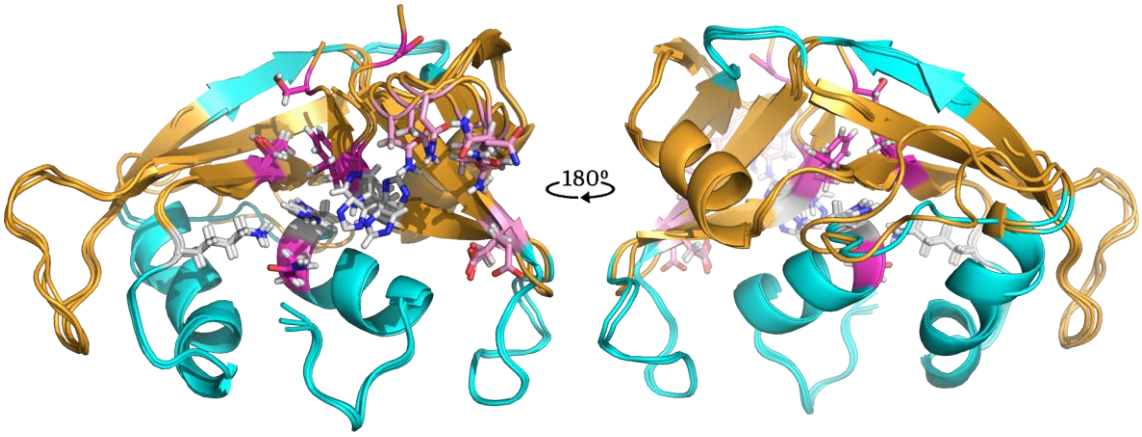

Additional Figure 4. Overlapping of RNase 3/1-v1 (6YMT.pdb), RNase 3/1-v2 (6YBC.pdb) and RNase 3/1-v3 (6SSN.pdb) crystal structures. In light blue, the fragments of RNase 3, in orange, the RNase 1 skeleton. In grey, the catalytic triad, in pink the B_1 subsite and in magenta the B_2 subsite. The picture was drawn with PyMOL 1.7.2 (Schrödinger, LLC).

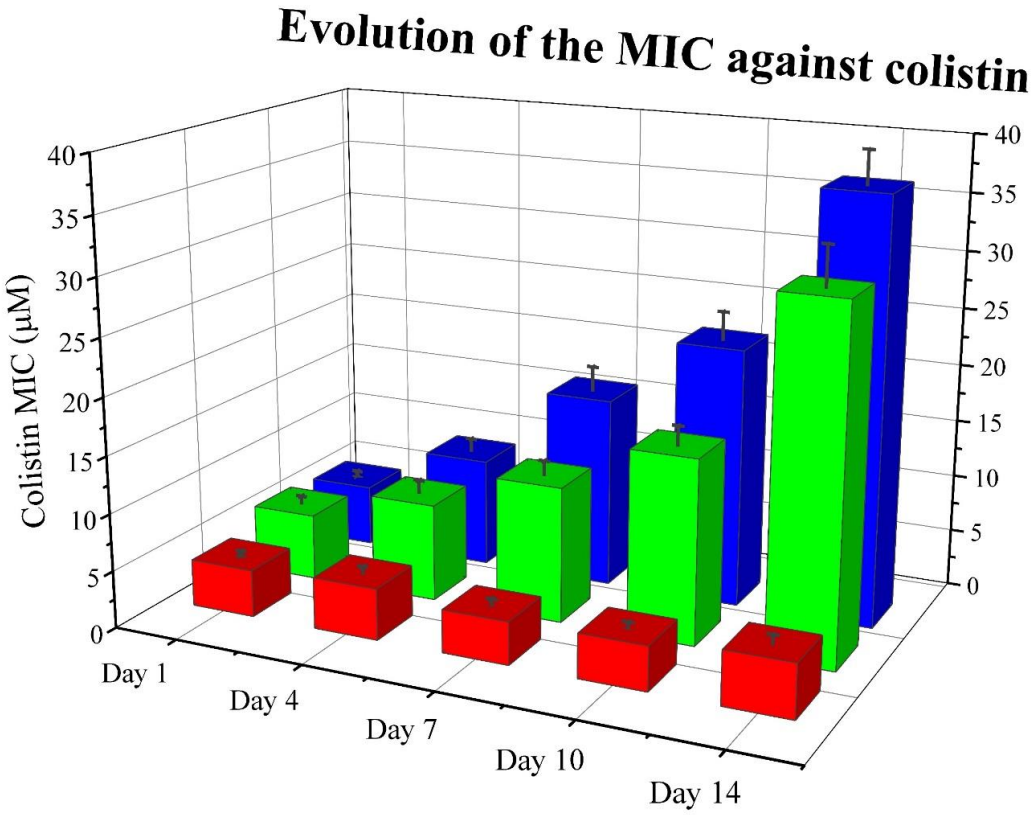

Additional Figure 5. Evolution of the mean MIC value for colistin after 14 days of exposition at each assayed condition. Red corresponds to the negative control, blue to the colistin alone and green to the colistin + RNase 3/1 condition. Data from selected days is shown. Error bars show the standard error of the mean. Taken from *Prats-Ejarque et al. 2019*[186].

	Escherichia coli CF073		***Pseudomonas aeruginosa (PAO1)***		***Acinetobacter baumannii (ATCC 15308)***		**MRC-5 cytotoxicity**		
μM	**MBC**	**MIC**	**MBC**	**MIC**	**MBC**	**MIC**	**IC_{50} (4 h)**	**IC_{50} (24 h)**	**IC_{50} (48 h)**
ECP(5–17P24–36)	0.6125 – 1,25	10 – 20	0.3125 – 0.625	> 20	0.3125 – 0.625	> 20	276.23 ± 25.23	N.D.	N.D.
D-ECP(5–17P24–36)	0.3125 – 0.625	1.25 – 2.5	0.3125 – 0.625	10 – 20	-	1.25 – 2.5	84.76 ± 7.37	26.02 ± 2.99	11.29 ± 6.25
Dab-ECP(5–17P24–36)	2.5 – 5	10 – 20	0.625 – 1.25	> 20	-	> 20	106.91 ± 14.59	-	-
Orn-ECP(5–17P24–36)	2.5 – 5	> 20	1.25 – 2.5	> 20	-	> 20	N.D.	-	-
HArg-ECP(5–17P24–36)	0.3125 – 0.625	10 – 20	0.3125 – 0.625	> 20	-	> 20	27.37 ± 5.19	-	-

Additional Table 1. Comparison of the bactericidal activity between ECP(5–17P24–36), peptide variants that incorporate non-standard amino acids and its D-enantiomer. MBC and MIC were determined as the lowest concentration of peptide where no cells were detected by CFU counting, in HEPES 20 mM pH 7.4, 100 mM NaCl or Mueller-Hinton broth, respectively. MRC-5 cytotoxicity was determined by the MTT essay. N.D. means that, at the highest concentration tested (300 μM), no reduction of cell viability was detected. Peptides were designed in collaboration with Dr. Marc Torrent (Dpt. of Biochemistry and Molecular Biology, UAB) and Prof. David Andreu (Dpt. of Experimental and Health Sciences) and synthesized at the UPF Peptide Synthesis core facility.

7. REFERENCES

1. Cuchillo, C. M., Nogués, M. V. & Raines, R. T. Bovine Pancreatic Ribonuclease: Fifty Years of the First Enzymatic Reaction Mechanism. *Biochemistry* **50,** 7835–7841 (2011).

2. Pizzo, E. & D'Alessio, G. The success of the RNase scaffold in the advance of biosciences and in evolution. *Gene* **406,** 8–12 (2007).

3. Rosenberg, H. F. RNase A ribonucleases and host defense: an evolving story. *J. Leukoc. Biol.* **83,** 1079–1087 (2008).

4. Lomax, J. E., Eller, C. H. & Raines, R. T. Comparative functional analysis of ribonuclease 1 homologs: Molecular insights into evolving vertebrate physiology. *Biochem. J.* **474,** 2219–2233 (2017).

5. Hooper, L. V, Stappenbeck, T. S., Hong, C. V & Gordon, J. I. Angiogenins: a new class of microbicidal proteins involved in innate immunity. *Nat. Immunol.* **4,** 269–273 (2003).

6. Goncalves, K. A., Silberstein, L., Li, S., Severe, N., Hu, M. G., Yang, H., Scadden, D. T. & Hu, G. fu. Angiogenin Promotes Hematopoietic Regeneration by Dichotomously Regulating Quiescence of Stem and Progenitor Cells. *Cell* **166,** 894–906 (2016).

7. Xu, L., Liao, W. L., Lu, Q. J., Li, C. G., Yuan, Y., Xu, Z. Y., Huang, S. D. & Chen, H. Z. ANG Promotes Proliferation and Invasion of the Cell of Lung Squamous Carcinoma by Directly Up-Regulating HMGA2. *J. Cancer* **7,** 862–871 (2016).

8. Sorrentino, S. The eight human 'canonical' ribonucleases: Molecular diversity, catalytic properties, and special biological actions of the enzyme proteins. *FEBS Lett.* **584,** 2194–2200 (2010).

9. Koczera, P., Martin, L., Marx, G. & Schuerholz, T. The ribonuclease a superfamily in humans: Canonical RNases as the buttress of innate immunity. *Int. J. Mol. Sci.* **17,** (2016).

10. Lu, L., Li, J., Moussaoui, M. & Boix, E. Immune modulation by human secreted RNases at the extracellular space. *Front. Immunol.* **9,** 1–20 (2018).

11. Fisher, B. M., Schultz, L. W. & Raines, R. T. Coulombic Effects of Remote Subsites on the Active Site of Ribonuclease A. *Biochemistry* **37,** 17386–17401 (1998).

12. Raines, R. T. Ribonuclease A. *Chem. Rev.* **98,** 1045–1066 (1998).

13. Parés, X., Nogués, M. V, de Llorens, R. & Cuchillo, C. M. Structure and function of ribonuclease A binding subsites. *Essays Biochem.* **26,** 89–103 (1991).

14. Moussaoui, M., Guasch, A., Boix, E., Cuchillo, C. M. & Nogués, M. V. The role of non-catalytic binding subsites in the endonuclease activity of bovine pancreatic ribonuclease A. *J. Biol. Chem.* **271,** 4687–4692 (1996).

15. Nogués, M. V., Moussaoui, M., Boix, E., Vilanova, M., Ribó, M. & Cuchillo, C. M. The contribution of noncatalytic phosphate-binding subsites to the mechanism of bovine pancreatic ribonuclease A. *Cell. Mol. Life Sci.* **54,** 766–774 (1998).

16. Boix, E., Blanco, J. a., Nogués, M. V. & Moussaoui, M. Nucleotide binding architecture for secreted cytotoxic endoribonucleases. *Biochimie* **95,** 1087–1097 (2013).

17. De Llorens, R., Arús, C., Parés, X. & Cuchillo, C. M. Chemical and computer graphics studies on the topography of the ribonuclease a active site cleft. A model of the enzymepentanucleotide substrate complex. *Protein Eng. Des. Sel.* **2,** 417–429 (1989).

18. McPherson, A., Brayer, G. D. & Morrison, R. D. Crystal structure of RNase A complexed with d(pA)4. *J. Mol. Biol.* **189,** 305–327 (1986).

19. Birdsall, D. L. & McPherson, A. Crystal structure disposition of thymidylic acid tetramer in complex with ribonuclease A. *J. Biol. Chem.* **267,** 22230–22236 (1992).

20. Fontecilla-Camps, J. C., De Llorens, R., Le Du, M. H. & Cuchillo, C. M. Crystal structure of ribonuclease A·d(ApTpApApG) complex. Direct evidence for extended substrate recognition. *J. Biol. Chem.* **269,** 21526–21531 (1994).

21. Boix, E., Nogués, M. V., Schein, C. H., Benner, S. a. & Cuchillo, C. M. Reverse Transphosphorylation by Ribonuclease A Needs an Intact p2-binding Site: Point mutations at LYS-7 and ARG-10 alter the catalytic properties of the enzyme. *J. Biol. Chem.* **269,** 2529–2534 (1994).

22. Boqué, L., Coll, M. G., Vilanova, M., Cuchillo, C. M. & Fita, I. Structure of ribonuclease a derivative II at 2.1-Å resolution. *J. Biol. Chem.* **269,** 19707–19712 (1994).

23. Shapiro, R. Structural features that determine the enzymatic potency and specificity of human angiogenin: Threonine-80 and residues 58-70 and 116-123. *Biochemistry* **37,** 6847–6856 (1998).

24. Boix, E., Nikolovski, Z., Moiseyev, G. P., Rosenberg, H. F., Cuchillo, C. M. & Nogués, M. V. Kinetic and Product Distribution Analysis of Human Eosinophil Cationic Protein Indicates a Subsite Arrangement That Favors Exonuclease-type Activity. *J. Biol. Chem.* **274,** 15605–15614 (1999).

25. Cuchillo, C. M., Moussaoui, M., Barman, T., Travers, F. & Nogués, M. V. The exo- or endonucleolytic preference of bovine pancreatic ribonuclease A depends on its subsites structure and on the substrate size. *Protein Sci.* **11,** 117–128 (2002).

26. Moussaoui, M., Cuchillo, C. M. & Nogués, M. V. A phosphate-binding subsite in bovine pancreatic ribonuclease A can be converted into a very efficient catalytic site. *Protein Sci.* **16,** 99–109 (2007).

27. Sorrentino, S. Human extracellular ribonucleases: Multiplicity, molecular diversity and catalytic properties of the major RNase types. *Cell. Mol. Life Sci.* **54,** 785–794 (1998).

28. Tarragona-Fiol, A., Eggelte, H. J., Harbron, S., Sanchez, E., Taylorson, C. J., Ward, J. M. & Rabin, B. R. Identification by site-directed mutagenesis of amino acids in the subsite of bovine pancreatic ribonuclease A. *"Protein Eng. Des. Sel.* **6,** 901–906 (1993).

29. Gagné, D. & Doucet, N. Structural and functional importance of local and global conformational fluctuations in the RNase A superfamily. *FEBS J.* **280,** 5596–5607 (2013).

30. Narayanan, C., Gagné, D., Reynolds, K. A. & Doucet, N. Conserved amino acid networks modulate discrete functional properties in an enzyme superfamily. *Sci. Rep.* **7,** 3207 (2017).

31. Narayanan, C., Bernard, D. N., Bafna, K., Gagné, D., Agarwal, P. K. & Doucet, N. Ligand-induced variations in structural and dynamical properties within an enzyme superfamily. *Front. Mol. Biosci.* **5,** 1–12 (2018).

32. Boix, E. & Nogués, M. V. Mammalian antimicrobial proteins and peptides: overview on the RNase A superfamily members involved in innate host defence.

Mol. Biosyst. **3,** 317–335 (2007).

33. Sorrentino, S. & Libonati, M. Structure-function relationships in human ribonucleases: Main distinctive features of the major RNase types. *FEBS Lett.* **404,** 1–5 (1997).

34. Cho, S., Beintema, J. J. & Zhang, J. The ribonuclease A superfamily of mammals and birds: Identifying new members and tracing evolutionary histories. *Genomics* **85,** 208–220 (2005).

35. Goo, S. M. & Cho, S. The expansion and functional diversification of the mammalian ribonuclease a superfamily epitomizes the efficiency of multigene families at generating biological novelty. *Genome Biol. Evol.* **5,** 2124–2140 (2013).

36. Sievers, F. & Higgins, D. G. Clustal Omega for making accurate alignments of many protein sequences. *Protein Sci.* **27,** 135–145 (2018).

37. Robert, X. & Gouet, P. Deciphering key features in protein structures with the new ENDscript server. *Nucleic Acids Res.* **42,** 320–324 (2014).

38. Gupta, S. K., Haigh, B. J., Griffin, F. J. & Wheeler, T. T. The mammalian secreted RNases: Mechanisms of action in host defence. *Innate Immun.* (2012). doi:10.1177/1753425912446955

39. Sorrentino, S., Naddeo, M., Russo, A. & D'Alessio, G. Degradation of double-stranded RNA by human pancreatic ribonuclease: Crucial role of noncatalytic basic amino acid residues. *Biochemistry* **42,** 10182–10190 (2003).

40. Johnson, R. J., McCoy, J. G., Bingman, C. A., Phillips, G. N. & Raines, R. T. Inhibition of Human Pancreatic Ribonuclease by the Human Ribonuclease Inhibitor Protein. *J. Mol. Biol.* **368,** 434–449 (2007).

41. Rutkoski, T. J. & Raines, R. T. Evasion of ribonuclease inhibitor as a determinant of ribonuclease cytotoxicity. *Curr. Pharm. Biotechnol.* **9,** 185–189 (2008).

42. Lomax, J. E., Bianchetti, C. M., Chang, A., Phillips, G. N., Fox, B. G. & Raines, R. T. Functional evolution of ribonuclease inhibitor: Insights from birds and reptiles. *J. Mol. Biol.* **426,** 3041–3056 (2014).

43. Rosenberg, H. F. The eosinophil ribonucleases. *Cell. Mol. Life Sci.* **54,** 795–803 (1998).

44. Torrent, M., Pulido, D., Nogués, M. V. & Boix, E. Exploring New Biological Functions of Amyloids: Bacteria Cell Agglutination Mediated by Host Protein Aggregation. *PLoS Pathog.* **8,** (2012).

45. Rosenberg, H. F., Dyer, K. D. & Foster, P. S. Eosinophils: changing perspectives in health and disease. *Nat. Rev. Immunol.* **13,** 9–22 (2013).

46. Malik, A. & Batra, J. K. Antimicrobial activity of human eosinophil granule proteins: involvement in host defence against pathogens. *Crit. Rev. Microbiol.* **38,** 168–181 (2012).

47. Acharya, K. R. & Ackerman, S. J. Eosinophil granule proteins: Form and function. *J. Biol. Chem.* **289,** 17406–17415 (2014).

48. Rosenberg, H. F., Dyer, K. D., Lee Tiffany, H. & Gonzalez, M. Rapid evolution of a unique family of primate ribonuclease genes. *Nat. Genet.* **10,** 219–223 (1995).

49. Zhang, J., Rosenberg, H. F. & Nei, M. Positive Darwinian selection after gene duplication in primate ribonuclease genes. *Proc. Natl. Acad. Sci. U. S. A.* **95,** 3708–13 (1998).

50. Domachowske, J. B., Dyer, K. D., Bonville, C. A. & Rosenberg, H. F. Recombinant Human Eosinophil-Derived Neurotoxin/RNase 2 Functions as an Effective Antiviral Agent against Respiratory Syncytial Virus. *J. Infect. Dis.* **177,** 1458–1464 (1998).

51. Rosenberg, H. Eosinophil-Derived Neurotoxin / RNase 2: Connecting the Past, the Present and the Future. *Curr. Pharm. Biotechnol.* **9,** 135–140 (2008).

52. Rosenberg, H. F. Eosinophil-derived neurotoxin (EDN/RNase 2) and the mouse eosinophil-associated RNases (mEars): Expanding roles in promoting host defense. *Int. J. Mol. Sci.* **16,** 15442–15455 (2015).

53. Carreras, E., Boix, E., Rosenberg, H. F., Cuchillo, C. M. & Nogués, M. V. Both aromatic and cationic residues contribute to the membrane-lytic and bactericidal activity of eosinophil cationic protein. *Biochemistry* **42,** 6636–6644 (2003).

54. Lien, P., Kuo, P., Chen, C., Chang, H.-H., Fang, S., Wu, W., Lai, Y., Pai, T. & Chang, M. D. In Silico Prediction and In Vitro Characterization of Multifunctional Human RNase3. *Biomed Res. Int.* **2013,** 1–12 (2013).

55. Boix, E., Salazar, V. a., Torrent, M., Pulido, D., Nogués, M. V. & Moussaoui, M. Structural determinants of the eosinophil cationic protein antimicrobial activity. *Biol. Chem.* **393,** 801–815 (2012).

56. Singh, A. & Batra, J. K. Role of unique basic residues in cytotoxic, antibacterial and antiparasitic activities of human eosinophil cationic protein. *Biol. Chem.* **392,** 337–346 (2011).

57. Rosenberg, H. F. Recombinant human eosinophil cationic protein. Ribonuclease activity is not essential for cytotoxicity. *J. Biol. Chem.* **270,** 7876–7881 (1995).

58. Lu, L., Wei, R., Prats-Ejarque, G., Goetz, M., Wang, G., Torrent, M. & Boix, E. Human RNase3 immune-modulation by catalytic-dependent and independent modes in a macrophage-cell line infection model. *Cell Mol. Life Sci.* Accepted Manuscript (2020).

59. Zhou, H.-M. & Strydom, D. J. The amino acid sequence of human ribonuclease 4, a highly conserved ribonuclease that cleaves specifically on the 3' side of uridine. *Eur. J. Biochem.* **217,** 401–410 (1993).

60. Terzyan, S. S., Peracaula, R., De Llorens, R., Tsushima, Y., Yamada, H., Seno, M., Gomis-Rüth, F. X. & Coll, M. The three-dimensional structure of human RNase 4, unliganded and complexed with d(Up), reveals the basis for its uridine selectivity. *J. Mol. Biol.* **285,** 205–214 (1999).

61. Fett, J. W., Strydom, D. J., Lobb, R. R., Alderman, E. M., Bethune, J. L., Riordan, J. F. & Vallee, B. L. Isolation and Characterization of Angiogenin, an Angiogenic Protein from Human Carcinoma Cells. *Biochemistry* **24,** 5480–5486 (1985).

62. Shapiro, R., Fett, J. W., Strydom, D. J. & Vallee, B. L. Isolation and characterization of a human colon carcinoma-secreted enzyme with pancreatic ribonuclease-like activity. *Biochemistry* **25,** 7255–7264 (1986).

63. Lyons, S. M., Fay, M. M., Akiyama, Y., Anderson, P. J. & Ivanov, P. RNA biology of angiogenin: Current state and perspectives. *RNA Biol.* **14,** 171–178 (2017).

64. Wang, Y. N., Lee, H. H., Chou, C. K., Yang, W. H., Wei, Y., Chen, C. Te, Yao, J., Hsu, J. L., Zhu, C., Ying, H., Ye, Y., Wang, W. J., Lim, S. O., Xia, W., Ko, H. W., Liu, X., Liu, C. G., Wu, X., Wang, H., Li, D., Prakash, L. R., Katz, M. H., Kang, Y., Kim, M., Fleming, J. B., Fogelman, D., Javle, M., Maitra, A. & Hung, M. C. Angiogenin/Ribonuclease 5 Is an EGFR Ligand and a Serum Biomarker for Erlotinib Sensitivity in Pancreatic Cancer. *Cancer Cell* **33,** 752-769.e8 (2018).

65. Spencer, J. D., Schwaderer, A. L., Wang, H., Bartz, J., Kline, J., Eichler, T., Desouza, K. R., Sims-Lucas, S., Baker, P. & Hains, D. S. Ribonuclease 7, an antimicrobial peptide upregulated during infection, contributes to microbial defense of the human urinary tract. *Kidney Int.* **83,** 615–625 (2013).

66. Becknell, B., Eichler, T. E., Beceiro, S., Li, B., Easterling, R. S., Carpenter, A. R., James, C. L., McHugh, K. M., Hains, D. S., Partida-Sanchez, S. & Spencer, J. D. Ribonucleases 6 and 7 have antimicrobial function in the human and murine urinary tract. *Kidney Int.* **87,** 151–161 (2014).

67. Amatngalim, G. D., van Wijck, Y., de Mooij-Eijk, Y., Verhoosel, R. M., Harder, J., Lekkerkerker, A. N., Janssen, R. A. J. & Hiemstra, P. S. Basal Cells Contribute to Innate Immunity of the Airway Epithelium through Production of the Antimicrobial Protein RNase 7. *J. Immunol.* **194,** 3340–3350 (2015).

68. Rosenberg, H. F. & Dyer, K. D. Molecular cloning and characterization of a novel human ribonuclease (RNase k6): increasing diversity in the enlarging ribonuclease gene family. *Nucleic Acids Res.* **24,** 3507–3513 (1996).

69. Deming, M. S., Dyer, K. D., Bankier, A. T., Piper, M. B., Dear, P. H. & Rosenberg, H. F. Ribonuclease k6: Chromosomal mapping and divergent rates of evolution within the RNase A gene superfamily. *Genome Res.* **8,** 599–607 (1998).

70. Dyer, K. D., Rosenberg, H. F. & Zhang, J. Isolation, characterization, and evolutionary divergence of mouse RNase 6: Evidence for unusual evolution in rodents. *J. Mol. Evol.* **59,** 657–665 (2004).

71. Zhang, J., Dyer, K. D. & Rosenberg, H. F. Evolution of the rodent eosinophil-associated RNase gene family by rapid gene sorting and positive selection. *Proc. Natl. Acad. Sci.* **97,** 4701–4706 (2000).

72. McDevitt, A. L., Deming, M. S., Rosenberg, H. F. & Dyer, K. D. Gene structure and enzymatic activity of mouse eosinophil-associated ribonuclease 2. *Gene* **267,** 23–30 (2001).

73. Saitou, N. & Nei, M. The neighbor-joining method: a new method for reconstructing phylogenetic trees. *Mol. Biol. Evol.* **4,** 406–425 (1987).

74. Felsenstein, J. Confidence limits on phylogenies: an approach using the bootstrap. *Evolution (N. Y).* **39,** 783–791 (1985).

75. Zuckerkandl, E. & Pauling, L. in *Evol. Genes Proteins* (eds. Bryson, V. & Vogel, H. J.) 97–166 (Academic Press, 1965). doi:10.1016/B978-1-4832-2734-4.50017-6

76. Tamura, K., Stecher, G., Peterson, D., Filipski, A. & Kumar, S. MEGA6: Molecular evolutionary genetics analysis version 6.0. *Mol. Biol. Evol.* **30,** 2725–2729 (2013).

77. Jelicic, K., Cimbro, R., Nawaz, F., Huang, D. W., Zheng, X., Yang, J., Lempicki, R. a, Pascuccio, M., Van Ryk, D., Schwing, C., Hiatt, J., Okwara, N., Wei, D., Roby, G., David, A., Hwang, I. Y., Kehrl, J. H., Arthos, J., Cicala, C. & Fauci, A. S. The HIV-1 envelope protein gp120 impairs B cell proliferation by inducing TGF-β1 production and FcRL4 expression. *Nat. Immunol.* **14,** 1256–65 (2013).

78. Pulido, D., Arranz-Trullén, J., Prats-Ejarque, G., Velázquez, D., Torrent, M., Moussaoui, M. & Boix, E. Insights into the Antimicrobial Mechanism of Action of Human RNase6: Structural Determinants for Bacterial Cell Agglutination and Membrane Permeation. *Int. J. Mol. Sci.* **17,** 552 (2016).

79. Torrent, M., Cuyás, E., Carreras, E., Navarro, S., López, O., De La Maza, A., Nogués, M. V., Reshetnyak, Y. K. & Boix, E. Topography studies on the membrane interaction mechanism of the eosinophil cationic protein. *Biochemistry* **46,** 720–733 (2007).

80. Prats-Ejarque, G., Arranz-Trullen, J., Blanco, J. A., Pulido, D., Nogues, M. V., Moussaoui, M. & Boix, E. The first crystal structure of human RNase 6 reveals a novel substrate-binding and cleavage site arrangement. *Biochem. J.* **473,** 1523–1536 (2016).

81. Spencer, J. D., Schwaderer, A. L., Dirosario, J. D., McHugh, K. M., McGillivary, G., Justice, S. S., Carpenter, A. R., Baker, P. B., Harder, J. & Hains, D. S. Ribonuclease 7 is a potent antimicrobial peptide within the human urinary tract. *Kidney Int.* **80,** 174–180 (2011).

82. Harder, J. RNase 7, a Novel Innate Immune Defense Antimicrobial Protein of Healthy Human Skin. *J. Biol. Chem.* **277,** 46779–46784 (2002).

83. Wang, H., Schwaderer, A. L., Kline, J., Spencer, J. D., Kline, D. & Hainsa, D. S. Contribution of structural domains to the activity of ribonuclease 7 against uropathogenic bacteria. *Antimicrob. Agents Chemother.* **57,** 766–774 (2013).

84. Ryu, S., Song, P. I., Seo, C. H., Cheong, H. & Park, Y. Colonization and infection of the skin by S. aureus: Immune system evasion and the response to cationic antimicrobial peptides. *Int. J. Mol. Sci.* **15,** 8753–8772 (2014).

85. Zhang, J., Dyer, K. D. & Rosenberg, H. F. RNase 8, a novel RNase A superfamily ribonuclease expressed uniquely in placenta. *Nucleic Acids Res.* **30,** 1169–1175 (2002).

86. Zhang, J. Disulfide-bond reshuffling in the evolution of an ape placental ribonuclease. *Mol. Biol. Evol.* **24,** 505–512 (2007).

87. Rudolph, B., Podschun, R., Sahly, H., Schubert, S., Schröder, J. M. & Harder, J. Identification of RNase 8 as a novel human antimicrobial protein. *Antimicrob. Agents Chemother.* **50,** 3194–3196 (2006).

88. Rosenberg, H. F. & Domachowske, J. B. Eosinophils, eosinophil ribonucleases, and their role in host defense against respiratory virus pathogens. *J. Leukoc. Biol.* **70,** 691–698 (2001).

89. Yamada, K. J., Barker, T., Dyer, K. D., Rice, T. a., Percopo, C. M., Garcia-Crespo, K. E., Cho, S., Lee, J. J., Druey, K. M. & Rosenberg, H. F. Eosinophil-associated Ribonuclease 11 Is a Macrophage Chemoattractant. *J. Biol. Chem.* **290,** 8863–8875 (2015).

90. Torrent, M., Odorizzi, F., Nogués, M. V., Boix, E., Nogues, M. V & Boix, E. Eosinophil cationic protein aggregation: identification of an N-terminus amyloid prone region. *Biomacromolecules* **11,** 1983–1990 (2010).

91. Torrent, M., Pulido, D., de la Torre, B. G., García-Mayoral, M. F., Nogués, M. V., Bruix, M., Andreu, D. & Boix, E. Refining the Eosinophil Cationic Protein Antibacterial Pharmacophore by Rational Structure Minimization. *J. Med. Chem.* **54,** 5237–5244 (2011).

92. Torrent, M., Pulido, D., Valle, J., Nogués, M. V., Andreu, D. & Boix, E. Ribonucleases as a host-defence family: evidence of evolutionarily conserved antimicrobial activity at the N-terminus. *Biochem. J.* **456,** 99–108 (2013).

93. Boix, E., Torrent, M., Sánchez, D. & Nogués, M. V. The antipathogen activities of eosinophil cationic protein. *Curr. Pharm. Biotechnol.* **9,** 141–152 (2008).

94. Torrent, M., Navarro, S., Moussaoui, M., Nogu?s, M. V. & Boix, E. Eosinophil Cationic Protein High-Affinity Binding to Bacteria-Wall Lipopolysaccharides and

Peptidoglycans. *Biochemistry* **47,** 3544–3555 (2008).

95. Munita, J. M. & Arias, C. A. Mechanisms of Antibiotic Resistance. *Microbiol. Spectr.* **4,** 1–24 (2016).

96. Wilson, D. N. Ribosome-targeting antibiotics and mechanisms of bacterial resistance. *Nat. Rev. Microbiol.* **12,** 35–48 (2014).

97. Davies, J. & Wright, G. D. Bacterial resistance to aminoglycoside antibiotics. *Trends Microbiol.* **5,** 234–240 (1997).

98. Abraham, E. P. & Chain, E. An enzyme from bacteria able to destroy penicillin. *Nature* **146,** 837 (1940).

99. Dcosta, V. M., King, C. E., Kalan, L., Morar, M., Sung, W. W. L., Schwarz, C., Froese, D., Zazula, G., Calmels, F., Debruyne, R., Golding, G. B., Poinar, H. N. & Wright, G. D. Antibiotic resistance is ancient. *Nature* **477,** 457–461 (2011).

100. Pagès, J. M., James, C. E. & Winterhalter, M. The porin and the permeating antibiotic: A selective diffusion barrier in Gram-negative bacteria. *Nat. Rev. Microbiol.* **6,** 893–903 (2008).

101. Nikaido, H. Molecular Basis of Bacterial Outer Membrane Permeability Revisited. *Microbiol. Mol. Biol. Rev.* **67,** 593–656 (2003).

102. Poole, K. Efflux-mediated antimicrobial resistance. *J. Antimicrob. Chemother.* **56,** 20–51 (2005).

103. Piddock, L. J. V. Clinically Relevant Chromosomally Encoded Multidrug Resistance Efflux Pumps in Bacteria. *Clin. Microbiol. Rev.* **19,** 382–402 (2006).

104. Piddock, L. J. V. Multidrug-resistance efflux pumps ? not just for resistance. *Nat. Rev. Microbiol.* **4,** 629–636 (2006).

105. Aldred, K. J., Kerns, R. J. & Osheroff, N. Mechanism of quinolone action and resistance. *Biochemistry* **53,** 1565–1574 (2014).

106. Oren, Z. & Shai, Y. Mode of Action of Linear Ampiphatic alpha-Helica Antimicrobial Peptides. *Pept. Sci.* **47,** 451–463 (1998).

107. Hancock, R. E. W. & Diamond, G. The role of cationic antimicrobial peptides in innate host defences. *Trends Microbiol.* **8,** 402–410 (2000).

108. Perron, G. G., Zasloff, M. & Bell, G. Experimental evolution of resistance to an antimicrobial peptide. *Proc. R. Soc. London B* **273,** 251–256 (2006).

109. Lai, Y. & Gallo, R. L. AMPed up immunity: how antimicrobial peptides have multiple roles in immune defense. *Trends Immunol.* **30,** 131–141 (2009).

110. Diamond, G., Beckloff, N., Weinberg, A. & Kisich, K. The Roles of Antimicrobial Peptides in Innate Host Defense. *Curr. Pharm. Des.* **15,** 2377–2392 (2009).

111. Schittek, B., Hipfel, R., Sauer, B., Bauer, J., Kalbacher, H., Stevanovic, S., Schirle, M., Schroeder, K., Blin, N., Meier, F., Rassner, G. & Garbe, C. Dermcidin: A novel human antibiotic peptide secreted by sweat glands. *Nat. Immunol.* **2,** 1133–1137 (2001).

112. Lai, R., Liu, H., Hui Lee, W. & Zhang, Y. An anionic antimicrobial peptide from toad Bombina maxima. *Biochem. Biophys. Res. Commun.* **295,** 796–799 (2002).

113. Bechinger, B., Zasloff, M. & Opella, S. J. Structure and Dynamics of the Antibiotic Peptide PGLa in Membranes by Solution and Solid-State Nuclear Magnetic Resonance Spectroscopy. *Biophys. J.* **74,** 981–987 (1998).

114. Brogden, K. A. Antimicrobial peptides: pore formers or metabolic inhibitors in bacteria? *Nat. Rev. Microbiol.* **3,** 238–250 (2005).

115. Wiesner, J. & Vilcinskas, A. Antimicrobial peptides: The ancient arm of the human immune system. *Virulence* **1,** 440–464 (2010).

116. Nakatsuji, T. & Gallo, R. L. Antimicrobial Peptides: Old Molecules with New Ideas. *J. Invest. Dermatol.* **132,** 887–895 (2012).

117. Zhu, S. Evidence for myxobacterial origin of eukaryotic defensins. *Immunogenetics* **59,** 949–954 (2007).

118. Gifford, J. L., Hunter, H. N. & Vogel, H. J. Lactoferricin: A lactoferrin-derived peptide with antimicrobial, antiviral, antitumor and immunological properties. *Cell. Mol. Life Sci.* **62,** 2588–2598 (2005).

119. Harris, F., Dennison, S. & Phoenix, D. Anionic Antimicrobial Peptides from Eukaryotic Organisms. *Curr. Protein Pept. Sci.* **10,** 585–606 (2009).

120. Bahar, A. A. & Ren, D. Antimicrobial peptides. *Pharmaceuticals* **6,** 1543–1575 (2013).

121. Brandenburg, L. O., Merres, J., Albrecht, L. J., Varoga, D. & Pufe, T. Antimicrobial peptides: Multifunctional drugs for different applications. *Polymers (Basel).* **4,** 539–560 (2012).

122. Yeaman, M. R. Mechanisms of Antimicrobial Peptide Action and Resistance. *Pharmacol. Rev.* **55,** 27–55 (2003).

123. Nguyen, L. T., Haney, E. F. & Vogel, H. J. The expanding scope of antimicrobial peptide structures and their modes of action. *Trends Biotechnol.* **29,** 464–472 (2011).

124. Tang, M. & Hong, M. Structure and mechanism of β-hairpin antimicrobial peptides in lipid bilayers from solid-state NMR spectroscopy. *Mol. Biosyst.* **5,** 317–322 (2009).

125. Epand, R. M. & Epand, R. F. Bacterial membrane lipids in the action of antimicrobial agents. *J. Pept. Sci.* **17,** 298–305 (2011).

126. Friedrich, C., Scott, M. G., Karunaratne, N., Yan, H. & Hancock, R. E. W. Salt-resistant alpha-helical cationic antimicrobial peptides. *Antimicrob. Agents Chemother.* **43,** 1542–1548 (1999).

127. Yeaman, M. R., Bayer, A. S., Koo, S. P., Foss, W. & Sullam, P. M. Platelet microbicidal proteins and neutrophil defensin disrupt the Staphylococcus aureus cytoplasmic membrane by distinct mechanisms of action. *J. Clin. Invest.* **101,** 178–187 (1998).

128. Jiao, N., Yang, Y. & Luo, T. Membrane potential based characterization by flow cytometry of physiological states in an aerobic anoxygenic phototrophic bacterium. *Aquat. Microb. Ecol.* **37,** 149–158 (2004).

129. Benarroch, J. M. & Asally, M. The Microbiologist's Guide to Membrane Potential Dynamics. *Trends Microbiol.* **xx,** 1–11 (2020).

130. Otto, M. *Bacterial Evasion of Antimicrobial Peptides by Biofilm Formation*. *Antimicrob. Pept. Hum. Dis. Curr. Top. Microbiol. Immunol.* **306,** (Springer, 2006).

131. Batoni, G., Maisetta, G., Lisa Brancatisano, F., Esin, S. & Campa, M. Use of Antimicrobial Peptides Against Microbial Biofilms: Advantages and Limits. *Curr. Med. Chem.* **18,** 256–279 (2011).

132. Bechinger, B. & Gorr, S. U. Antimicrobial Peptides: Mechanisms of Action and Resistance. *J. Dent. Res.* **96,** 254–260 (2017).

133. Lewis, L. A., Choudhury, B., Balthazar, J. T., Martin, L. E., Ram, S., Rice, P. A., Stephens, D. S., Carlson, R. &

Shafer, W. M. Phosphoethanolamine substitution of lipid A and resistance of Neisseria gonorrhoeae to cationic antimicrobial peptides and complement-mediated killing by normal human serum. *Infect. Immun.* **77,** 1112–1120 (2009).

134. Moffatt, J. H., Harper, M., Harrison, P., Hale, J. D. F., Vinogradov, E., Seemann, T., Henry, R., Crane, B., St. Michael, F., Cox, A. D., Adler, B., Nation, R. L., Li, J. & Boyce, J. D. Colistin resistance in Acinetobacter baumannii is mediated by complete loss of lipopolysaccharide production. *Antimicrob. Agents Chemother.* **54,** 4971–4977 (2010).

135. Takayama, K., Qureshi, N., Hyver, K., Honovich, J., Cotter, R. J., Mascagni, P. & Schneider, H. Characterization of a structural series of lipid A obtained from the lipopolysaccharides of Neisseria gonorrhoeae. Combined laser desorption and fast atom bombardment mass spectral analysis of high performance liquid chromatography-purified dimethyl deriv. *J. Biol. Chem.* **261,** 10624–31 (1986).

136. Mayer, H., Krauss, J. H., Yokota, A. & Weckesser, J. in *Endotoxin* (eds. Friedman, H., Klein, T. W., Nakano, M. & Nowotny, A.) 45–70 (Springer US, 1990). doi:10.1007/978-1-4757-5140-6_3

137. Bhat, U. R., Forsberg, L. S. & Carlson, R. W. Structure of lipid A component of Rhizobium leguminosarum bv. phaseoli lipopolysaccharide. Unique nonphosphorylated lipid a containing 2-amino-2- deoxygluconate, galacturonate, and glucosamine. *J. Biol. Chem.* **269,** 14402–14410 (1994).

138. Basu, S. S., White, K. A., Que, N. L. S. & Raetz, C. R. H. A deacylase in Rhizobium leguminosarum membranes that cleaves the 3-O- linked β-hydroxymyristoyl moiety of lipid A precursors. *J. Biol. Chem.* **274,** 11150–11158 (1999).

139. Gunn, J. S. Bacterial modification of LPS and resistance to antimicrobial peptides. *J. Endotoxin Res.* **7,** 57–62 (2001).

140. del Castillo, F. J., del Castillo, I. & Moreno, F. Construction and characterization of mutations at codon 751 of the Escherichia coli gyrB gene that confer resistance to the antimicrobial peptide microcin B17 and alter the activity of DNA gyrase. *J. Bacteriol.* **183,** 2137–40 (2001).

141. Guo, L., Lim, K. B., Poduje, C. M., Daniel, M., Gunn, J. S., Hackett, M. & Miller, S. I. Lipid A acylation and bacterial resistance against vertebrate antimicrobial peptides. *Cell* **95,** 189–198 (1998).

142. Guina, T., Yi, E. C., Wang, H., Hackett, M. & Miller, S. I. A PhoP-Regulated Outer Membrane Protease of Salmonella enterica Serovar Typhimurium Promotes Resistance to Alpha-Helical Antimicrobial Peptides. *J. Bacteriol.* **182,** 4077–4086 (2000).

143. Shafer, W. M., Qu, X. D., Waring, A. J. & Lehrer, R. I. Modulation of Neisseria gonorrhoeae susceptibility to vertebrate antibacterial peptides due to a member of the resistance/nodulation/division efflux pump family. *Proc. Natl. Acad. Sci. U. S. A.* **95,** 1829–1833 (1998).

144. Ackerman, S. J., Loegering, D. a, Venge, P., Olsson, I., Harley, J. B., Fauci, a S. & Gleich, G. J. Distinctive cationic proteins of the human eosinophil granule: major basic protein, eosinophil cationic protein, and eosinophil-derived neurotoxin. *J. Immunol.* **131,** 2977–2982 (1983).

145. Ackerman, S. J., Gleich, G. J., Loegering, D. A., Richardson, B. A. & Butterworth, A. E. Comparative toxicity of purified human eosinophil granule cationic proteins for schistosomula of Schistosoma mansoni. *Am. J. Trop. Med. Hyg.* **34,** 735–745 (1985).

146. Lehrer, R. I., Szklarek, D., Barton, A., Ganz, T., Hamann, K. J. & Gleich, G. J. Antibacterial properties of eosinophil major basic protein and eosinophil cationic protein. *J. Immunol.* **142,** 4428–34 (1989).

147. Tischendorf, F. W., Brattig, N. W., Büttner, D. W., Pieper, A. & Lintzel, M. Serum levels of eosinophil cationic protein, eosinophil-derived neurotoxin and myeloperoxidase in infections with filariae and schistosomes. *Acta Trop.* **62,** 171–182 (1996).

148. Hancock, R. E. & Scott, M. G. The role of antimicrobial peptides in animal defenses. *Proc. Natl. Acad. Sci. U. S. A.* **97,** 8856–61 (2000).

149. Torrent, M., de la Torre, B. G., Nogués, V. M., Andreu, D. & Boix, E. Bactericidal and membrane disruption activities of the eosinophil cationic protein are largely retained in an N-terminal fragment. *Biochem. J.* **421,** 425–434 (2009).

150. Pulido, D., Prats-Ejarque, G., Villalba, C., Albacar, M., González-López, J. J., Torrent, M., Moussaoui, M. & Boix, E. A novel RNase 3/ECP peptide for Pseudomonas aeruginosa biofilm eradication. Combining antimicrobial, lipopolysaccharide binding and cell agglutinating activities. *Antimicrob. Agents Chemother.* **60,** 6313–6325 (2016).

151. Villalba, C. Estudi de les funcions de defensa de les ribonucleases humanes d'eosinòfils. (2015).

152. Adams, P. D., Afonine, P. V., Bunkóczi, G., Chen, V. B., Davis, I. W., Echols, N., Headd, J. J., Hung, L. W., Kapral, G. J., Grosse-Kunstleve, R. W., McCoy, A. J., Moriarty, N. W., Oeffner, R., Read, R. J., Richardson, D. C., Richardson, J. S., Terwilliger, T. C. & Zwart, P. H. PHENIX: A comprehensive Python-based system for macromolecular structure solution. *Acta Crystallogr. Sect. D Biol. Crystallogr.* **66,** 213–221 (2010).

153. Emsley, P. & Cowtan, K. Coot: Model-building tools for molecular graphics. *Acta Crystallogr. Sect. D Biol. Crystallogr.* **60,** 2126–2132 (2004).

154. Borkakoti, N. The active site of ribonuclease A from the crystallographic studies of Ribonuclease-A-Inhibitor complexes. *Eur. J. Biochem.* **132,** 89–94 (1983).

155. Wlodawer, A., Svensson, L. A., Sjoelin, L. & Gilliland, G. L. Structure of phosphate-free ribonuclease A refined at 1.26 Å. *Biochemistry* **27,** 2705–2717 (1988).

156. deMel, V. S. J., Martin, P. D., Doscher, M. S. & Edwards, B. F. P. Structural changes that accompany the reduced catalytic efficiency of two semisynthetic ribonuclease analogs. *J. Biol. Chem.* **267,** 247–256 (1992).

157. Berisio, R., Lamzin, V. S., Sica, F., Wilson, K. S., Zagari, a & Mazzarella, L. Protein titration in the crystal state. *J. Mol. Biol.* **292,** 845–54 (1999).

158. Gotte, G., Laurents, D. V. & Libonati, M. Three-dimensional domain-swapped oligomers of ribonuclease A: Identification of a fifth tetramer, pentamers and hexamers, and detection of trace heptameric, octameric and nonameric species. *Biochim. Biophys. Acta - Proteins Proteomics* **1764,** 44–54 (2006).

159. Gotte, G., Laurents, D. V., Merlino, A., Picone, D. & Spadaccini, R. Structural and functional relationships of natural and artificial dimeric bovine ribonucleases: New scaffolds for potential antitumor drugs. *FEBS Lett.* **587,** 3601–3608 (2013).

160. Liao, Y. di. A pyrimidine-guanine sequence-specific ribonuclease from Rana catesbeiana (bullfrog) oocytes. *Nucleic Acids Res.* **20,** 1371–1377 (1992).

161. Irie, M., Nitta, K. & Nonaka, T. Biochemistry of frog ribonucleases. *Cell. Mol. Life Sci.* **54,** 775–784 (1998).

162. Luscombe, N. M. Amino acid-base interactions: a three-dimensional analysis of protein-DNA interactions at an atomic level. *Nucleic Acids Res.* **29,** 2860–2874 (2001).

163. Prats-Ejarque, G., Lu, L., Salazar, V. A., Moussaoui, M. & Boix, E. Evolutionary Trends in RNA Base Selectivity Within the RNase A Superfamily. *Front. Pharmacol.* **10,** 1–17 (2019).

164. Hsu, C. H., Chang, C. F., Liao, Y. Di, Wu, S. H. & Chen, C. Solution structure and base specificity of cytotoxic RC-RNase 2 from Rana catesbeiana. *Arch. Biochem. Biophys.* **584,** 70–78 (2015).

165. Prats-Ejarque, G., Blanco, J. A., Salazar, V. A., Nogués, V. M., Moussaoui, M. & Boix, E. Characterization of an RNase with two catalytic centers. Human RNase6 catalytic and phosphate-binding site arrangement favors the endonuclease cleavage of polymeric substrates. *Biochim. Biophys. Acta - Gen. Subj.* **1863,** 105–117 (2019).

166. Uggerhøj, L. E., Poulsen, T. J., Munk, J. K., Fredborg, M., Sondergaard, T. E., Frimodt-Moller, N., Hansen, P. R. & Wimmer, R. Rational Design of Alpha-Helical Antimicrobial Peptides: Do's and Don'ts. *ChemBioChem* **16,** 242–253 (2015).

167. Oliva, R., Chino, M., Pane, K., Pistorio, V., De Santis, A., Pizzo, E., D'Errico, G., Pavone, V., Lombardi, A., Del Vecchio, P., Notomista, E., Nastri, F. & Petraccone, L. Exploring the role of unnatural amino acids in antimicrobial peptides. *Sci. Rep.* **8,** 1–16 (2018).

168. Joo, H. S., Fu, C. I. & Otto, M. Bacterial strategies of resistance to antimicrobial peptides. *Philos. Trans. R. Soc. B Biol. Sci.* **371,** (2016).

169. Doucet, N., Watt, E. D. & Loria, J. P. The flexibility of a distant loop modulates active site motion and product release in ribonuclease A. *Biochemistry* **48,** 7160–7168 (2009).

170. Gagné, D., French, R. L., Narayanan, C., Simonović, M., Agarwal, P. K. & Doucet, N. Perturbation of the Conformational Dynamics of an Active-Site Loop Alters Enzyme Activity. *Structure* **23,** 2256–2266 (2015).

171. Torrent, M., Sánchez, D., Buzón, V., Nogués, M. V., Cladera, J. & Boix, E. Comparison of the membrane interaction mechanism of two antimicrobial RNases: RNase 3/ECP and RNase 7. *Biochim. Biophys. Acta - Biomembr.* **1788,** 1116–1125 (2009).

172. Pulido, D., Torrent, M., Andreu, D., Nogués, M. V. & Boix, E. Two human host defense ribonucleases against mycobacteria, the eosinophil cationic protein (RNase 3) and RNase 7. *Antimicrob. Agents Chemother.* **57,** 3797–805 (2013).

173. Dickson, K. A., Haigis, M. C. & Raines, R. T. Ribonuclease Inhibitor: Structure and Function. *Prog. Nucleic Acid Res. Mol. Biol.* **80,** 349–374 (2005).

174. Prats-Ejarque, G., Lorente, H., Lu, L., Vázquez, S., Fernández-Millán, P. & Boix, E. Design of an RNase chimera for antimicrobial therapy. *Int. J. Mol. Sci.* To be submitted (2020).

175. Boix, E., Leonidas, D. D., Nikolovski, Z., Nogués, M. V., Cuchillo, C. M. & Acharya, K. R. Crystal structure of eosinophil cationic protein at 2.4 A resolution. *Biochemistry* **38,** 16794–16801 (1999).

176. García-Mayoral, M. F., Moussaoui, M., De La Torre, B. G., Andreu, D., Boix, E., Nogués, M. V., Rico, M., Laurents, D. V & Bruix, M. NMR structural determinants of eosinophil cationic protein binding to membrane and heparin mimetics. *Biophys. J.* **98,** 2702–2711 (2010).

177. Noda, N. N., Ohsumi, Y. & Inagaki, F. Atg8-family interacting motif crucial for selective autophagy. *FEBS Lett.* **584,** 1379–1385 (2010).

178. Birgisdottir, Å. B., Lamark, T. & Johansen, T. The LIR motif - crucial for selective autophagy. *J. Cell Sci.* **126,** 3237–3247 (2013).

179. Wild, P., McEwan, D. G. & Dikic, I. The LC3 interactome at a glance. *J. Cell Sci.* **127,** 3–9 (2014).

180. Yang, Z. & Klionsky, D. J. An overview of the molecular mechanism of autophagy. *Curr. Top. Microbiol. Immunol.* **335,** 1–32 (2009).

181. Klionsky, D. & Deretic, V. Autophagy: molecular mechanisms and disease outcomes. *Nat. Rev. Mol. Cell Biol.* 2011 (2011). at <http://www.bostonbiochem.com/sites/bostonbiochem.com/files/new-scientific-poster-autophagy-molecular-mechanisms-and-disease-outcomes.pdf>

182. Johansen, T. & Lamark, T. Selective Autophagy: ATG8 Family Proteins, LIR Motifs and Cargo Receptors. *J. Mol. Biol.* **432,** 80–103 (2020).

183. Rozenknop, A., Rogov, V. V., Rogova, N. Y., Löhr, F., Güntert, P., Dikic, I. & Dötsch, V. Characterization of the interaction of GABARAPL-1 with the LIR motif of NBR1. *J. Mol. Biol.* **410,** 477–487 (2011).

184. Lu, L., Arranz-Trullén, J., Prats-Ejarque, G., Pulido, D., Bhakta, S. & Boix, E. Human Antimicrobial RNases Inhibit Intracellular Bacterial Growth and Induce Autophagy in Mycobacteria-Infected Macrophages. *Front. Immunol.* **10,** (2019).

185. González Plaza, J. J. Small RNAs as Fundamental Players in the Transference of Information During Bacterial Infectious Diseases. *Front. Mol. Biosci.* **7,** (2020).

186. Prats-Ejarque, G., Li, J., Ait-Ichou, F., Lorente, H. & Boix, E. Testing a Human Antimicrobial RNase Chimera Against Bacterial Resistance. *Front. Microbiol.* **10,** 1–14 (2019).

8. AGRAÏMENTS

Al llarg d'aquests anys, han estat moltes les persones que m'han ajudat, directa, o indirectament, en poder fer aquesta tesi. La llista és molt llarga, i intentaré no deixar-me a ningú.

Primer de tot, voldria agrair a l'Ester per la direcció d'aquesta tesi, tant a nivell científic com personal. Es fa molt difícil trobar un grup de recerca en el qual es pugui tenir tanta autonomia, estant sempre a sobre per quan és necessari. Molts IP haurien d'aprendre'n. Al Mohammed, per ser-hi sempre que tenia algun problema, i trobar-hi una solució, per inusual que fos. A la Victòria, per les seves valuoses aportacions en les reunions de grup i per estar "infiltrada" a l'escola de Doctorat.

A tot el grup de Ribos, passat, present, i futur. Lu, for all the good times, long days at the lab and to complain together against science. We have been working together a lot of time, and after first teaching you, then you ended slaving me, also from China. Your spirit has remained in the lab, so now I go to SAF, by bike everywhere, and I work all day all night. If that keeps like this, I'll learn Chinese soon, and then I'll visit you! Helena, em poses en un compromís perquè ara em podràs tornar els vòmits d'arcoiris, però vaja XD. Podria posar un "Gràcies" i quedar-me tant ample, però seria lleig. També podria fer la conya fàcil d'agrair-te portar-me els tuppers i la llibreta, però no hi cauré, així que t'agrairé una cosa indiscutible, i és que vas portar alegria al lab en un moment que en faltava. Has fet bé deixant la ciència però... se t'ha trobat a faltar. Pablo, por todos los buenos consejos, ya sean de lab o de montaña, por los cafés y por todas las conversaciones arreglando el mundo (de momento no lo hemos conseguido parece xD). Jiarui, it seems yesterday that you arrived and you we were going around the lab with the board, and now you are almost finishing the PhD. It is really nice to have an optimistic and happy person as you in the lab, who always smile despite science. I a tots els altres Ribos que han estat o seguiran sent-hi, pels bons moments al lab, cafès, dinars, experiments intempestius, etc. Raúl, Vivian, Sergi, Andrea, Alba, Kamillah, Fatima...

A tota la gent de la torre. En pocs llocs de treball, almenys en el nostre sector, hi ha un ambient tant bo i es fan tantes coses junts. Als Pros; Samu y Francisca, por todas las fiestas, juegos, mojitos y birras en vuestra casa (bueno, y fuera de ella) y por organizar el 99 % de las veces que quedamos, Jaime por haber conseguido un éxito tras otro en la comisión de fiestas, nadie va a poder superar nuestro legado. Esta tesis es otro éxito de la comisión de fiestas. Al Jordi, la ment més preclara de les olimpíades bioquímiques i ja quasi l'únic que encara em superes en antiguitat, pels submarinos i les locuras científiques. Algun dia ho hem de tornar a provar. Valen, per animar sempre les converses amb el teu toc, diguem-ne, picant ;) A les RMN-kinàsiques; Lucía i Fanny, per introduir-me en el "meravellós" món dels westerns, Shuang, I've been doubting if to put you here or in Ribos xD. I hope you don't miss Spain very much, we both know it's hard to work in China. A Pilar, por la compañía, las conversaciones, las fiestas, birras, rutas, y un largo etcétera. Por aguantar mis ralladas y animarme, aunque no me dejara. En fin, por todos y cada uno de los buenos momentos… y también por los vergonzosos 😁. Y, por supuesto, por hacer de tu casa mi segundo hogar, pese a que la primera vez no fue mi mejor carta de presentación XD. No te vayas muy lejos cuando termines… Als PFs, nous i vells. Jofre, Gisela i Laia, fundadors de Doctorands Bioquímica, per ajudar-me quan començava a rondar per aquí, pels dinars al solàrium, calçotades... Gabri, crec que no m'arrisco si dic que no hi ha hagut pitjors estudiants al Màster de Bioquímica que nosaltres dos. Em deus una birra per les dinàmiques, per cert! ADHs, Raquel i Julio, pels xanxulleos i deixar-me sempre totes les coses rares que necessitava pels cristalls. Als veïns de DNAs, Dani (el meu traficant de fenol preferit), Marta, per totes les vegades que us he vingut a demanar coses (i les que vindran). Al grup de System Bio... bah, al grup de Plantes. Dani,

Javi, i sobretot a la Núria, per les deu mil vegades que he vingut a molestar-te pel Tecan, campana o similars... I evidentment, per totes les sortides i festes junts, per posar sempre aquesta alegria tant teva i... malgrat que mengis formatge. Jara, hemos sido los profes más chungos de Genética y nos marcamos buenos tours entre Lleida y Tarragona. I a la resta de gent de l'IBB, Santo (vamos que ya lo tienes!!), Marcos, Marta, Cris... No sou de la torre, però els dies de Nadal, la *fondue* de l'IBB ho compensa.

Al Santi i la Magda per tota l'ajuda i paciència amb nosaltres, tant per les pràctiques com per fer que tots els aparells de la Unitat segueixin funcionant. A l'Helena, per tots els tampons, pels milers de plaques de Petri, per les urgències a primera hora del matí per preparar-ne corrents, per escoltar la meva indignació amb el món cada dijous i per intentar que el lab, malgrat la meva tendència a l'entropia, estigui una mica presentable. Al Joan Carles per poder arreglar tots els problemes amb els proveïdors més estrambòtics possibles. Al Salva, per tots els bons consells quan tenia dubtes i per la paciència amb descuits i urgències. A tots els no-predocs del departament que en un moment o altre m'heu ajudat, ja sigui amb consells, suggeriments o reactius exòtics; Marc, Josep, Alícia, Inma, David...

A la gent de Micro, Estela, Esther, Marta, Sandra, Marc, Paula per tenir-me sempre rondant per allà i fer del vostre el meu segon lab, ensenyar-me a treballar amb cultius i micobacteris, malgrat que el tema dels exosomes va acabar com va acabar...

To all the BioNMR group in Patras, for the time I stayed there, and particularly to George, Maria and Katerina for your hospitality and helping me all the time I needed.

A tots els companys de la CGT, dels quals he après que, amb la lluita, si no ens resignem, podem guanyar. Merce, David, Ermen, Sara (el Dimas i la Muriel et volen conèixer, els hi deus un sopar!), Guillem, Rubén, Mireia, Marc (el meu dissenyador gràfic personal), Òscar, Rafa, Maca... Les birres després de guanyar una vaga són les millors que es poden fer, així que haurem de guanyar-ne més! María, yo esto de la coordinadora no sé cómo va a ir, pero solo para conocerte ya valió la pena subir a Madrid.

A tota la gent que ha format Doctorandes en Lluita. No esperàvem que amb tant poc temps poguéssim aconseguir tant. Crec que hem fet un grup que val molt la pena mantenir i estem canviant la percepció de què és un doctorat, lo que era molt important des de fa ja massa anys. Laura, després de la primera Doctora en Lluita ara vinc jo, ja veig *Postdocs en Lluita* a l'horitzó, i ara, internacional! I no pot faltar l'altra Laura, la meva advocada de capçalera, per tota la turra que t'he clavat, ja siguin legals o d'utopies pirates. Ànim amb la tesi, Transoxiana necessita gent com tu. I a tota la resta de Doctorandes en Lluita, Paula, Almudena, Carol, Lara, Joan, Berta...

Als bioquímics croquetaires (i més recentment, club d'escalada XD), Cris, Vicente, Aleix, Laura, Marta i Manu, per tots els sopars, estius, esquiades, patos etílics... en els quals no es desconnectava de la tesi, perquè era el principal tema de conversa, però bé, se li treia ferro i en rajàvem junts, que també és important. I record també als exiliats, Carlos i Gisela!

A l'Andguipo, Pol, Andreu i Navarro, per recordar-me que hi ha vida fora del laboratori, malgrat que sempre ho he posat difícil, tot i que no he estat l'únic... (òstia Andre, acabo de recordar que vivies amb mi i el Navarro! A tu et sona?). Ja vam anar a Miravete i fins i tot a Romania, falten los Cerros de Úbeda, i la Mongòlia Ulterior. S'hi pot anar des del camí de Santiago? Així fem 3 punts de la llista d'una tacada. Jo ara sóc doctor, i més aviat que tard estaré a l'atur així que... busquem uns mesos.

A la meva família. Als meus pares per aguantar-me el cansament i mal humor i portar-me tants cops al laboratori en caps de setmana o hores intempestives. A l'Helena, que em sembla que, vist que després de conèixer les RNases al meu lab, vas decidir fer Psicologia, potser no et va molar gaire el tema XDD. I a part de l'Helena, no pot faltar una menció al meu cunyat, l'Alejandro, company de lluites i de tantes altres coses. Per les festes i els bons moments, per dissenyar vagues entre birra i birra, per compartir inhumanes jornades lab-sindicat (no penso tornar a matinar per anar a Lleida!!), per les infructíferes, però apassionants converses...

Finalment, i per suposat, a la Clara. Per acompanyar-me durant tot aquest temps, per suportar el mal humor i les frustracions, per ajudar-me en tot el que podies, per aguantar les xapes infumables, per corregir-me els articles, per fer-me (o almenys intentar-ho) canviar de xip i d'obsessió... En definitiva, per estar sempre amb mi i al meu costat, tant quan et necessitava com, quan (ingenu de mi) em pensava que no.

I per acabar, convé recordar, per a futures ocasions, que, *The No, you have*.